AWARD NUMBER: W81XWH-15-1-0236

TITLE: Phosphoproteomic Assessment of Therapeutic Kinases for Personalized Therapy in Castration-Resistant Prostate Cancer

PRINCIPAL INVESTIGATOR: Justin M. Drake

CONTRACTING ORGANIZATION: Rutgers, The State University of New Jersey
New Brunswick NJ 08903

REPORT DATE: October 2016

TYPE OF REPORT: Annual

PREPARED FOR: U.S. Army Medical Research and Materiel Command
Fort Detrick, Maryland 21702-5012

REPORT DOCUMENTATION PAGE

Form Approved
OMB No. 0704-0188

1. REPORT DATE	2. REPORT TYPE	3. DATES COVERED
October 2016	Annual	15 Sep 2015 - 14 Sep 2016

4. TITLE AND SUBTITLE

Phosphoproteomic Assessment of Therapeutic Kinases for Personalized Therapy in Castration-Resistant Prostate Cancer

5a. CONTRACT NUMBER

5b. GRANT NUMBER
81XWH-15-1-0236

5c. PROGRAM ELEMENT NUMBER

6. AUTHOR(S)
Justin M. Drake

E-Mail: justin.drake@cinj.rutgers.edu

5d. PROJECT NUMBER

5e. TASK NUMBER

5f. WORK UNIT NUMBER

7. PERFORMING ORGANIZATION NAME(S) AND ADDRESS(ES)
Rutgers, The State University of New Jersey
195 Little Albany Street
New Brunswick, NJ 08903-1914

8. PERFORMING ORGANIZATION REPORT NUMBER

9. SPONSORING / MONITORING AGENCY NAME(S) AND ADDRESS(ES)

U.S. Army Medical Research and Materiel Command
Fort Detrick, Maryland 21702-5012

10. SPONSOR/MONITOR'S ACRONYM(S)

11. SPONSOR/MONITOR'S REPORT NUMBER(S)

12. DISTRIBUTION / AVAILABILITY STATEMENT

Approved for Public Release; Distribution Unlimited

13. SUPPLEMENTARY NOTES

14. ABSTRACT
Due to the overwhelming evidence for kinase activation in metastatic CRPC tissues, our objective is to utilize a targeted mass spectrometry (MS) approach for the evaluation of current druggable kinases in human prostate cancer biopsies that will ultimately guide personalized therapy decisions. We hypothesize that targeted MS can be effectively used for the stratification of prostate cancer patients based on detection of activated kinases in pre-clinical and biopsy tissues. We have begun to evaluate activated kinases using pre-designed phosphopeptides via targeted MS. To date, we have evaluated 111 kinase phosphopeptide standards and were able to detect nearly 75% via targeted MS, nearly half of which at 400 attomole sensitivity. We are currently evaluating phosphopeptide enrichment methods to detect these phosphopeptide standards in small tissue lysate amounts equivalent to a biopsy in cell lines where known genetic alterations in kinases exist. Those experiments are ongoing prior to moving into clinical tissues.

15. SUBJECT TERMS
Phosphoproteomics, metastatic, castration resistant prostate cancer, kinase, mass spectrometry

16. SECURITY CLASSIFICATION OF:			17. LIMITATION OF ABSTRACT	18. NUMBER OF PAGES	19a. NAME OF RESPONSIBLE PERSON
a. REPORT	b. ABSTRACT	c. THIS PAGE			USAMRMC
Unclassified	Unclassified	Unclassified	Unclassified	56	19b. TELEPHONE NUMBER *(include area code)*

Table of Contents

Page

INTRODUCTION

Prostate cancer is the most common diagnosed and second leading cause of epithelial cancer-related death in men[1]. One of the biggest challenges during cancer treatment is to define the patient subsets that will best respond to appropriate therapies. In prostate cancer, all patients are essentially treated the same and there are currently no subtypes to stratify for therapy purposes. Molecular targets for metastatic castration resistant prostate cancer (CRPC) include translocations[2], somatic mutations[3], and DNA amplifications[4] but targeting AR is still the main focus for current therapies. As resistance to AR therapeutic agents become more common, AR independent pathways such as kinase signaling need to be considered as new therapeutic options, although activating mutations of kinases in metastatic CRPC are very rare[3]. This is a major clinical problem and the development of new biomarkers that can either predict disease progression (diagnostic) or to stratify patients for effective personalized therapy (predictive) are urgently needed. Our strategy is to develop biomarkers geared towards the activated kinases in metastatic CRPC using targeted mass spectrometry (MS) approaches for clinical diagnostics. Our goal is to generate a minimal set, but if necessary up to 100 unique phosphopeptides that behave as surrogates for kinase activation that can be used pre-clinically and clinically to evaluate endogenous kinase signaling, as resistance mechanisms to conventional therapies, and as biomarkers for patient stratification leading to therapy decisions.

KEYWORDS

- Castration resistant prostate cancer
- Phosphoproteomics
- Metastasis
- Kinase
- Mass spectrometry
- Biomarker

ACCOMPLISHMENTS

What were the major goals of the project?

The major aims of the project are to:
Aim 1: To establish quantitative methods to detect activated kinases for clinical diagnostics.
Aim 2: To measure activated kinases in pre-clinical xenograft models of prostate cancer.
Aim 3: To assess efficacy of targeted SIM MS in clinical CRPC tissues for personalized therapy.

What was accomplished under these goals?

For Aim 1, we were able to design phosphopeptides for up to 111 different kinases of interest (including several phosphosites for a few select kinases). We have ordered and received all 111 phosphopeptide standards (not heavy labeled) for initial testing on the mass spectrometer (MS) in 2 separate batches. This initial experiment goal is to determine if we can detect these phosphopeptide standards on the MS and at what sensitivity when spike into a complex lysate. We spiked in serial dilutions of our phosphopeptide standards beginning at 250 femtomoles/ul down to 0.4 femtomoles/ul into 0.25ug/ul of Arabidopsis lysate tryptic digest (**Figure 1A, B**). Arabidopsis was used because the kinase sequences corresponding to our human kinase phosphopeptides would not be homologous to the Arabidopsis sequences allowing us to directly detect them on the MS without having to heavy label them. Of these, we identified 82/111 (74%) via MS and 39/111 (35%) were detected at 400 attomoles; nearly sensitive enough for detection in biopsy tissues (**Figure 1C-E**). **Figure 1** is showing just one example of our kinase phosphopeptide standards and how they are analyzed via MS. We have data for all 111 kinases similar to **Figure 1.**

We have also begun evaluating phosphopeptide enrichment strategies to determine the best sample preparation that is necessary to achieve optimum sensitivity. For this experiment, we purchased a commercial set of N^{15} heavy labeled phosphopeptides that correspond to kinase activation loops from the company JPT. This set will

allow us to begin testing our enrichment strategies while we are developing are final targeted phosphopeptide list to be generated in house. We initially designed the experiment to test 2 variables: 1) when to spike in the heavy labeled phosphopeptides (**Figure 2A-C**) and 2) whether phosphopeptide enrichment is necessary (**Figure 2D-F**). We have prepared these samples are in the process of analyzing them via MS. Task 1 is completed and Tasks 2 and 3 are underway.

For Aim 2, we assessed some cancer cell lines that had known actionable mutations for preliminary analyses. This was done so that we could use these lines as a means to detect the activated kinases via our phosphopeptide standards as we know which kinase(s) should be activated. The cell lines chosen were UACC903 (BRAF V600E) melanoma line, H1650 (EGFR mutant) NSCLC line, and HCC1954 (HER amplified) breast cancer line. Xenografts were grown for each tumor in the flank of mice and the tumors were then lysed using 6M guanidinium HCl lysis buffer prior to protein measurements. The tumors were then subjected to a series of workflows to evaluate different enrichment strategies (**Figure 2**). The preparations have been completed and are currently under evaluation via MS to determine which approach provides the best sensitivity and detection. Task 4 is currently being evaluated and Task 5 has yet to begin.

For Aim 3, we have the human subjects protocol approved by the IRB at Rutgers Cancer Institute of New Jersey as well as the Department of Defense. This is the first step to begin acquiring tissues for analysis in Task 6. Task 7 has yet to begin.

What opportunities for training and professional development has the project provided?
Nothing to report.

How were the results disseminated to communities of interest?
Nothing to report.

What do you plan to do during the next reporting period to accomplish the goals?
I will have hired a full time postdoctoral fellow beginning in January to help finish up Aim 1 and begin Aims 2 and 3. We plan to have the enrichment strategies confirmed, tested, and finalized in our pre-clinical models and plan to begin Aim 3 using the clinical tissue biopsies. We anticipate Tasks 2 and 3 in Aim 1, Tasks 4 and 5 in Aim 2, and Task 6 in Aim 3 to be completed or nearly completed by the end of Year 2.

IMPACT

What was the impact on the development of the principal discipline(s) of the project?
Therapeutic targeting of tyrosine kinases in late stage prostate cancer are still underdeveloped. We have begun investigation into new ways that we can detect activated, non-mutated kinases in pre-clinical and clinical tissues for potential biomarkers leading to better prognosis and therapies.

What was the impact on other disciplines?
To date, this is minimal, but we anticipate the results of our studies have the broad capability of expanding to other cancer types where detection of activated kinases might be important. This could include ovarian cancer, triple negative breast cancer, and osteosarcomas.

What was the impact on technology transfer?
Nothing to report.

What was the impact on society beyond science and technology?
Nothing to report.

CHANGES/PROBLEMS

Changes in approach and reasons for change.

Nothing to report.

Actual or anticipated problems or delays and actions or plans to resolve them.

At the beginning of this award, I recently acquired a tenure-track faculty position and was in the process of setting up and developing my lab, which included up to 6 months just to receive all the equipment necessary to do research. This also included hiring staff for this project. While we have made some significant progress on this project, there were some delays in the 1st year related to my new position that will not be an issue in year 2. I initially hired a postdoctoral fellow to work on this project but after 3 months left for another position. I am about to hire another postdoc to work on this project to begin January 1, 2017. This new hire will significantly impact (in a positive way) the project timeline.

Another issue we came across is that some of our designed phosphopeptide isoforms could not be separated. An example is for IGF1R at Y1165 or Y1166 (**Figure 3**). For phosphopeptides that have phosphorylated residues adjacent to one another, it may be difficult to distinguish these peaks. Therefore, to resolve this issue, we will pick one of the phosphopeptides and leave the other one out. In instances such as this, both phosphopeptides are usually required for activation so the assumption can be made that if one is phosphorylated, then the kinase is activated.

Changes that had a significant impact on expenditures

Nothing to report.

Significant changes in use or care of human subjects, vertebrate animals, biohazards, and/or select agents.

Nothing to report.

Significant changes in use or care of human subjects.

Nothing to report.

Significant changes in use or care of vertebrate animals.

Nothing to report.

Significant changes in use of biohazards and/or select agents.

Nothing to report.

PRODCUTS

Publications, conference papers, and presentations.

Journal publications (Note: These publications were not a direct result of this project but related.)

Faltermeier CM, **Drake JM**, Clark PM, Smith BA, Zong Y, Volpe C, Mathis C, Morrissey C, Castor B, Huang J, Witte ON (2016) Functional Screen Identifies Kinases Driving Prostate Cancer Visceral and Bone Metastasis. *PNAS*. 113(2):E172-E181. PMCID: PMC4720329.

-Featured in a commentary by Feng and Kothari in PNAS

Drake JM*,#, Paull, EO*, Graham NA, Lee JK, Smith, BA, Titz, B, Stoyanova TS, Faltermeier CM, Carlin DE, Flemming DT, Wong CK, Newton Y, Sudha S, Vashisht AA, Huang J, Wohlschlegel JA, Graeber TG, Witte ON#, Stuart JM# (2016) Phosphoproteome Integration Reveals Patient-Specific Networks in Prostate Cancer. *Cell.* 166(4):1041-1054. *Authors contributed equally to this work. #Co-corresponding author.

-Editor's choice commentary in Science Translational Medicine

Stoyanova T, Riedinger M, Lin S, Faltermeier CM, Smith BA, Zhang KX, Going C, Goldstein AS, Lee JK, **Drake JM**, Rice M, Hsu E, Nowroozizadeh B, Castor B, Orellana SY, Blum SM, Cheng D, Pienta KJ, Reiter R, Pitteri S, Huang J, Witte ON (2016) Activation of Notch1 Synergizes with Multiple Pathways in Promoting Castration Resistant Prostate Cancer. *PNAS*. In press

Books or other non-periodical, one time publications.
Nothing to report.

Other publications, conference papers, and presentations.
Poster Presentations
Department of Defense IMPaCT Meeting – August 4-5, 2016 Baltimore, MD (see appendices)

Invited Presentations
Institute for Quantitative Biomedicine: Cancer Genomics and Proteomics Research Working Group Meeting Rutgers University, Piscataway, NJ, "Identification of activated signaling pathways in lethal prostate cancer." September 2015

Department of Pharmacology and Therapeutics Seminar Series, Roswell Park Cancer Institute, Buffalo, NY, "Identification of signaling pathways in metastatic prostate cancer." May 2016

Website(s) or other Internet site(s)
Nothing to report.

Technologies or techniques.
Nothing to report.

Inventions, patent applications, and/or licenses.
Nothing to report.

Other products.
Nothing to report.

PARTICIPANTS & OTHER COLLABORATING ORGANIZATIONS
What individuals have worked on the project?

Name:	*Sangeeta Bafna*
Project Role:	*Postdoctoral Fellow*
Researcher Identifier (e.g. ORCID ID):	*NA*
Nearest person month worked:	*3*
Contribution to Project:	*Dr. Bafna began developing the phosphopeptide list for biomarker development and started to work on the wet lab experiments to test these phosphopeptides using targeted mass spectrometry approaches related to Aims 1 and 2.*
Funding Support:	*NA*

Name:	*Zhen Li*
Project Role:	*Laboratory Manager*
Researcher Identifier (e.g. ORCID ID):	*NA*
Nearest person month worked:	*1*
Contribution to Project:	*Dr. Li began working with the mass spectrometry facility at Rutgers University to begin testing the phosphopeptides and sensitivity determination related to Aim 1.*
Funding Support:	*NA*

Has there been a change in the active other support of the PD/PI(s) or senior/key personnel since the last reporting period?
Nothing to report.

What organizations were involved as partners?
Dr. Thomas G. Graeber
Organization Name: University of California, Los Angeles
Location of Organization: Los Angeles, CA
Partner's Contribution to the Project: Collaboration

Dr. Peter Lobel
Organization Name: Rutgers University
Location of Organization: Piscataway, NJ
Partner's Contribution to the Project: Collaboration

SPECIAL REPORTING REQUIREMENTS
None

APPENDICES (see attached)
- Supporting Data (Figures 1-3)
- Publication in *PNAS*
- Publication in *Cell*
- Publication in *PNAS*
- Department of Defense IMPaCT Meeting Abstract

REFERENCES

1. Siegel, R.L., Miller, K.D. & Jemal, A. Cancer statistics, 2015. *CA Cancer J Clin* **65**, 5-29 (2015).
2. Tomlins, S.A., *et al.* Recurrent fusion of TMPRSS2 and ETS transcription factor genes in prostate cancer. *Science* **310**, 644-648 (2005).
3. Grasso, C.S., *et al.* The mutational landscape of lethal castration-resistant prostate cancer. *Nature* **487**, 239-243 (2012).
4. Taylor, B.S., *et al.* Integrative genomic profiling of human prostate cancer. *Cancer Cell* **18**, 11-22 (2010).

Phosphopeptides were added into Arabidopsis tryptic digest (0.25ug/ul)

- Serial dilutions: 250fmol/ul, 50fmol/ul, 10fmol/ul, 2fmol/ul, 0.4fmol/ul

A

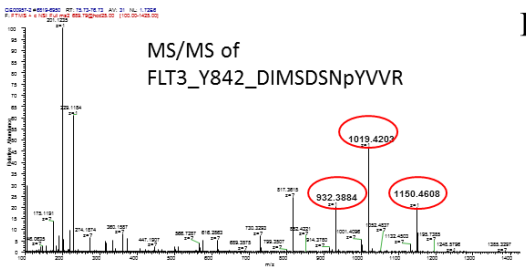

B

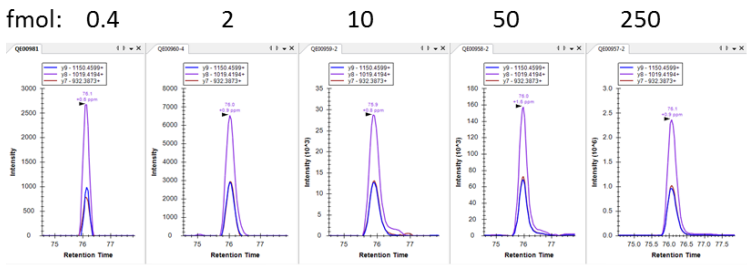

C

Amount on column(fmol)	Peak Area
250	7.89E+07
50	6.59E+06
10	1.17E+06
2	2.30E+05
0.4	6.64E+04

D

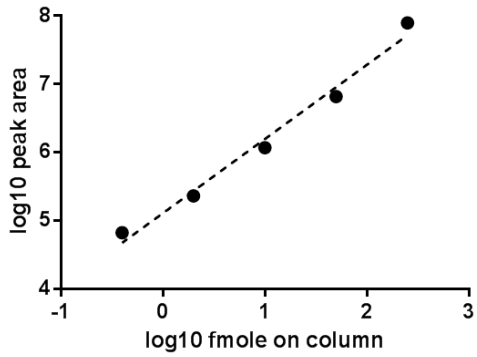

E

Batch #:

1	39/52 (75%) phosphopeptides have been identified at 400 amole 13/52 (25%) phosphopeptides were not quantified (low or no peptide detected)
2	43/59 (73%) phosphopeptides have been identified 16/59 (27%) phosphopeptides were not quantified (no peptide detected)
Total	82/111 (74%) phosphopeptides have been identified

Figure 1. Targeted MS/MS Quantification. A. Mass spectrum of the detection of one of our kinase phosphopeptide standards, FLT3 Y842. B. Area under the curve peak values for FLT3 Y842 at each serial dilution. C. The peak area for each serial dilution and the quantified line curve (C). For our 11 phosphopeptide standards, we were able to detect nearly 75% of them. Big progress has been made with these standards and we plan to move forward with them in our pre-clinical models in Aim 2.

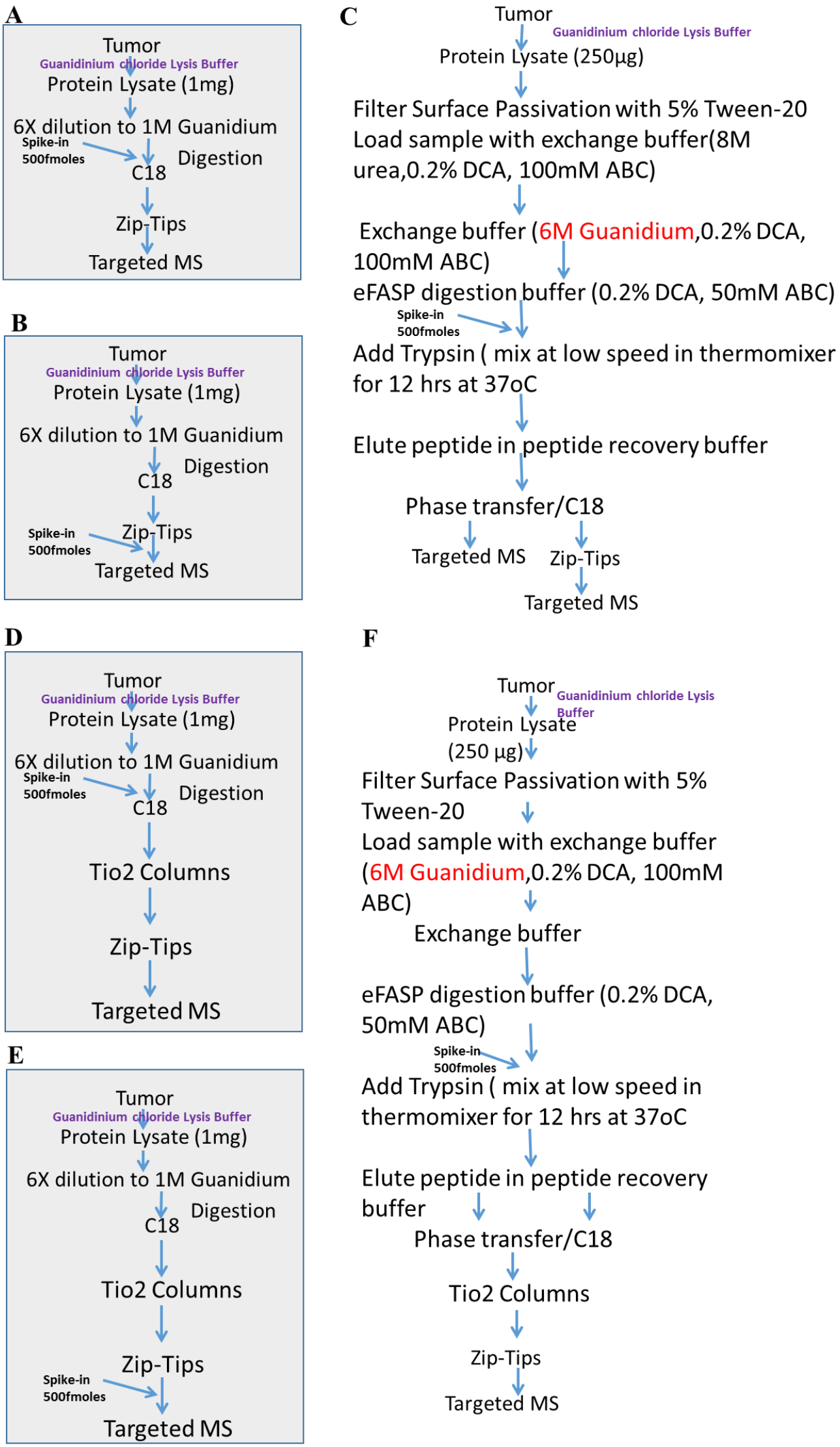

Figure 2. Advantages of targeted selected ion monitoring (SIM) over shotgun proteomics. Different phosphopeptide methods were used to determine the optimum sensitivity and when to spike in the heavy labeled phosphopeptides (A-C_ and enrichment protocols (D-F). Xenografts from 3 cell lines chosen: UACC903 (BRAF V600E) melanoma line, H1650 (EGFR mutant) NSCLC line, and HCC1954 (HER amplified) breast line. These tumors were then lysed and subjected to the methods described in this figure. These methods are currently being evaluated and our first trial experiment is completed and the samples have been just completed on the MS. We are now analyzing the samples.

A

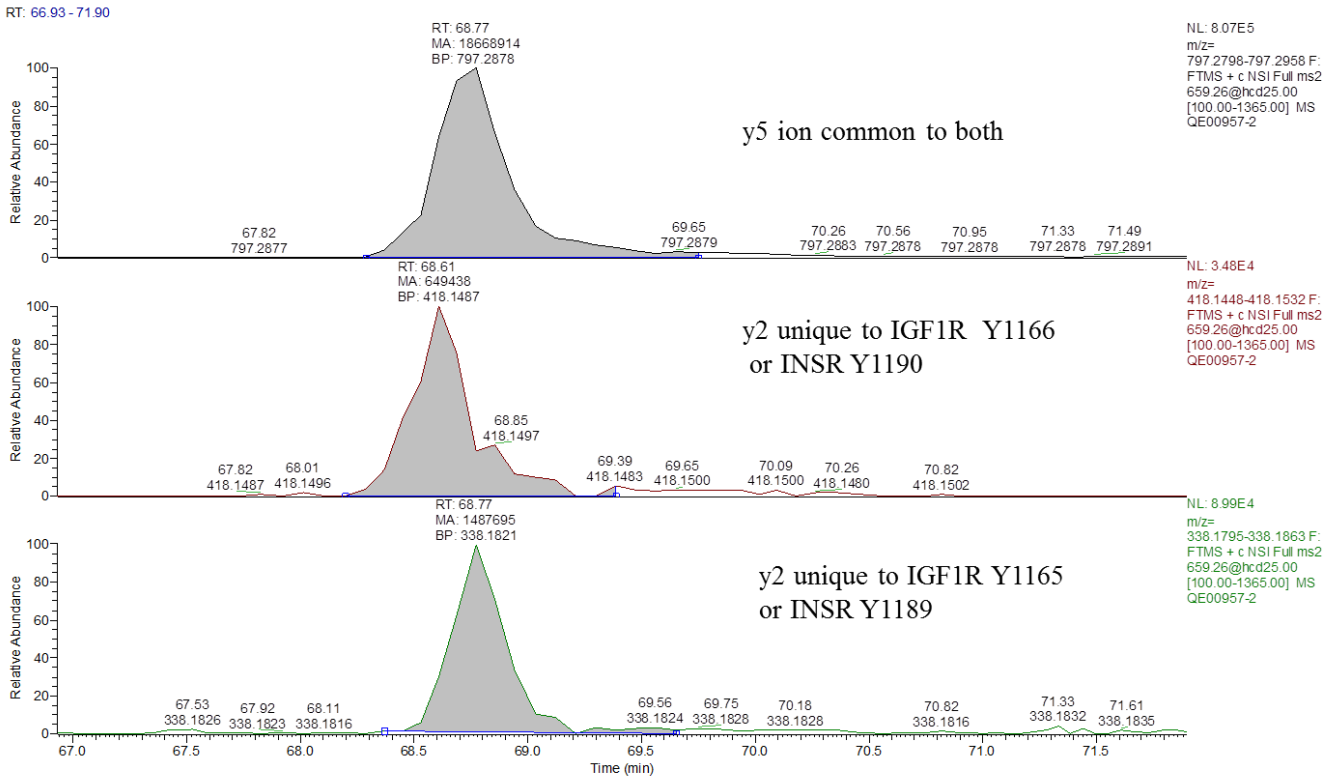

B

	b			y		b			y
D	1	116.0348	1317.504	9	D	1	116.0348	1317.504	9
I	2	229.1189	1202.477	8	I	2	229.1189	1202.477	8
Y	3	392.1822	1089.393	7	Y	3	392.1822	1089.393	7
E	4	521.2248	926.3294	6	E	4	521.2248	926.3294	6
T	5	622.2725	797.2868	5	T	5	622.2725	797.2868	5
D	6	737.2994	696.2391	4	D	6	737.2994	696.2391	4
Y	7	980.3288	581.2122	3	Y	7	900.3628	581.2122	3
Y	8	1143.392	338.1829	2	Y	8	1143.392	418.1489	2
R	9	1299.493	175.1196	1	R	9	1299.493	175.1196	1

Figure 3. Isoforms that were not separated by chromatography-IGF1R Y1165/Y1166 or INSR Y1189/Y1190. A. Chromatogram peaks for both phosphopeptides to IGF1R Y1165 or Y1166. These two phosphopeptides could not be distinguished from each other due to the same m/z (mass/charge) and elution times. The MS2 spectrum data (B) does not differentiate between Y1165 or Y1166 based on the y5 ion. To fix this issue, we plan to evaluate only one of the phosphopeptide standards as each signal IGF1R activity.

Functional screen identifies kinases driving prostate cancer visceral and bone metastasis

Claire M. Faltermeier[a], Justin M. Drake[b,1], Peter M. Clark[b], Bryan A. Smith[b], Yang Zong[c], Carmen Volpe[d], Colleen Mathis[b], Colm Morrissey[e], Brandon Castor[f], Jiaoti Huang[f,g,h,i,j], and Owen N. Witte[a,b,c,h,i,j,2]

[a]Molecular Biology Institute, University of California, Los Angeles, CA 90095; [b]Department of Microbiology, Immunology and Molecular Genetics, University of California, Los Angeles, CA 90095; [c]Howard Hughes Medical Institute, University of California, Los Angeles, CA 90095; [d]Division of Laboratory and Animal Medicine, University of California, Los Angeles, CA 90095; [e]Department of Urology, University of Washington, Seattle, WA 98195; [f]Department of Pathology and Laboratory Medicine, University of California, Los Angeles, CA 90095; [g]Department of Urology, University of California, Los Angeles, CA 90095; [h]Jonsson Comprehensive Cancer Center, University of California, Los Angeles, CA 90095; [i]David Geffen School of Medicine, University of California, Los Angeles, CA 90095; and [j]Eli and Edythe Broad Center of Regenerative Medicine and Stem Cell Research, University of California, Los Angeles, CA 90095

Contributed by Owen N. Witte, November 4, 2015 (sent for review September 17, 2015; reviewed by Theresa Guise and John T. Isaacs)

Mutationally activated kinases play an important role in the progression and metastasis of many cancers. Despite numerous oncogenic alterations implicated in metastatic prostate cancer, mutations of kinases are rare. Several lines of evidence suggest that nonmutated kinases and their pathways are involved in prostate cancer progression, but few kinases have been mechanistically linked to metastasis. Using a mass spectrometry-based phosphoproteomics dataset in concert with gene expression analysis, we selected over 100 kinases potentially implicated in human metastatic prostate cancer for functional evaluation. A primary in vivo screen based on overexpression of candidate kinases in murine prostate cells identified 20 wild-type kinases that promote metastasis. We queried these 20 kinases in a secondary in vivo screen using human prostate cells. Strikingly, all three RAF family members, MERTK, and NTRK2 drove the formation of bone and visceral metastasis confirmed by positron-emission tomography combined with computed tomography imaging and histology. Immunohistochemistry of tissue microarrays indicated that these kinases are highly expressed in human metastatic castration-resistant prostate cancer tissues. Our functional studies reveal the strong capability of select wild-type protein kinases to drive critical steps of the metastatic cascade, and implicate these kinases in possible therapeutic intervention.

kinases | metastasis | prostate cancer | bone metastasis

Metastatic prostate cancer is responsible for the deaths of ~30,000 men in the United States each year (1, 2). Ninety percent of patients develop bone metastases, and other major sites of metastases include lymph nodes, liver, adrenal glands, and lung (3). First-line treatments for metastatic disease are androgen deprivation therapies that block androgen synthesis or signaling through the androgen receptor (AR) (2). Inevitably, metastatic prostate cancer becomes resistant to androgen blockade. Second-line treatments such as chemotherapy (docetaxel, cabazitaxel) and radiation only extend survival 2–4 mo (4, 5).

Identifying new therapeutic targets for metastatic prostate cancer has proven difficult. Exome and whole-genome sequencing of human metastatic prostate cancer tissues have found frequent mutations and/or chromosomal aberrations in numerous genes, including *AR*, *TP53*, *PTEN*, *BRCA2*, and *MYC* (6–11). The precise functional contribution of these genes to prostate cancer metastasis remains unknown. Genomic and phosphoproteomic analyses have also revealed that metastatic prostate cancer is molecularly heterogeneous, which has complicated the search for common therapeutic targets (12). Few murine models of prostate cancer develop metastases. Mice having prostate-specific homozygous deletions in *SMAD4* and *PTEN* or expression of mutant *KRAS* develop metastases in visceral organs but rarely in bone (13–15).

Targeting genetically altered constitutively active protein kinases such as BCR-ABL in chronic myelogenous leukemia and $BRAF^{V600E}$ in melanoma has led to dramatic clinical responses (16). Although numerous oncogenic alterations have been identified in prostate cancer, DNA amplifications, translocations, or other mutations resulting in constitutive activity of kinases are rare (6, 9, 17). Genome sequencing of metastatic prostate cancer tissues from >150 patients found translocations involving the kinases BRAF and CRAF in <1% of patients (8, 18). Although uncommon, these genomic aberrations cause enhanced BRAF and CRAF kinase activity and suggest that kinase-driven pathways can be crucial in prostate cancer. Multiple lines of evidence indicate that nonmutated kinases may contribute to prostate cancer progression, castration resistance, and metastasis. SRC kinase synergizes with AR to drive the progression of early-stage prostatic intraepithelial neoplasia to advanced adenocarcinoma (19). SRC, BMX, and TNK2 kinases promote castration resistance by phosphorylating and stabilizing AR (20–22). Moreover, FGFR1, AKT1, and EGFR kinases activate pathways in prostate cancer cells to drive epithelial-to-mesenchymal transition and angiogenesis, both of which are key steps in metastasis (23–25). Despite the strong evidence implicating kinases in advanced prostate cancer, a systematic analysis of the functional role of kinases in prostate cancer metastasis has been lacking.

Metastasis of epithelial-derived cancers encompasses a complex cascade of steps, including (*i*) migration and invasion through

Significance

Therapies are urgently needed to treat metastatic prostate cancer. Mutationally activated and wild-type kinases such as BCR-ABL and BTK are effective therapeutic targets in multiple cancers. Genetically altered kinases are rare in prostate cancer. Wild-type kinases may be implicated in prostate cancer progression, but their therapeutic potential in metastatic prostate cancer remains unknown. Using phosphoproteomics and gene expression datasets, we selected 125 wild-type kinases implicated in human prostate cancer metastasis to screen for metastatic ability in vivo. The RAF family, MERTK, and NTRK2 drove prostate cancer bone and visceral metastasis and were highly expressed in human metastatic prostate cancer tissues. These studies reveal that wild-type kinases can drive metastasis and that the RAF family, MERTK, and NTRK2 may represent important therapeutic targets.

Author contributions: C.M.F. and O.N.W. designed research; C.M.F., J.M.D., P.M.C., B.A.S., Y.Z., C.V., and C. Mathis performed research; C. Morrissey and B.C. contributed new reagents/analytic tools; C.M.F., P.M.C., J.H., and O.N.W. analyzed data; and C.M.F. and O.N.W. wrote the paper.

Reviewers: T.G., Indiana University; and J.T.I., Johns Hopkins Oncology Center.

The authors declare no conflict of interest.

Freely available online through the PNAS open access option.

[1]Present address: Rutgers Cancer Institute of New Jersey and Department of Medicine, Rutgers-Robert Wood Johnson Medical School, New Brunswick, NJ 08901.

[2]To whom correspondence should be addressed. Email: owenwitte@mednet.ucla.edu.

This article contains supporting information online at www.pnas.org/lookup/suppl/doi:10.1073/pnas.1521674112/-/DCSupplemental.

surrounding stroma/basement membrane, (*ii*) intravasation and survival in circulation/lymphatics, (*iii*) extravasation through the vasculature, and (*iv*) survival and growth at a secondary site (26). With the exception of genetically engineered mouse models, no single experimental assay can model all steps of the metastatic cascade. As a result, most screens for genes involved in metastasis have focused on testing one step of the cascade. The migration/invasion step of metastasis is commonly interrogated in vitro by determining the ability of cells to invade through small pores in a membrane (27–29). Genes that function in other steps, or those dependent on the in vivo microenvironment to promote metastasis, are likely to be overlooked in these screens.

Multiple groups have performed in vivo screens for regulators of metastasis by manipulating cell lines in vitro with shRNA libraries or using genome editing techniques, and injecting cells either subcutaneously or into the tail vein of mice (30, 31). These methods are advantageous, because they interrogate multiple steps of the metastatic cascade (survival in circulation, extravasation, and colonization and growth at a secondary site) in a physiologically relevant environment. However, the majority of in vivo screens conducted so far have been based on loss-of-function genetics. These screens are limited to inhibiting the function of proteins expressed by a particular cell line. Using a gain-of-function in vivo screen, we sought to identify kinases that activate pathways leading to prostate cancer metastasis.

Results

Identifying Potential Metastasis-Promoting Kinases Using an Integrated Approach Combining Genomic/Transcriptomic, Phosphoproteomic, and Literature Data. The human kinome encodes over 500 kinases, many of which likely have a limited role in prostate cancer. We reasoned our results would have more relevance if we screened only kinases with evidence of enhanced expression and/or activity in human metastatic prostate cancer. Because no single analysis is both accurate and comprehensive in predicting relevant kinases, three different data sources were investigated. The database cBioPortal contains multiple genomic/transcriptomic datasets from patients with metastatic prostate cancer (6, 9, 32). Five hundred and five kinases were queried for increased RNA expression or genomic amplification in >10% of metastatic patient samples. From this analysis 54 kinases were identified (Table S1). However, high mRNA expression or genomic amplification of a kinase does not always correlate with kinase activity. Identification of phosphorylated kinases or their substrates by phosphoproteomics can better predict kinase activity. Analysis of our previously published phosphoproteomics dataset (33) identified 52 additional kinases with enriched activity in metastatic samples in comparison with benign or localized prostate cancer. Previously published functional studies also provide strong evidence of kinase activity. Searching PubMed using the terms "kinase," "prostate cancer," "metastasis," and "castration resistance" followed by prioritization of articles based on strength of functional data yielded an additional 19 kinases. Our selection method provided 125 kinases for further interrogation of their metastasis-promoting ability (Fig. 1 and Table S1).

Development of an in Vivo Lung Colonization Screen. We devised an in vivo lung colonization screen to test the metastasis-promoting ability of the 125 candidate kinases. A gain-of-function screening design was chosen given our interest in testing whether enhanced expression of a kinase is sufficient to drive metastasis. Additionally, it is unlikely that all 125 kinases are expressed in any single prostate cell line for loss-of-function studies.

Kinases were cloned into a lentiviral expression vector and stably overexpressed in Cap8 cells derived from PTEN null mice (34) (Fig. S1). Cap8 cells have minimal to no metastatic ability in vivo but metastasize when overexpressing a mutationally activated kinase, SRC^{Y529F} (Fig. S2). A luciferase reporter vector was also expressed in Cap8 cells to monitor their metastatic behavior in vivo by bioluminescence imaging (BLI).

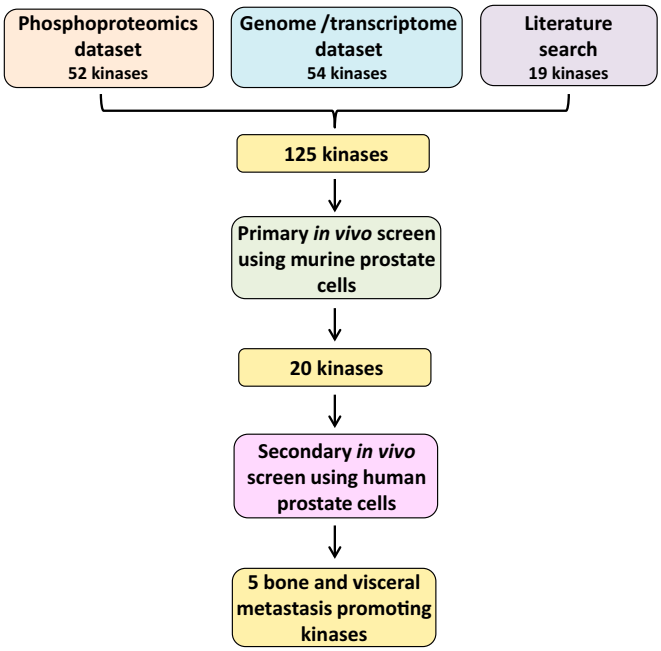

Fig. 1. Schematic summary of the screen for metastasis-promoting kinases. One hundred twenty-five candidate kinases were identified from a combination of genomic/transcriptomic, phosphoproteomic, and literature data. The primary screen entailed expressing all 125 kinases individually in a murine cell line followed by tail vein injection of cells into recipient mice. Twenty kinases strongly promoted lung colonization in vivo. The 20 kinases identified in the primary screen were subjected to a secondary in vivo screen using human prostate cells. Five kinases promoted bone and visceral metastasis in the human cell context.

Testing all 125 kinases as a "pool" in a single mouse would bias our screen toward kinases that are rapid inducers of metastatic colonization. Instead, we decided to test groups of five kinases per mouse to enable identification of kinases with varied metastatic potencies. Groups were selected by choosing five kinases with different molecular weights. Cap8 cells were stably transduced with individual kinases to make 125 different Cap8-kinase cell lines. Equal numbers of five different Cap8-kinase cell lines were pooled and injected into the tail vein of immunocompromised CB17 mice. Because all kinases were cloned with a V5 C-terminal tag (Fig. S1), the metastasis-promoting kinase in each group could be identified by Western blot analysis of the metastatic tissue with a V5 antibody (Fig. 2*A*).

In Vivo Colonization Screen Identifies 20 Kinases That Promote Metastasis in Murine Prostate Cancer Cells. From our screen of 125 kinases, we identified 20 kinases that promoted lung metastasis in vivo (Fig. 2 *B*–*D*). The most rapid detection of metastasis occurred 2 wk after injection, and was attributed to kinases NTRK2 and MAP3K8. Kinases MAP3K15, MERTK, and all members of the RAF family of kinases (ARAF, BRAF, and CRAF) drove the formation of significant lung metastasis within 3 wks. Kinases promoting metastasis but having a longer latency included FGFR1 (6 wk), SRC (6 wk), and BMX (7 wk) (Figs. 2*D* and 3*A*). Both FGFR1 and SRC have previously described roles in prostate cancer metastasis, which provides support for the validity of our screen (35, 36). Several small lung nodules were recovered at necropsy in 2/5 control mice after 10 wk (Fig. S3*B*). Albeit weak, the inherent metastatic ability of Cap8 cells in our model system implies that the 20 kinases identified are "enhancers of metastasis." It is still unclear whether they are actually "drivers" of de novo metastasis.

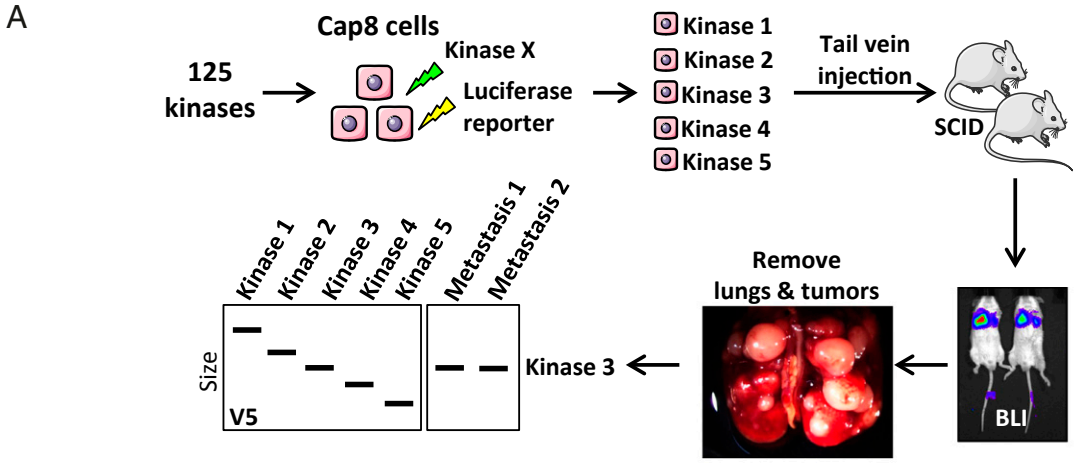

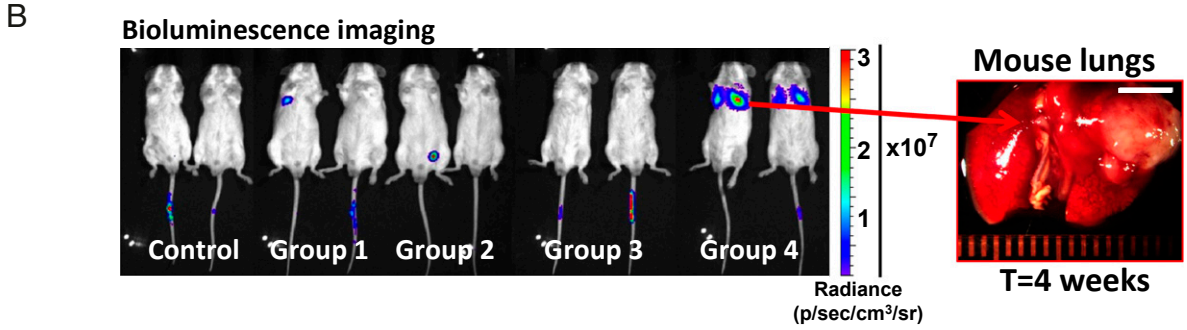

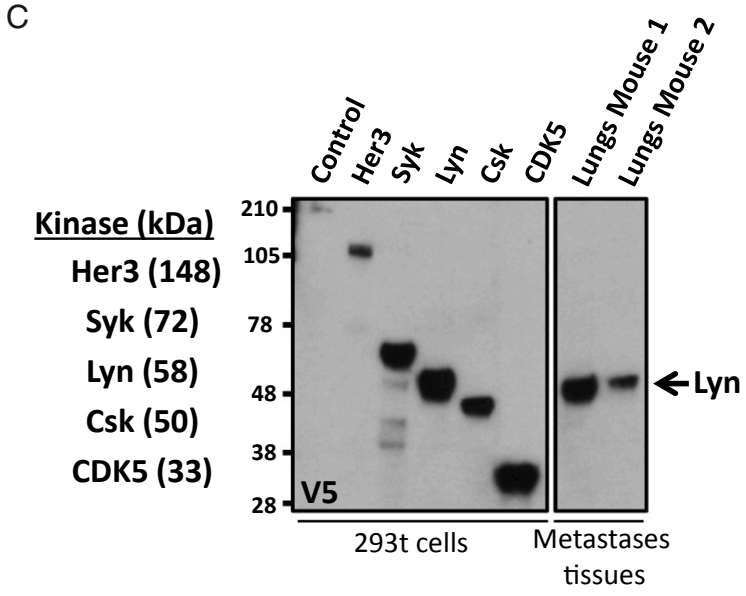

D

Kinase	Latency (weeks)	Kinase	Latency (weeks)
MAP3K8	2	MAP3K2	4
NTRK2	2	NTRK3	4
ARAF	3	PIK3Ca	4
BRAF	3	EGFR	5
CRAF	3	EPHA2	5
MAP3K15	3	HER2	5
MERTK	3	PDGFRa	5
FGFR3	4	FGFR1	6
FLT3	4	SRC	6
LYN	4	BMX	7

Fig. 2. In vivo screen of 125 candidate kinases identifies 20 kinases with metastasis-promoting ability when expressed in murine prostate cells. (*A*) Schematic diagram of the screen testing the metastatic ability of 125 kinases. Kinases were expressed individually in Cap8 cells, pooled into groups of five kinases (each with a different molecular weight), and injected into the tail vein of CB17 SCID mice. Bioluminescence imaging (BLI) was used to detect metastases that were subsequently removed for Western blot analysis. Because all kinases have a C-terminal V5 tag, the Western blot was probed with a V5 antibody to determine which size kinase was enriched in the metastasis tissues. (*B*) Composite BLI image of four different groups of mice. BLI images for each group were taken separately, but at the same time point. Each group was injected with a different set of five kinases. Corresponding bright field image of lungs removed from one of the group 4 mice is shown. sr noted in the units for radiance and refers to steradian. (Scale bar, 5 mm.) (*C*, *Left*) Names and molecular weights of five kinases in a representative group. Western blot analysis of 293t cells overexpressing kinases demonstrates that kinases can be differentiated by size using a V5 antibody. (*C*, *Right*) Western blot of lung tumors removed from mice injected with Cap8 cells overexpressing a group of kinases. By size alignment, the kinase enriched in the metastatic tissue from this particular group was identified as Lyn. (*D*) List of kinases identified in the primary lung colonization screen. Latency columns refer to the interval of time (in weeks) between time of injection and time at which metastatic burden detected by BLI and/or physical symptoms necessitated euthanasia.

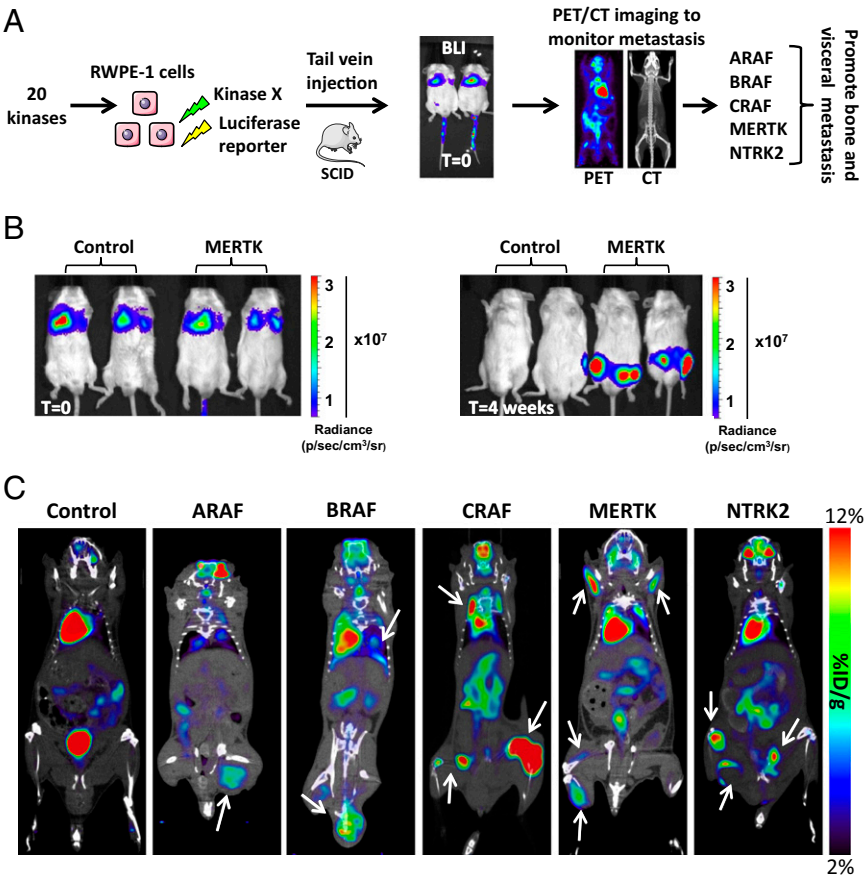

Kinase	Mice	Bone & visceral	Visceral only	No mets	Latency range (M)	Avg. latency (M)	Bone tumor burden
ARAF	8	7	1	0	2-6	4.3	Small
BRAF	4	2	1	1	4-5	4.5	Small
CRAF	6	4	1	1	1-4	2.5	Large
MERTK	6	5	0	1	2-5	3.0	Large
NTRK2	6	4	2	0	2-6	3.3	Large

Fig. 3. Screen of 20 kinases in human prostate cells identifies 5 kinases that drive bone and visceral metastasis. (*A*) Schema of the secondary screen. The 20 kinases identified in the primary screen were expressed in human prostate cells (RWPE-1 cells) and injected into the tail vein of mice. Immediately postinjection, mice were imaged by BLI to verify proper injection. Mice were monitored for metastasis by PET/CT imaging. (*B*) Representative BLI of mice injected with control or MERTK-expressing cells. At time (T) = 0, luciferase signal was detected in the lungs and, by T = 4 wk, luciferase signal was detected in the hind legs. (*C*) PET/CT images of mice injected with control cells or cells expressing the kinases ARAF, BRAF, CRAF, MERTK, and NTRK2. White arrows indicate anatomical sites of high glycolytic activity corresponding to sites of tumor growth. Scale bar on right corresponds to percent injected dose (ID) per gram (g) of tissue. (*D*) Table summarizing the outcomes of tail vein injections of RWPE-1 cells overexpressing ARAF, BRAF, CRAF, MERTK, and NTRK2. Listed are the number of mice tested per kinase, sites of metastatic colonization ("bone & visceral" or "visceral only"), latency (time point at which metastatic burden necessitated euthanasia), and tumor burden. The anatomical sites classified as visceral were lungs and lymph nodes. avg., average; M, month; mets, metastasis.

Screening in Human Prostate Cells Identifies Five Kinases That Drive Bone and Visceral Metastasis in Vivo. To identify which of the 20 candidate kinases drive rather than enhance metastasis in a human cell context, we next assayed their ability to promote metastasis when overexpressed in nonmalignant human prostate cells. The RWPE-1 cell line is derived from normal human prostate epithelium and immortalized with HPV-18 E6/E7 oncogenes (37). RWPE-1 cells do not form colonies in soft agar, nor are they tumorigenic in nude mice (37).

RWPE-1 cells expressing a luciferase reporter gene were separately infected with lentiviruses expressing each of the 20 kinases. Each kinase cell line was individually injected into the tail vein of NOD scid gamma (NSG) mice (Fig. 3*A*). Following tail vein injection, most cells are assumed to get lodged in the small capillaries of the lung rather than travel through the systemic circulation (38). This assumption is consistent with the BLI of mice conducted immediately after injection, showing tumor cells in the lungs but not in other anatomical sites (Fig. 3*B*).

Strikingly, mice injected with cells overexpressing the kinases MERTK, ARAF, BRAF, CRAF, and NTRK2 did not show symptoms of lung metastasis but rather developed hind leg weakness. Mice injected with CRAF-, MERTK-, and NTRK2-expressing RWPE-1 cells were the first to show symptoms 1–2 mo postinjection. A longer latency of up to 6 mo was observed in mice injected with cells expressing ARAF and BRAF. Using BLI, signal was detected in the hind legs (Fig. 3*B*). Although BLI is extremely sensitive, it lacks the precision to accurately predict the location of a metastasis, especially when signal is outside the lungs. Positron-emission tomography combined with computed tomography (PET/CT) is tissue depth-independent and enables precise identification of tumor localization based on cancer cell metabolic activity (39). PET/CT imaging of mice injected with cells expressing MERTK, ARAF, BRAF, CRAF, and NTRK2 showed high [^{18}F]FDG accumulation in the bones, lungs, and lymph nodes (Fig. 3*C*). Control mice were negative for [^{18}F]FDG accumulation in all corresponding anatomical sites (Fig. 3*C*). Further assessment of the CT scans suggested that the bone metastases in mice injected with cells expressing MERTK, ARAF, BRAF, CRAF, and NTRK2 are likely osteolytic.

Histological evaluation of tissues confirmed tumor cell colonization of the lungs, lymph nodes, and bone (femur, tibia, ilium, and vertebra) (Fig. 4 and Figs. S4 and S5). The RAF family members and NTRK2 drove the formation of lung and lymph node metastasis with a similar incidence, whereas MERTK-overexpressing cells did not colonize the lungs (Fig. 3*D*). Although not quantitative,

we observed by histology that metastases driven by CRAF, MERTK, and NTRK2 were extensive, with tumor cells often replacing large areas of bone marrow in the long bones, pelvis, and spine (Figs. 3*D* and 4). In contrast, small metastatic deposits were observed in the femur and spine of mice injected with cells expressing ARAF and BRAF (Fig. 4). To verify that each metastasis expressed the respective kinase and originated from human RWPE-1 cells, bone tissue sections underwent immunohistochemical (IHC) analysis for kinases (MERTK, ARAF, BRAF, CRAF, and NTRK2), HLA, prostate-specific antigen (PSA), and the epithelial cell marker E-cadherin. As shown in Fig. 4, strong IHC staining of each respective kinase, HLA, E-cadherin, and PSA was detected in all bone metastases.

After 8 mo, mice injected with RWPE-1 cells expressing PIK3Cα, MAP3K8, FGFR3, and NTRK3 developed lung, lymph node, and bone micrometastases. None of the mice injected with RWPE-1 cells expressing the other 12 kinases developed metastasis assessed by BLI and histology after 9 mo. Altogether, the functional data described indicate that RAF family members, NTRK2, and MERTK have strong metastasis-promoting ability in both human and mouse prostate cell lines and drive the formation of bone metastasis.

MERTK, NTRK2, and RAF Family Members Are Expressed in Human Prostate Cancer Bone and Visceral Metastasis Tissues. ARAF, BRAF, and CRAF were originally selected for the screen based on predicted activity from our human metastatic prostate cancer phosphoproteomics dataset. Due to the sequence similarity of the RAF kinases (40), some common phosphopeptide substrates could be shared by all three RAF family members. Which RAF family members are relevant to human metastatic prostate cancer remains unclear. MERTK and NTRK2 were added to the screen based on evidence of their role in lung (41), melanoma (42), and glioblastoma metastasis (43), but neither kinase has been previously implicated in prostate cancer metastasis.

To seek evidence of the relevance and therapeutic potential of candidate kinases, we evaluated their expression by immunohistochemistry in metastatic, localized, and benign human prostate cancer tissue samples. The University of Washington's Prostate Cancer Rapid Autopsy Program provided tissue microarrays (TMAs) containing 33 different patients' bone and visceral metastases for staining. We also obtained from the University of California, Los Angeles (UCLA), TMAs containing tissue from 115 patients with benign and medium- to high-grade localized prostate cancer (Gleason 7–9). Because an estimated 10% of patients with

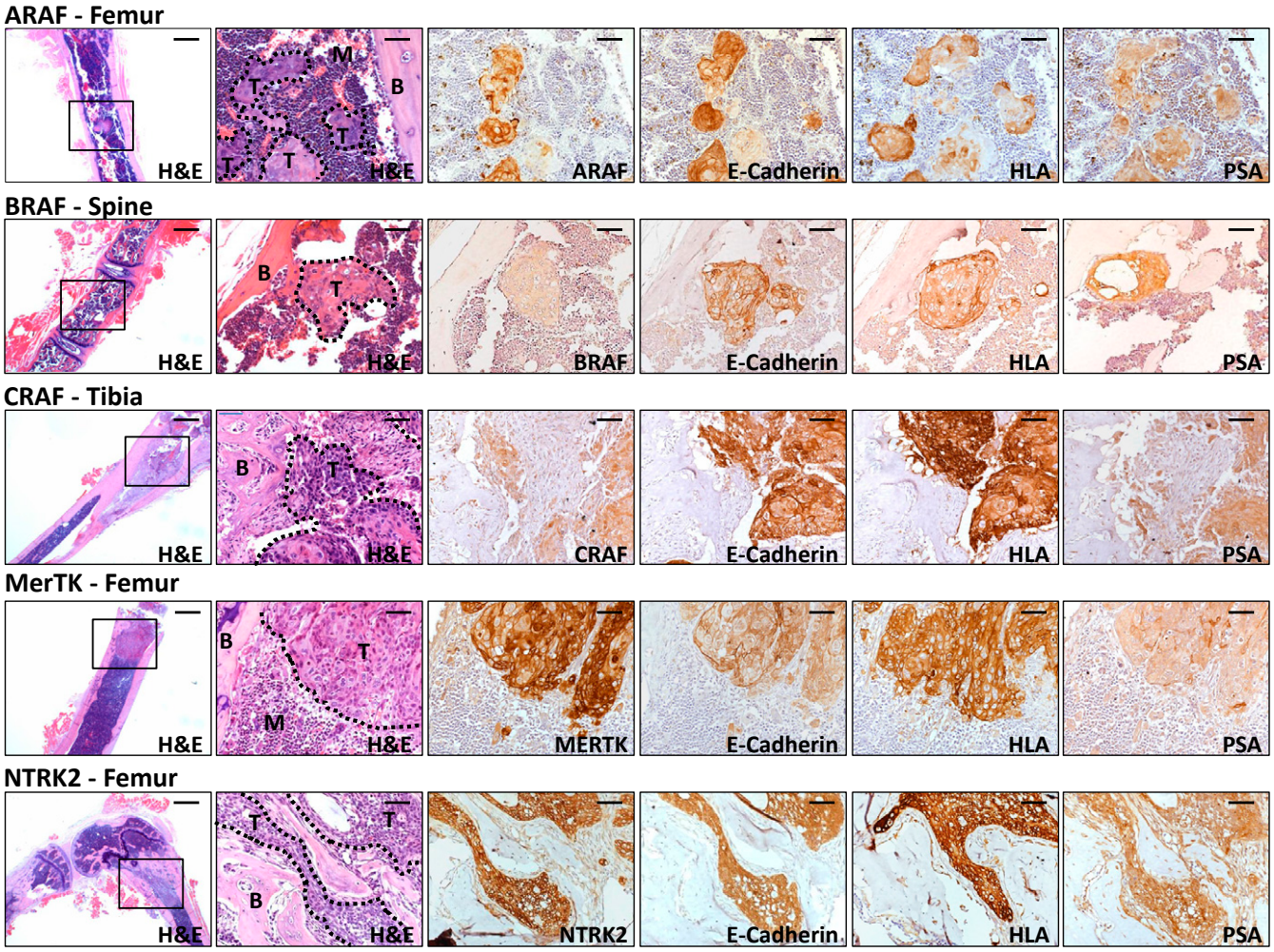

Fig. 4. Histological analysis of bones recovered from mice injected with cells expressing ARAF, BRAF, CRAF, MERTK, and NTRK2 confirms that metastases are of human prostate epithelial cell origin. (*Left* two columns) H&E stains of the affected bones removed from mice injected with RWPE-1 cells expressing the five metastasis-promoting kinases. Images in *Right* five columns are 20× magnification of the area outlined by a black box in the first column. Tumor areas are outlined by black dotted lines and indicated by "T." Bone and bone marrow are marked with "B" and "M," respectively. (*Right* four columns) IHC staining of bone metastasis for overexpressed kinase, E-cadherin, HLA class I, and PSA. [Scale bars, 320 μm (*Left*) and 40 μm (*Right* five columns).]

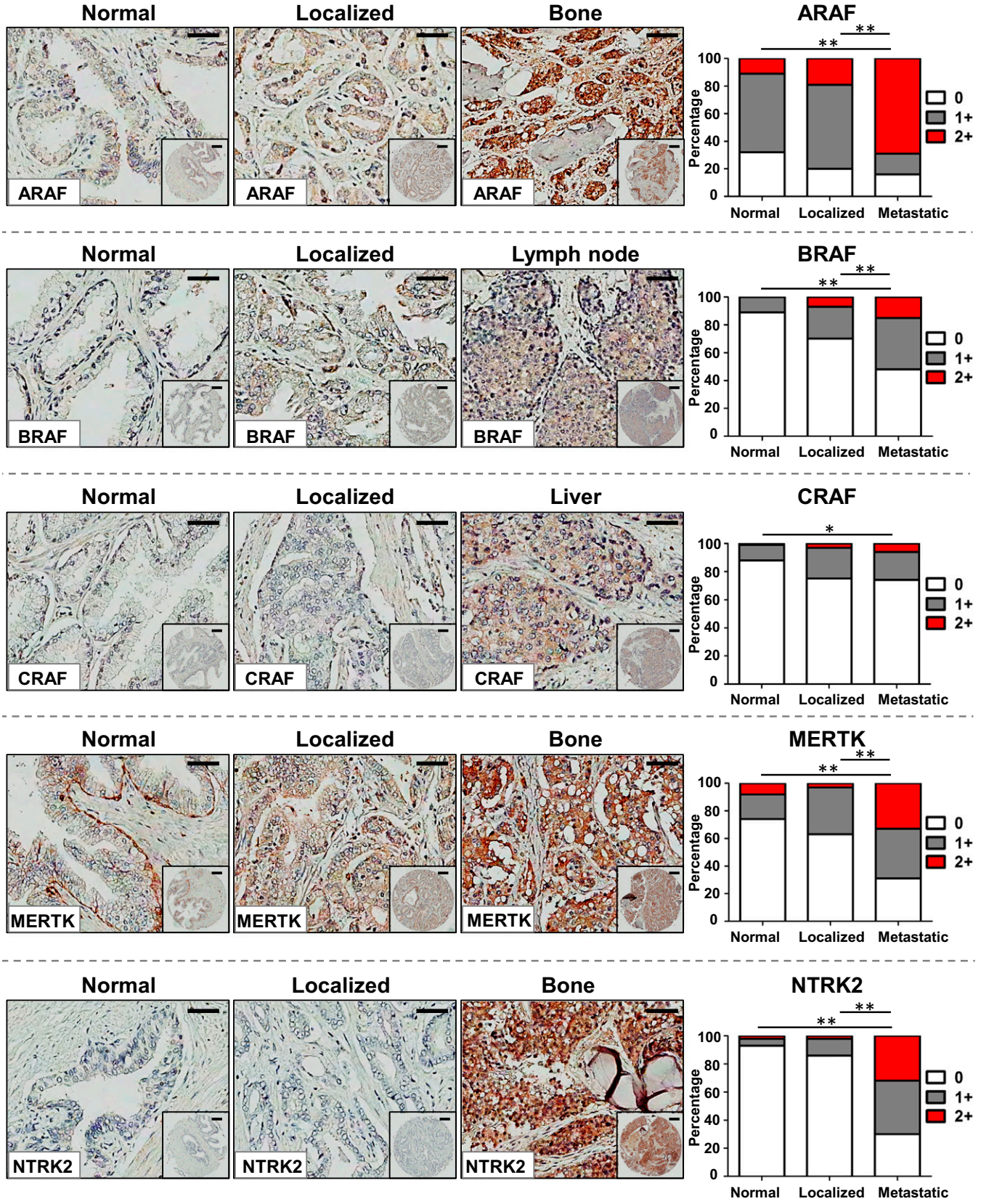

Fig. 5. High levels of the five metastasis-promoting kinases are detected in human prostate cancer metastasis tissues. (*Left*) IHC staining for ARAF, BRAF, CRAF, MERTK, and NTRK2 in representative samples from TMAs containing tissue sections from normal prostate tissue, localized prostate cancer (Gleason 7–9), and metastatic prostate cancer. [Scale bars, 50 μm (large images) and 100 μm (small images).] (*Right*) Quantification of kinase expression in TMAs based on staining intensity. No immunoreactivity was scored as 0, whereas positive immunoreactivity was scored as 1 or 2 based on intensity. The distributions of scores between normal + metastatic tissues and localized + metastatic tissues were subjected to χ^2 statistical analysis. Significance: $^*P \leq 0.05$, $^{**}P \leq 0.01$.

Gleason 7 prostate cancer develop metastasis (44), we hypothesized that the metastasis-promoting kinases would have low expression in the majority of benign and localized prostate cancer tissues in comparison with metastatic prostate cancer tissues.

Consistent with our hypothesis, we found ARAF, BRAF, MERTK, and NTRK2 to be highly expressed in metastatic tissues in comparison with benign or localized prostate cancer tissues (Fig. 5). Remarkably, 69% of metastatic tissues (68/99 samples) had strong ARAF staining (scored as 2+), whereas only 11% of normal (11/102 samples) and 19% of localized prostate cancer tissues (20/105 samples) had ARAF staining of similar intensity. Strong BRAF, MERTK, and NTRK2 staining was detected in 15% (15/100 samples), 33% (32/98 samples), and 32% (31/96 samples) of metastatic tissues, but less than ∼10% of normal and localized prostate cancer tissues were scored 2+ for these three kinases. CRAF-positive staining was higher in metastases (26%, 26/99 samples) in comparison with normal prostate tissue (12%, 11/92 samples). However, no difference in CRAF staining was observed between localized (25%, 24/95 samples) and metastatic prostate cancer. We cannot exclude the possibility that the activation state of CRAF may be different between localized and metastatic prostate cancer samples. Overall, the IHC staining results provide evidence that MERTK, NTRK2, and the RAF family members are expressed and could be functionally relevant in human metastatic prostate cancer. Based on expression, ARAF, BRAF, MERTK, and NTRK2 are more likely to have a functional role in metastasis rather than in early-stage prostate cancer.

Discussion

The strong metastatic ability of RAF family members in our model is consistent with previous reports describing alterations of this pathway in human prostate cancer metastasis. Based on copy number alterations and transcriptome and mutational data, Taylor et al. found that RAS/RAF signaling is dysregulated in 43% of primary tumors and >90% of metastasis (9). Recently, two studies identified BRAF and CRAF fusion proteins with predicted constitutive kinase activity in a small subset (<0.05%) of advanced localized and metastatic prostate cancer tumors (8, 18). We found overexpression of CRAF in the human prostate cell line RWPE-1 to be a more potent driver of bone metastasis (with regard to metastatic burden and time point at which metastases necessitated euthanasia) than ARAF or BRAF. Despite its lower metastatic potency, ARAF expression in human metastatic prostate cancer tissues was much higher than BRAF or CRAF expression. It is possible that ARAF is the dominant RAF family member functioning in human prostate cancer metastasis.

The mechanism by which RAF family members drive metastasis and in particular bone colonization is unknown. Using Madin–Darby canine kidney (MDCK) cells, Lehmann et al. showed that dimerization of CRAF not only induces ERK/MAPK pathway activation but also leads to TGF-β secretion (45). Because the TGF-β signaling pathway is considered one of the key pathways driving prostate cancer bone metastasis (46), CRAF may contribute to metastasis by promoting autocrine TGF-β secretion. Much less is known about the role of ARAF in tumorigenesis, but a recent study showed that ARAF homodimerization or heterodimerization with BRAF enhanced the metastatic ability of lung cancer cells (47).

We also show that MERTK is a potent inducer of prostate cancer metastasis. As a member of the TAM family of tyrosine kinases, MERTK is best-known for its role in promoting phagocytosis of apoptotic cells and dampening the proinflammatory cytokine response (48). MERTK is overexpressed and/or has functional activity in multiple cancers but is rarely genetically amplified or mutated (48). We demonstrate that wild-type MERTK has functional activity in metastasis and is highly expressed in human prostate cancer metastasis tissues. Lending support to our findings are studies demonstrating that MERTK drives migration and invasion in glioblastoma and melanoma cells (42, 43). The downstream pathways activated by MERTK include the RAF/ERK/MAPK, AKT, Stat, and NF-κB pathways (48). Given the metastatic potency of the RAF pathway in our model, MERTK may be dependent on this pathway for its metastatic ability.

NTRK2 and NTRK3, belonging to the neurotrophin family of tyrosine kinases, were also identified in our screen as strong promoters of prostate cancer metastasis. Expression analyses have previously implicated these kinases in prostate cancer. NTRK2 and NTRK3 were undetectable in normal prostate epithelial cells but positive in bone metastasis tissues (49). The precise function of the neurotrophin tyrosine kinases in prostate cancer is unknown. In multiple cancer types, NTRK2 promotes resistance to anoikis (detachment-induced apoptosis), which is a key step in the metastatic cascade (28, 50). Preventing anoikis could be part of the mechanism by which NTRK2 contributes to prostate cancer metastasis.

One of the most interesting features of our metastatic model is the high frequency of metastasis to the lumbar spine, femur, pelvis, and tibia. This bone metastasis pattern is similar to sites of prostate cancer bone metastasis in humans, with the lumbar vertebrae being most common, followed by ribs, pelvis, and long bones (51). Greater than 80% of mice injected with cells overexpressing ARAF (7/8 mice) and MERTK (5/6 mice) developed bone metastasis, whereas BRAF, CRAF, and NTRK2 promoted bone metastasis in at least 50% of mice. In comparison, the few genetically engineered mouse models that develop prostate cancer metastasis have a lower penetrance (12.5–25%) of bone metastases (52–54). Intracardiac or direct bone injection of human prostate cancer cell lines results in a higher frequency of metastasis, but the incidence and location of bone metastasis vary widely between studies (55, 56). The similarities of our model to human prostate cancer and the high frequency of bone metastasis may increase the feasibility of studying the biological mechanisms of prostate cancer bone metastasis. Integrins and chemoattractants such as αVβ3 and SCF1 likely contribute to prostate cancer bone tropism, and our model could provide insights into how certain kinase pathways regulate these bone homing factors (57, 58).

Our results underscore the potential contribution of wild-type kinases to prostate cancer metastasis and provide rationale for therapeutically targeting MERTK, NTRK2, and RAF family members. Currently, there are no selective Food and Drug Administration (FDA)-approved inhibitors of MERTK or NTRK2. The multikinase inhibitor foretinib inhibits MERTK in addition to c-MET and VEGFR (59). Because c-MET inhibition is effective in some patients with metastatic prostate cancer, targeting both MERTK and c-Met with foretinib may be a promising therapeutic approach (60). Pan-NTRK family member inhibitors are excellent therapeutic candidates for prostate cancer, because they would block the bone metastasis-promoting functions of NTRK2 and NTRK3, and NTRK1-mediated bone pain (61). Sorafenib is an FDA-approved small-molecule inhibitor targeting RAF family members and other kinases such as VEGFR-2, VEGFR-3, and PDGF-β (62). Clinical studies involving a small number of patients have suggested that sorafenib may have therapeutic benefit in patients with castration-resistant prostate cancer (63, 64). Due to reports of paradoxical RAF inhibitor-mediated RAF activation, inhibiting the direct downstream targets of RAF, MEK1/MEK2, may be a better approach (65). Trametinib, an inhibitor of MEK1/MEK2, is currently in phase II clinical trials for patients with advanced prostate cancer (66). Future studies should focus on inhibition of MERTK, NTRK2, and RAF pathways in metastatic models to provide additional rationale for targeting these kinases in patients with metastatic prostate cancer.

Methods

Cell Culture and Reagents. Cap8 cells were obtained from the laboratory of Hong Wu, University of California, Los Angeles (UCLA), and propagated in DMEM supplemented with 10% (vol/vol) FBS (Gibco), 25 μg/mL bovine

pituitary extract (Lonza), 5 μg/mL human insulin (Gibco), 6 ng/mL recombinant human epidermal growth factor (PeproTech), glutamine (1 mM), penicillin (100 U/mL), and streptomycin (100 μg/mL) (34). RWPE-1 cells were purchased from ATCC and cultured in keratinocyte serum-free medium (K-SFM) (Gibco) supplemented with 0.05 mg/mL bovine pituitary extract (Gibco), 5 ng/mL EGF (Gibco), penicillin (100 U/mL), and streptomycin (100 μg/mL). 293t cells used for lentiviral production were cultured in DMEM supplemented with 10% (vol/vol) FBS, glutamine (1 mM), penicillin (100 U/mL), and streptomycin (100 μg/mL).

Cloning of Kinases. We obtained the Center for Cancer Systems Biology–Dana-Farber Cancer Institute–Broad Human Kinase ORF collection consisting of 559 kinases in pDONR-223 Gateway entry vectors. The plasmid kit (Addgene Kit 1000000014) was a gift from William Hahn and David Root, Broad Institute of Harvard and Massachusetts Institute of Technology, Boston. Using the pcDNA 6.2/V5-DEST (Invitrogen), we cloned the attR1-ccdB-CmR-attR2-V5-SV40-blasticidin cassette into the previously described third-generation lentiviral FUCGW vector (67). The FU-R1-R2-V5-SV40-Blasti-CGW vector (Fig. S1) is optimized for our screen based on the V5 tag enabling kinase detection with V5 antibody and selection of kinase-expressing cells using blasticidin. Kinases in pDONR-223 vectors were cloned into FU-R1-R2-V5-SV40-Blasti-CGW using LR Clonase II (Invitrogen) and sequenced to verify the wild-type sequence. Wild-type BRAF and RPS6KA4 were not included in the ORF kinase collection. We acquired these ORFs from the Harvard PlasmID Repository and subcloned them into the FUCGW vector.

Virus Production. Third-generation lentiviruses were prepared by calcium phosphate precipitation transfection of 293t cells with plasmids expressing kinases (FU-kinase-V5-SV40-Blasti-CGW) or luciferase (FU-ILYW). The lentiviruses were prepared as described (67).

Western Blot. Whole-cell lysates were prepared in RIPA lysis buffer (150 nM NaCl, 1% Nonidet P-40, 0.5% sodium deoxycholate, 0.1% SDS, 50 mM Tris, pH 8.0) with phosphatase inhibitor (cocktails 2 and 3; Sigma) and protease inhibitor cocktail (Roche). Equal amounts of protein were separated by 4–20% (mass/vol) Tris-Hepes SDS/PAGE (Thermo Fisher), followed by immunoblotting analysis with the indicated antibodies.

Kinase protein expression was detected using a V5 antibody (Invitrogen R960-25; 1:2,500). Because AXL and BRAF lacked a V5 tag, we verified their expression using an AXL antibody (Cell Signaling 4977; 1:1,000) and a BRAF antibody (Cell Signaling 55C6; 1:1,000).

Animal Studies. All animal experiments were performed according to the protocol approved by the Division of Laboratory Medicine at the University of California, Los Angeles. NOD.CB17-Prkdc^{scid}/J mice (for the primary screen) and NOD-scid gamma (for the secondary screen) were purchased from Jackson Laboratories. For all experiments, male mice between 6 and 8 wk of age were used.

Primary in Vivo Kinase Screen.

Infection of cells and tail vein injections. Cap8 cells were infected with lentivirus expressing luciferase and YFP (FU-ILYW) at a multiplicity of infection (MOI) of 10. Three days later, cells were sorted based on YFP expression using a BD FACSAria. Cap8-ILYW cells were expanded and frozen in aliquots so that all experiments would start at the same cell passage number. Upon starting an experiment, Cap8-ILYW cells were thawed and propagated for 5 d followed by infection with kinases individually at an MOI of 8 in media containing polybrene (8 μg/mL). Twenty-four hours after infection, media was removed and replaced with media containing 13 μg/mL blasticidin (InvivoGen). Cells underwent blasticidin selection for 5 d, followed by propagation for 48 h in complete media (without blasticidin). Instead of screening 125 kinases individually in vivo, we tested groups of 5 kinases in each mouse. Five kinases with different molecular weights were selected for each group. Each group was prepared by counting 2×10^5 cells of each of the five kinase cell lines and pooling the kinase cell lines together in 200 μL HBSS (Life Technologies). Using a 27-G needle, 200 μL (1×10^6 total cells) was injected into the lateral tail vein of CB17 mice in duplicate. D-luciferin substrate was injected i.p. into mice, followed by BLI to verify proper tail vein injection of kinase-expressing Cap8-ILYW cells (indicated by luciferase signal in the lungs). Mice were monitored for physical symptoms of metastasis (labored breathing, cachexia, difficulty moving) and by biweekly BLI. Upon detection of metastasis, mice were euthanized and lung tumors were dissected and stored at −80 °C.

Identification of metastasis-promoting kinase. Lung tumors were thawed, homogenized, and sonicated in RIPA lysis buffer. After a high-speed spin, protein concentration of the supernatant was measured in preparation for Western blotting. Because all kinases had a V5 C-terminal tag, the Western blot was probed with a V5 antibody to determine which size kinase was enriched in the metastasis tissues. To aid in identifying the enriched kinase, we included on our Western blot lysate from 293t cells expressing the five kinase cell lines individually. This Western blot was used as a reference of the individual kinase sizes. For the majority of the metastasis tissues analyzed by Western blot, only one out of the five kinases was enriched. If >1 kinase was identified in the metastasis tissues by Western blot, tail vein injections using cell lines expressing each of the kinases were repeated.

Secondary in Vivo Kinase Screen.

Infection of cells and tail vein injections. The same infection method described for the primary screen was used to transduce RWPE-1 cells with a lentivirus expressing luciferase followed by lentiviruses expressing the 20 kinases (identified in the primary screen). RWPE-1 cells expressing kinases were selected with 15 μg/mL blasticidin for 5 d and prepared for tail vein injection following the method described for the primary screen. However, instead of screening 5 kinases at a time, the 20 kinases were tested individually. Kinase-expressing RWPE-1 cells (1×10^6) were injected into the lateral tail vein of NSG mice in duplicate. D-luciferin substrate was injected i.p. into mice, followed by BLI to verify proper tail vein injection. Mice were monitored for physical symptoms of metastasis and by biweekly BLI. Upon symptom detection or positive BLI signal, mice underwent PET/CT imaging and were euthanized the following day. Macroscopic tumors and bones were removed and prepared for histology. Three biological replicates were performed for each of the five kinases (ARAF, BRAF, CRAF, NTRK2, and MERTK).

Imaging.

Bioluminescence imaging. BLI was conducted using an IVIS Lumina II (PerkinElmer). D-luciferin (150 mg/kg) was injected intraperitoneally. After 15 min, anesthetized mice [using 2.5% (vol/vol) isoflurane] were imaged. BLI analysis was performed using Living Image software, version 4.0 (PerkinElmer).

PET imaging. Mice were placed on a heated platform and anesthetized with 1.5% (vol/vol) isoflurane for the entirety of the experiment. Approximately 740 kBq of ^{18}F-labeled 2-fluoro-2-deoxyglucose ([^{18}F]FDG; obtained from the UCLA Department of Nuclear Medicine) was injected into the tail vein. After 1 h, the mice were imaged for 10 min on a Genisys 4 imager (Sofie Biosciences) followed by a high-resolution computed tomography scan on a CrumpCAT imager (UCLA).* PET and CT images were manually coregistered. Images were analyzed using AMIDE medical imaging software (68).

Immunohistochemistry. Metastatic tissues were removed from the mice and fixed in 10% (vol/vol) formalin overnight and paraffin-embedded. Bones were decalcified before paraffin embedding. Four-micrometer-thick sections were stained with hematoxylin and eosin for representative histology. For IHC analysis of TMAs, sections were heated at 65 °C for 1 h followed by deparaffinization in xylene and rehydration in 100%, 95%, and 70% (vol/vol) ethanol. Antigen retrieval was performed by heating samples at 95° for 20 min in 0.01 M citrate buffer (pH 6.0). Endogenous peroxidase activity was blocked with 3% (vol/vol) H_2O_2 for 10 min, followed by blocking for nonspecific binding with 2.5% (vol/vol) horse serum (Vector Laboratories) for 1 h. Primary antibodies (see below) were diluted in 2.5% (vol/vol) horse serum and incubated on slides overnight at 4 °C. Following three washes with 1× PBS, slides were incubated with anti-mouse HRP or anti-rabbit HRP secondary antibodies (Dako) for 1 h at 25 °C. Slides were developed using the liquid DAB+ Substrate Chromogen System (Dako), counterstained with hematoxylin, dehydrated, and mounted.

MERTK protocol. IHC staining for MERTK was conducted as described (69). Briefly, we followed the same primary antibody protocol as described above, but to increase the sensitivity of MERTK staining we used a biotinylated secondary antibody (goat anti-rabbit IgG; Boster Biotechnology), followed by peroxidase-conjugated streptavidin (SABC; SA1022; Boster Biotechnology). The slide development protocol was followed as described above.

Antibodies. The following primary antibodies and dilutions were used: E-cadherin (BD clone 36; 1:250), PSA (Dako; 1:2,000), HLA class I ABC (Abcam 70328; 1:350), ARAF (Abcam 200653; 1:700), BRAF (Cell Signaling 55C6; 1:100), CRAF (Cell Signaling 9422; 1:100), MERTK (Abcam 52968; 1:300), and NTRK2 (Cell Signaling 4607; 1:250). Dilutions were optimized on sections using metastatic tissues recovered from mice injected with RWPE-1 cells overexpressing each kinase. To ensure specificity and lack of cross-reactivity of RAF family member antibodies, we stained ARAF-overexpressing tissue with BRAF and CRAF antibodies, BRAF-overexpressing tissue with CRAF and ARAF antibodies, and CRAF-overexpressing tissue with ARAF and BRAF antibodies.

*Taschereau R, Vu NT, Chatziioannou AF, 2014 Institute of Electrical and Electronics Engineers Nuclear Science Symposium & Medical Imaging Conference, November 8–15 2014, Seattle, WA.

Clinical Prostate Tissue Microarrays.

Human metastatic prostate cancer tissue microarrays.

Tissue acquisition. Samples were obtained from patients who died of metastatic castration resistant prostate cancer (CRPC) and who signed written informed consent for a rapid autopsy performed within 6 h of death, under the aegis of the Prostate Cancer Donor Program at the University of Washington (70). The Institutional Review Board of the University of Washington approved this study. Visceral metastases were identified at the gross level, bone biopsies were obtained according to a template from 20 different sites, and metastases were identified at a histological level.

Tissue microarray construction. One hundred and three CRPC metastases (including 45 visceral metastases and 58 bone metastases) from 33 autopsy patients (up to four sites per patient) were fixed in buffered formalin [bone metastases were decalcified in 10% (vol/vol) formic acid] and embedded in paraffin. A TMA was made using duplicate 1-mm-diameter cores from these tissues.

Human benign prostate and localized prostate cancer tissue microarrays. Construction of TMAs was approved by UCLA's Institutional Review Board. Samples were obtained from prostatectomy specimens performed at UCLA between 2001 and 2010. A total of 115 cases of high-grade prostate adenocarcinoma (combined Gleason score 7–9) were selected. Three cores of tumor and three cores of corresponding benign prostate were obtained from each case and transferred to two recipient TMA blocks.

Scoring of TMAs. TMAs were scored 0, 1, and 2 based on intensity of staining, with 0 indicating no staining, 1 indicating weakly positive staining, and 2 indicating strongly positive staining. Two separate observers scored normal prostate, localized prostate cancer, and metastatic prostate cancer TMAs. TMAs and corresponding scores were reviewed by a board-certified pathologist. Because MERTK is expressed in normal human prostate basal cells and in macrophages, scores for MERTK were based on expression only in luminal cells. Representative images of TMAs were taken using a Zeiss Axio Imager A1 microscope. To optimize TMA images for print (Fig. 5), PowerPoint was used to equally adjust all images using the following parameters: sharpen (+25%), brightness (–33%), and contrast (+66%).

ACKNOWLEDGMENTS. We thank members of the O.N.W. laboratory for helpful comments and discussion. We are grateful to the patients and their families who were willing to participate in the University of Washington's Prostate Cancer Donor Program and the investigators Drs. Robert Vessella, Celestia Higano, Bruce Montgomery, Evan Yu, Peter Nelson, Paul Lange, Martine Roudier, and Lawrence True and the Rapid Autopsy team for their contributions to the University of Washington Medical Center Prostate Cancer Donor Rapid Autopsy Program. This research was supported by funding from the Pacific Northwest Prostate Cancer Specialized Program of Research Excellence (SPORE) (P50CA97186) and a P01 NIH grant (P01CA085859). We thank Dr. Daniel Margolis for radiological evaluation of PET/CT scans; UCLA Molecular Imaging Center and staff; H. Wu laboratory for cell lines; UCLA Translational Pathology Core Laboratory for assistance with tissue processing and H&E staining; and Donghui Cheng for help with FACS sorting. C.M.F. was supported by a California Institute of Regenerative Medicine Training Grant (TG2-01169) and USHHS Ruth L. Kirschstein Institutional National Research Service Award (T32 CA009056); J.M.D. was supported by the Department of Defense Prostate Cancer Research Program (W81XWH-14-1-0148); P.M.C. was supported by a California Institute of Regenerative Medicine Training Grant (TG2-01169), UCLA Scholars in Oncologic Molecular Imaging Program National Cancer Institute Grant (R25T CA098010), and UCLA in Vivo Cellular and Molecular Imaging Center Career Development Award (P50 CA086306); and B.A.S. was supported by a UCLA Tumor Immunology Training Grant (T32 CA00912). J.H. is supported by NIH Grants 5R01CA172603-02 [principal investigator (PI): J.H.], 2P30CA016042-39 (PI: Judith Gasson), 1R01CA181242-01A1 (PI: Chun Chao), and 1R01CA195505 (PI: Leonard Marks); Department of Defense Prostate Cancer Research Program W81XWH-12-1-0206 (PI: Lily Wu); UCLA SPORE in prostate cancer (PI: Robert Reiter); Prostate Cancer Foundation Honorable A. David Mazzone Special Challenge Award (PI: Robert Reiter); and UCLA Jonsson Comprehensive Cancer Center Impact Grant (PI: Sanaz Memarzadeh). O.N.W. is an Investigator of the Howard Hughes Medical Institute and is supported by a Prostate Cancer Foundation Challenge Award. J.H. and O.N.W. are supported by a Stand Up To Cancer–Prostate Cancer Foundation Prostate Dream Team Translational Research Grant (SU2C-AACR-DT0812). This research grant is made possible by the generous support of the Movember Foundation. Stand Up To Cancer is a program of the Entertainment Industry Foundation administered by the American Association for Cancer Research.

1. van Dodewaard-de Jong JM, et al. (2015) New treatment options for patients with metastatic prostate cancer: What is the optimal sequence? *Clin Genitourin Cancer* 13(4):271–279.
2. Nelson WG, De Marzo AM, Isaacs WB (2003) Prostate cancer. *N Engl J Med* 349(4): 366–381.
3. Bubendorf L, et al. (2000) Metastatic patterns of prostate cancer: An autopsy study of 1,589 patients. *Hum Pathol* 31(5):578–583.
4. de Bono JS, et al.; TROPIC Investigators (2010) Prednisone plus cabazitaxel or mitoxantrone for metastatic castration-resistant prostate cancer progressing after docetaxel treatment: A randomised open-label trial. *Lancet* 376(9747):1147–1154.
5. Parker C, et al.; ALSYMPCA Investigators (2013) Alpha emitter radium-223 and survival in metastatic prostate cancer. *N Engl J Med* 369(3):213–223.
6. Grasso CS, et al. (2012) The mutational landscape of lethal castration-resistant prostate cancer. *Nature* 487(7406):239–243.
7. Gundem G, et al.; ICGC Prostate UK Group (2015) The evolutionary history of lethal metastatic prostate cancer. *Nature* 520(7547):353–357.
8. Robinson D, et al. (2015) Integrative clinical genomics of advanced prostate cancer. *Cell* 161(5):1215–1228.
9. Taylor BS, et al. (2010) Integrative genomic profiling of human prostate cancer. *Cancer Cell* 18(1):11–22.
10. Hong MK, et al. (2015) Tracking the origins and drivers of subclonal metastatic expansion in prostate cancer. *Nat Commun* 6:6605.
11. Kumar A, et al. (2011) Exome sequencing identifies a spectrum of mutation frequencies in advanced and lethal prostate cancers. *Proc Natl Acad Sci USA* 108(41): 17087–17092.
12. Drake JM, et al. (2013) Metastatic castration-resistant prostate cancer reveals intrapatient similarity and interpatient heterogeneity of therapeutic kinase targets. *Proc Natl Acad Sci USA* 110(49):E4762–E4769.
13. Aytes A, et al. (2013) ETV4 promotes metastasis in response to activation of PI3-kinase and Ras signaling in a mouse model of advanced prostate cancer. *Proc Natl Acad Sci USA* 110(37):E3506–E3515.
14. Mulholland DJ, et al. (2012) Pten loss and RAS/MAPK activation cooperate to promote EMT and metastasis initiated from prostate cancer stem/progenitor cells. *Cancer Res* 72(7):1878–1889.
15. Ding Z, et al. (2011) SMAD4-dependent barrier constrains prostate cancer growth and metastatic progression. *Nature* 470(7333):269–273.
16. Zhang J, Yang PL, Gray NS (2009) Targeting cancer with small molecule kinase inhibitors. *Nat Rev Cancer* 9(1):28–39.
17. Drake JM, Lee JK, Witte ON (2014) Clinical targeting of mutated and wild-type protein tyrosine kinases in cancer. *Mol Cell Biol* 34(10):1722–1732.
18. Palanisamy N, et al. (2010) Rearrangements of the RAF kinase pathway in prostate cancer, gastric cancer and melanoma. *Nat Med* 16(7):793–798.
19. Cai H, Babic I, Wei X, Huang J, Witte ON (2011) Invasive prostate carcinoma driven by c-Src and androgen receptor synergy. *Cancer Res* 71(3):862–872.
20. Dai B, et al. (2010) Compensatory upregulation of tyrosine kinase Etk/BMX in response to androgen deprivation promotes castration-resistant growth of prostate cancer cells. *Cancer Res* 70(13):5587–5596.
21. Guo Z, et al. (2006) Regulation of androgen receptor activity by tyrosine phosphorylation. *Cancer Cell* 10(4):309–319.
22. Mahajan NP, et al. (2007) Activated Cdc42-associated kinase Ack1 promotes prostate cancer progression via androgen receptor tyrosine phosphorylation. *Proc Natl Acad Sci USA* 104(20):8438–8443.
23. Acevedo VD, et al. (2007) Inducible FGFR-1 activation leads to irreversible prostate adenocarcinoma and an epithelial-to-mesenchymal transition. *Cancer Cell* 12(6): 559–571.
24. Gan Y, et al. (2010) Differential roles of ERK and Akt pathways in regulation of EGFR-mediated signaling and motility in prostate cancer cells. *Oncogene* 29(35):4947–4958.
25. Conley-LaComb MK, et al. (2013) PTEN loss mediated Akt activation promotes prostate tumor growth and metastasis via CXCL12/CXCR4 signaling. *Mol Cancer* 12(1):85.
26. Nguyen DX, Bos PD, Massagué J (2009) Metastasis: From dissemination to organ-specific colonization. *Nat Rev Cancer* 9(4):274–284.
27. van Roosmalen W, et al. (2015) Tumor cell migration screen identifies SRPK1 as breast cancer metastasis determinant. *J Clin Invest* 125(4):1648–1664.
28. Douma S, et al. (2004) Suppression of anoikis and induction of metastasis by the neurotrophic receptor TrkB. *Nature* 430(7003):1034–1039.
29. Scott KL, et al. (2011) Proinvasion metastasis drivers in early-stage melanoma are oncogenes. *Cancer Cell* 20(1):92–103.
30. Chen S, et al. (2015) Genome-wide CRISPR screen in a mouse model of tumor growth and metastasis. *Cell* 160(6):1246–1260.
31. Duquet A, et al. (2014) A novel genome-wide in vivo screen for metastatic suppressors in human colon cancer identifies the positive WNT-TCF pathway modulators TMED3 and SOX12. *EMBO Mol Med* 6(7):882–901.
32. Cerami E, et al. (2012) The cBio Cancer Genomics Portal: An open platform for exploring multidimensional cancer genomics data. *Cancer Discov* 2(5):401–404.
33. Drake JM, et al. (2012) Oncogene-specific activation of tyrosine kinase networks during prostate cancer progression. *Proc Natl Acad Sci USA* 109(5):1643–1648.
34. Jiao J, et al. (2007) Murine cell lines derived from Pten null prostate cancer show the critical role of PTEN in hormone refractory prostate cancer development. *Cancer Res* 67(13):6083–6091.
35. Park SI, et al. (2008) Targeting SRC family kinases inhibits growth and lymph node metastases of prostate cancer in an orthotopic nude mouse model. *Cancer Res* 68(9): 3323–3333.
36. Yang F, et al. (2013) FGFR1 is essential for prostate cancer progression and metastasis. *Cancer Res* 73(12):3716–3724.
37. Bello D, Webber MM, Kleinman HK, Wartinger DD, Rhim JS (1997) Androgen responsive adult human prostatic epithelial cell lines immortalized by human papillomavirus 18. *Carcinogenesis* 18(6):1215–1223.

38. Fidler IJ (2003) The pathogenesis of cancer metastasis: The 'seed and soil' hypothesis revisited. *Nat Rev Cancer* 3(6):453–458.
39. Gambhir SS (2002) Molecular imaging of cancer with positron emission tomography. *Nat Rev Cancer* 2(9):683–693.
40. Leicht DT, et al. (2007) Raf kinases: Function, regulation and role in human cancer. *Biochim Biophys Acta* 1773(8):1196–1212.
41. Sinkevicius KW, et al. (2014) Neurotrophin receptor TrkB promotes lung adenocarcinoma metastasis. *Proc Natl Acad Sci USA* 111(28):10299–10304.
42. Schlegel J, et al. (2013) MERTK receptor tyrosine kinase is a therapeutic target in melanoma. *J Clin Invest* 123(5):2257–2267.
43. Wang Y, et al. (2013) Mer receptor tyrosine kinase promotes invasion and survival in glioblastoma multiforme. *Oncogene* 32(7):872–882.
44. Partin AW, et al. (1997) Combination of prostate-specific antigen, clinical stage, and Gleason score to predict pathological stage of localized prostate cancer. A multi-institutional update. *JAMA* 277(18):1445–1451.
45. Lehmann K, et al. (2000) Raf induces TGFbeta production while blocking its apoptotic but not invasive responses: A mechanism leading to increased malignancy in epithelial cells. *Genes Dev* 14(20):2610–2622.
46. Fournier PG, et al. (2015) The TGF-β signaling regulator PMEPA1 suppresses prostate cancer metastases to bone. *Cancer Cell* 27(6):809–821.
47. Mooz J, et al. (2014) Dimerization of the kinase ARAF promotes MAPK pathway activation and cell migration. *Sci Signal* 7(337):ra73.
48. Graham DK, DeRyckere D, Davies KD, Earp HS (2014) The TAM family: Phosphatidylserine sensing receptor tyrosine kinases gone awry in cancer. *Nat Rev Cancer* 14(12):769–785.
49. Dionne CA, et al. (1998) Cell cycle-independent death of prostate adenocarcinoma is induced by the trk tyrosine kinase inhibitor CEP-751 (KT6587). *Clin Cancer Res* 4(8): 1887–1898.
50. Geiger TR, Peeper DS (2007) Critical role for TrkB kinase function in anoikis suppression, tumorigenesis, and metastasis. *Cancer Res* 67(13):6221–6229.
51. Knudson G, et al. (1991) Bone scan as a stratification variable in advanced prostate cancer. *Cancer* 68(2):316–320.
52. Klezovitch O, et al. (2004) Hepsin promotes prostate cancer progression and metastasis. *Cancer Cell* 6(2):185–195.
53. Ding Z, et al. (2012) Telomerase reactivation following telomere dysfunction yields murine prostate tumors with bone metastases. *Cell* 148(5):896–907.
54. Grabowska MM, et al. (2014) Mouse models of prostate cancer: Picking the best model for the question. *Cancer Metastasis Rev* 33(2-3):377–397.
55. Jin JK, Dayyani F, Gallick GE (2011) Steps in prostate cancer progression that lead to bone metastasis. *Int J Cancer* 128(11):2545–2561.
56. Wu TT, et al. (1998) Establishing human prostate cancer cell xenografts in bone: Induction of osteoblastic reaction by prostate-specific antigen-producing tumors in athymic and SCID/bg mice using LNCaP and lineage-derived metastatic sublines. *Int J Cancer* 77(6):887–894.
57. McCabe NP, De S, Vasanji A, Brainard J, Byzova TV (2007) Prostate cancer specific integrin alphavbeta3 modulates bone metastatic growth and tissue remodeling. *Oncogene* 26(42):6238–6243.
58. Taichman RS, et al. (2002) Use of the stromal cell-derived factor-1/CXCR4 pathway in prostate cancer metastasis to bone. *Cancer Res* 62(6):1832–1837.
59. Knubel KH, et al. (2014) MerTK inhibition is a novel therapeutic approach for glioblastoma multiforme. *Oncotarget* 5(5):1338–1351.
60. Yakes FM, et al. (2011) Cabozantinib (XL184), a novel MET and VEGFR2 inhibitor, simultaneously suppresses metastasis, angiogenesis, and tumor growth. *Mol Cancer Ther* 10(12):2298–2308.
61. Ghilardi JR, et al. (2010) Administration of a tropomyosin receptor kinase inhibitor attenuates sarcoma-induced nerve sprouting, neuroma formation and bone cancer pain. *Mol Pain* 6:87.
62. Wilhelm SM, et al. (2008) Preclinical overview of sorafenib, a multikinase inhibitor that targets both Raf and VEGF and PDGF receptor tyrosine kinase signaling. *Mol Cancer Ther* 7(10):3129–3140.
63. Meyer A, et al. (2014) Role of sorafenib in overcoming resistance of chemotherapy-failure castration-resistant prostate cancer. *Clin Genitourin Cancer* 12(2):100–105.
64. Dahut WL, et al. (2008) A phase II clinical trial of sorafenib in androgen-independent prostate cancer. *Clin Cancer Res* 14(1):209–214.
65. Poulikakos PI, Zhang C, Bollag G, Shokat KM, Rosen N (2010) RAF inhibitors transactivate RAF dimers and ERK signalling in cells with wild-type BRAF. *Nature* 464(7287):427–430.
66. Zhao Y, Adjei AA (2014) The clinical development of MEK inhibitors. *Nat Rev Clin Oncol* 11(7):385–400.
67. Xin L, Ide H, Kim Y, Dubey P, Witte ON (2003) In vivo regeneration of murine prostate from dissociated cell populations of postnatal epithelia and urogenital sinus mesenchyme. *Proc Natl Acad Sci USA* 100(Suppl 1):11896–11903.
68. Loening AM, Gambhir SS (2003) AMIDE: A free software tool for multimodality medical image analysis. *Mol Imaging* 2(3):131–137.
69. Nguyen KQ, et al. (2014) Overexpression of MERTK receptor tyrosine kinase in epithelial cancer cells drives efferocytosis in a gain-of-function capacity. *J Biol Chem* 289(37):25737–25749.
70. Morrissey C, et al. (2013) Effects of androgen deprivation therapy and bisphosphonate treatment on bone in patients with metastatic castration-resistant prostate cancer: Results from the University of Washington Rapid Autopsy Series. *J Bone Miner Res* 28(2):333–340.

Resource

Cell

Phosphoproteome Integration Reveals Patient-Specific Networks in Prostate Cancer

Graphical Abstract

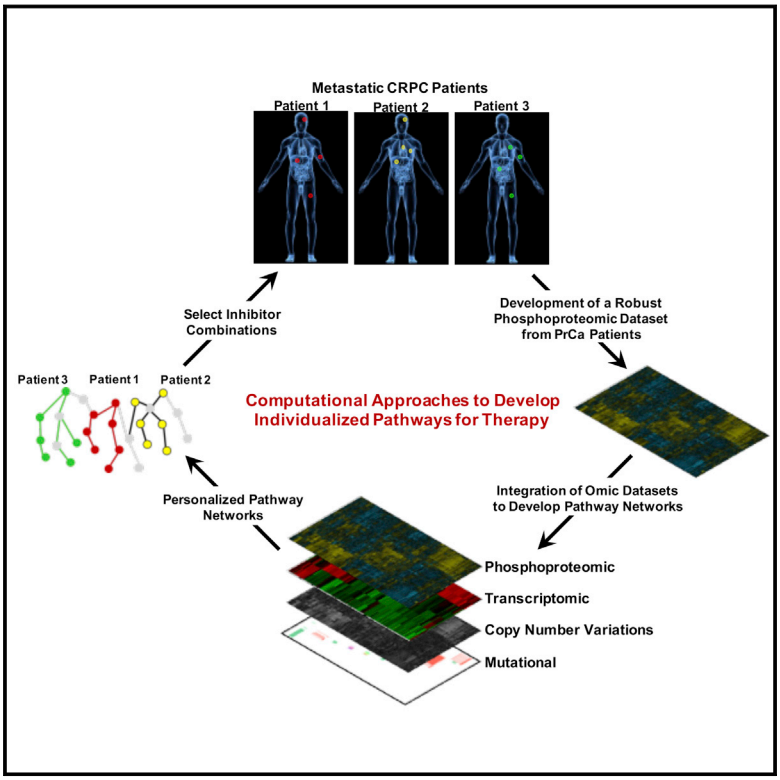

Authors

Justin M. Drake, Evan O. Paull, Nicholas A. Graham, ..., Thomas G. Graeber, Owen N. Witte, Joshua M. Stuart

Correspondence

justin.drake@cinj.rutgers.edu (J.M.D.), owenwitte@mednet.ucla.edu (O.N.W.), jstuart@ucsc.edu (J.M.S.)

In Brief

A multi-omic approach helps to pinpoint which protein kinase is the most promising therapeutic target in prostate cancer patients.

Highlights

- Provides a new phosphoproteomic encyclopedia of prostate cancer cells and tissues
- Integration of omics datasets reveal a map of activated signaling pathways in CRPC
- Development of personalized cancer hallmarks termed pCHIPS
- Patient-specific hierarchy of clinically actionable pathways for therapy

Accession Numbers

PXD002286

Drake et al., 2016, Cell *166*, 1–14
August 11, 2016
http://dx.doi.org/10.1016/j.cell.2016.07.007

CellPress

Please cite this article in press as: Drake et al., Phosphoproteome Integration Reveals Patient-Specific Networks in Prostate Cancer, Cell (2016), http://dx.doi.org/10.1016/j.cell.2016.07.007

Resource

Cell

Phosphoproteome Integration Reveals Patient-Specific Networks in Prostate Cancer

Justin M. Drake,[1,14,19,*] Evan O. Paull,[13,19] Nicholas A. Graham,[2,3,15] John K. Lee,[4,5] Bryan A. Smith,[1] Bjoern Titz,[2,3] Tanya Stoyanova,[1,16] Claire M. Faltermeier,[5] Vladislav Uzunangelov,[13] Daniel E. Carlin,[13,17] Daniel Teo Fleming,[13] Christopher K. Wong,[13] Yulia Newton,[13] Sud Sudha,[12] Ajay A. Vashisht,[6] Jiaoti Huang,[7,8,11,18] James A. Wohlschlegel,[6] Thomas G. Graeber,[2,3,7,9] Owen N. Witte,[1,3,10,11,*] and Joshua M. Stuart[13,*]

[1]Department of Microbiology, Immunology, and Molecular Genetics
[2]Crump Institute for Molecular Imaging
[3]Department of Molecular and Medical Pharmacology
[4]Division of Hematology and Oncology, Department of Medicine
[5]Molecular Biology Institute
[6]Department of Biological Chemistry
[7]Jonsson Comprehensive Cancer Center
[8]Department of Pathology and Laboratory Medicine
[9]California NanoSystems Institute
[10]Howard Hughes Medical Institute, David Geffen School of Medicine
University of California, Los Angeles, Los Angeles, CA 90095, USA
[11]Eli and Edythe Broad Center of Regenerative Medicine and Stem Cell Research, University of California, Los Angeles, Los Angeles, CA 90095, USA
[12]Department of Internal Medicine, University of Michigan Medical School, Ann Arbor, MI 48109, USA
[13]Department of Biomolecular Engineering, University of California, Santa Cruz, Santa Cruz, CA 95064, USA
[14]Rutgers Cancer Institute of New Jersey and Department of Medicine, Rutgers-Robert Wood Johnson Medical School, New Brunswick, NJ 08903, USA
[15]Mork Family Department of Chemical Engineering and Materials Science, University of Southern California, Los Angeles, CA 90089, USA
[16]Department of Radiology, Canary Center at Stanford for Cancer Early Detection, Stanford University, Palo Alto, CA 94304, USA
[17]Department of Medicine, University of California, San Diego, La Jolla, CA 92093, USA
[18]Department of Pathology, Duke University School of Medicine, Durham, NC 27710, USA
[19]Co-first author
*Correspondence: justin.drake@cinj.rutgers.edu (J.M.D.), owenwitte@mednet.ucla.edu (O.N.W.), jstuart@ucsc.edu (J.M.S.)
http://dx.doi.org/10.1016/j.cell.2016.07.007

SUMMARY

We used clinical tissue from lethal metastatic castration-resistant prostate cancer (CRPC) patients obtained at rapid autopsy to evaluate diverse genomic, transcriptomic, and phosphoproteomic datasets for pathway analysis. Using Tied Diffusion through Interacting Events (TieDIE), we integrated differentially expressed master transcriptional regulators, functionally mutated genes, and differentially activated kinases in CRPC tissues to synthesize a robust signaling network consisting of druggable kinase pathways. Using MSigDB hallmark gene sets, six major signaling pathways with phosphorylation of several key residues were significantly enriched in CRPC tumors after incorporation of phosphoproteomic data. Individual autopsy profiles developed using these hallmarks revealed clinically relevant pathway information potentially suitable for patient stratification and targeted therapies in late stage prostate cancer. Here, we describe phosphorylation-based cancer hallmarks using integrated personalized signatures (pCHIPS) that shed light on the diversity of activated signaling pathways in metastatic CRPC while providing an integrative, pathway-based reference for drug prioritization in individual patients.

INTRODUCTION

DNA and RNA sequencing data have been used to analyze key transcriptional targets, cell surface molecules, or pathways at work in cancer (Aytes et al., 2014; Cancer Genome Atlas Network, 2012a, 2012b; Cancer Genome Atlas Research Network, 2015; Grasso et al., 2012; Robinson et al., 2015; Taylor et al., 2010; Vaske et al., 2010). One goal from these approaches is to select mutations corresponding to genes or pathways from tumors and then match targeted therapies based on these lesions. However, missing from many genomic or transcriptomic analyses is further measurement and extension of the activated pathways that are found by such approaches using mass spectrometry-based phosphoproteomics.

Protein phosphorylation remains a critical, rate-limiting step for the regulation of signaling pathways over numerous biological events. Determining both the level of phosphorylation and what residues are phosphorylated on a given protein may inform us about the activity of kinases and phosphatases as well as

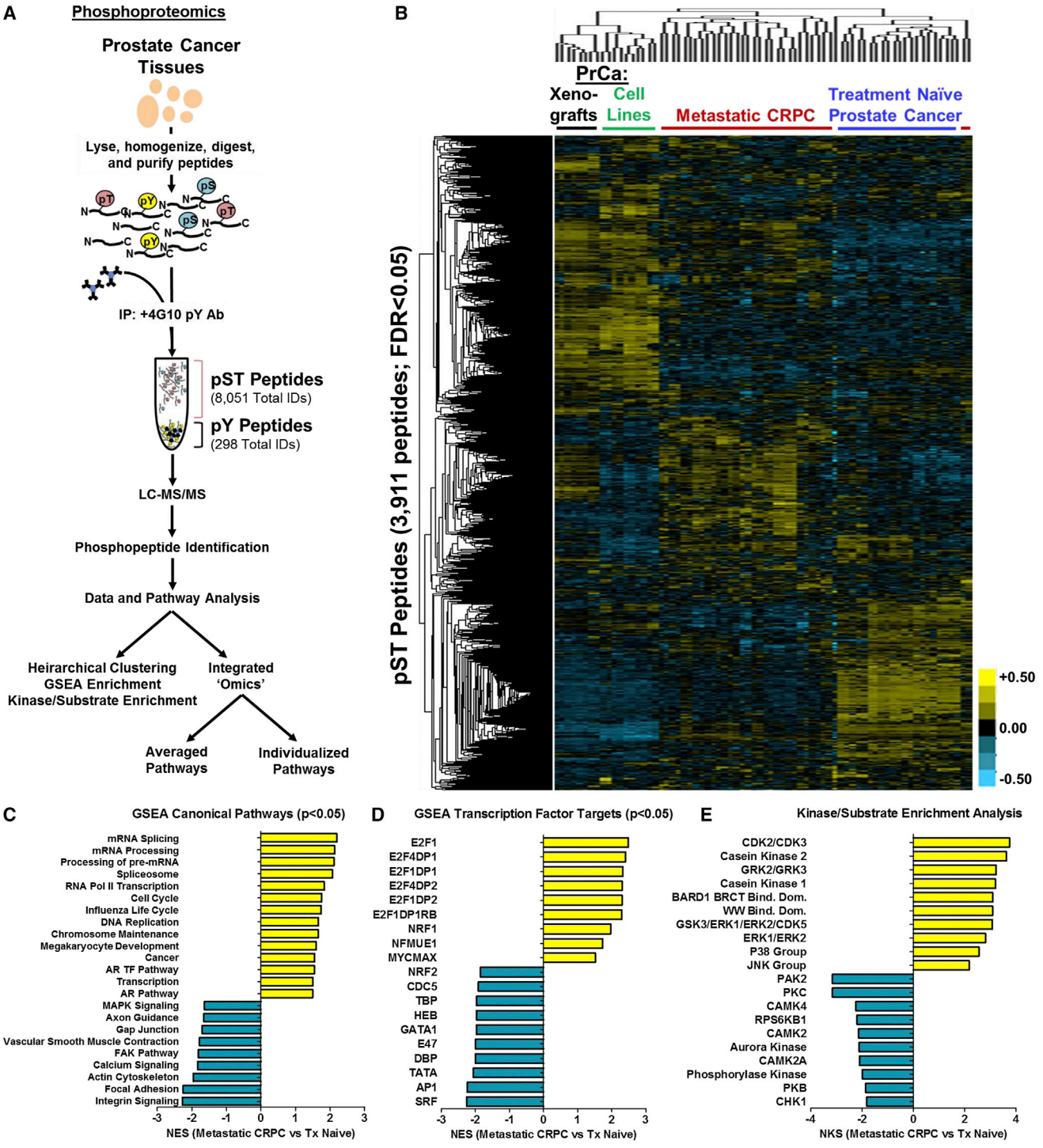

Figure 1. Characterization of the Phosphoproteome in Metastatic CRPC Tissues

(A) General workflow of the phosphopeptide enrichment and quantitative mass spectrometry protocol followed by data and pathway analyses. Analyses is described in the text.

(B) Unsupervised hierarchical clustering heatmap of phosphoserine and phosphothreonine peptides identified from prostate cancer cell lines and tissues. 3,911 unique phosphopeptides (rows) were significantly identified from over 36 samples (columns). Unsupervised hierarchical clustering was performed using the Cluster program with the Pearson correlation and pairwise complete linkage analysis.

(legend continued on next page)

uncover new functional information that was previously underappreciated. Cellular signaling can also be controlled through the recruitment of protein domains (such as SH2 and SH3) to specific phosphorylation sites on kinases (Pawson, 2004). Protein phosphorylation leads to a cascade of downstream signaling events important for cell maintenance and survival and dysregulation of this process has been implicated in many diseases including cancer (Hunter, 2009). It stands to reason that the implementation of phosphoproteomics, coupled with traditional mRNA-based approaches, may provide greater clues to these signaling events than either alone.

Recent computational advances allow for the simultaneous examination of genomic, phosphoproteomic, and transcriptional data, in the context of prior pathway knowledge (Cancer Genome Atlas Research Network, 2013, 2014a; Huang et al., 2013). These methods have the advantage of being able to detect events that are below the threshold of statistical significance when examining a single dataset in isolation, as well as finding evidence for functional interactions between proteins. For instance, a multistep systems-level approach was recently used to find genomic events that drive tumorigenesis in glioblastoma by first finding transcriptional "master regulators" that are predicted to control a large number of differentially expressed genes and then reversing pathway database interactions to look "upstream" for genomic events that may be influencing (and statistically associated with) the activity of regulators active in individual patients (Chen et al., 2014). Similarly, the TieDIE algorithm (Paull et al., 2013) was recently used in a study of thyroid papillary carcinoma to identify signaling pathways linking mutant BRAF and RAS genes to transcription factors and signaling proteins with altered activity in tumor samples. It was found that the small GTPase RHEB, a known regulator of mTOR activity, was a contributing factor to the differences observed between BRAF and RAS mutants (Cancer Genome Atlas Research Network, 2014a). Both of these analyses ranked candidate regulators according to multiple data types and pathway context, though the latter analysis focused on identifying intermediate "linking" genes that are strongly implicated by the combination of pathway context and the incorporation of multiple data types.

Here, we set out to define the global picture of signaling pathways in lethal prostate cancer through dataset integration. We developed a complete and extensive new dataset of the phosphoproteome in metastatic CRPC by extending our analysis to phosphoserine and phosphothreonine peptides and then combining this information with our previously published phosphotyrosine peptide data (Drake et al., 2013). To develop comprehensive pathway networks that are both enriched and activated in CRPC, we used TieDIE to integrate independent datasets of mutations, transcriptional changes, and phosphoproteome activities in an unbiased manner from a similar set of tumor samples obtained at rapid autopsy (Rubin et al., 2000). The integration of tissue samples from a single autopsy program allowed us to make inferences on the connections between the mRNA and phosphoproteome datasets. In addition, both mRNA and phosphoproteome data were available for several of the patients. Using this information, we introduce a new tool called phosphorylation-based cancer hallmarks using integrated personalized signatures (pCHIPS) to establish patient-specific pathways marking key signaling events for possible targeting.

RESULTS

Development of a Robust Phosphoproteomic Dataset for Integration

We analyzed the phosphoproteome of metastatic CRPC tissues, obtained via an IRB approved tissue procurement protocol from the University of Michigan (Rubin et al., 2000) and identified 297 phosphotyrosine (pY) peptides, (Drake et al., 2013) and 8,051 phosphoserine/phosphothreonine (pST) peptides from 54 total runs corresponding to 27 samples of interest (11 treatment-naive, 16 metastatic CRPC; Data S1A–S1C) using quantitative label free mass spectrometry (Figure 1A). Hierarchical clustering revealed similarities in the groupings of the samples compared to previously published pY peptide data (Drake et al., 2013). For example, cell lines were distinct from primary tissues and treatment naive localized prostate cancer clustered independently from metastatic CRPC tissues (Figure 1B). Within this dataset, we were able to directly identify phosphopeptides corresponding to 74 kinases, 18 of which were differentially phosphorylated (false discovery rate [FDR] <0.05, >1.5-fold) in metastatic CRPC tissues (Data S1D). To get an initial sense of the biological processes and pathways enriched in metastatic CRPC, we performed gene set enrichment analysis (GSEA) typically used for RNA-based datasets (Subramanian et al., 2005) as well as kinase-substrate enrichment analysis (KSEA) better tailored for phosphoproteomic-based datasets that we and others have previously established (Drake et al., 2012, 2013; Casado et al., 2013; Newman et al., 2013). GSEA of canonical processes and pathways detected over-representation of mRNA splicing and processing, DNA replication, and AR transcription factor pathways as well as loss of integrin signaling, focal adhesion, and axon guidance pathways in metastatic CRPC (Figure 1C). GSEA of transcription factor targets revealed several E2F family members as well as the MYC/Max complex to be over-represented in metastatic CRPC (Figure 1D; Data S1E). The enrichment of E2F target genes is intriguing as we have previously been able to connect a primary basal stem cell signature to small cell neuroendocrine carcinoma with this gene set (Smith et al., 2015). KSEA further implicated enrichment of several kinases in metastatic CRPC including cyclin-dependent kinases (CDK2/CDK3), casein kinase 2 (CSNK2A1), and β-adrenergic receptor kinases (ADRBK1/ADRBK2) (Figure 1E; Data S1F). Many of the genes and kinases identified through GSEA and KSEA

(C–E) Gene set enrichment analysis (GSEA) was performed to identify canonical pathways (C) and transcription factor targets (D) with activity either higher (right yellow bars) or lower (left blue bars) in metastatic CRPC compared to primary tissue. (E) Kinase/substrate enrichment analysis (KSEA) identified several unique kinases that were not directly sequenced by the mass spectrometer in the phosphoproteomic data. NES, normalized enrichment score; yellow, hyperphosphorylation; blue, hypophosphorylation in the heatmap (B).
See also Data S1A–S1F.

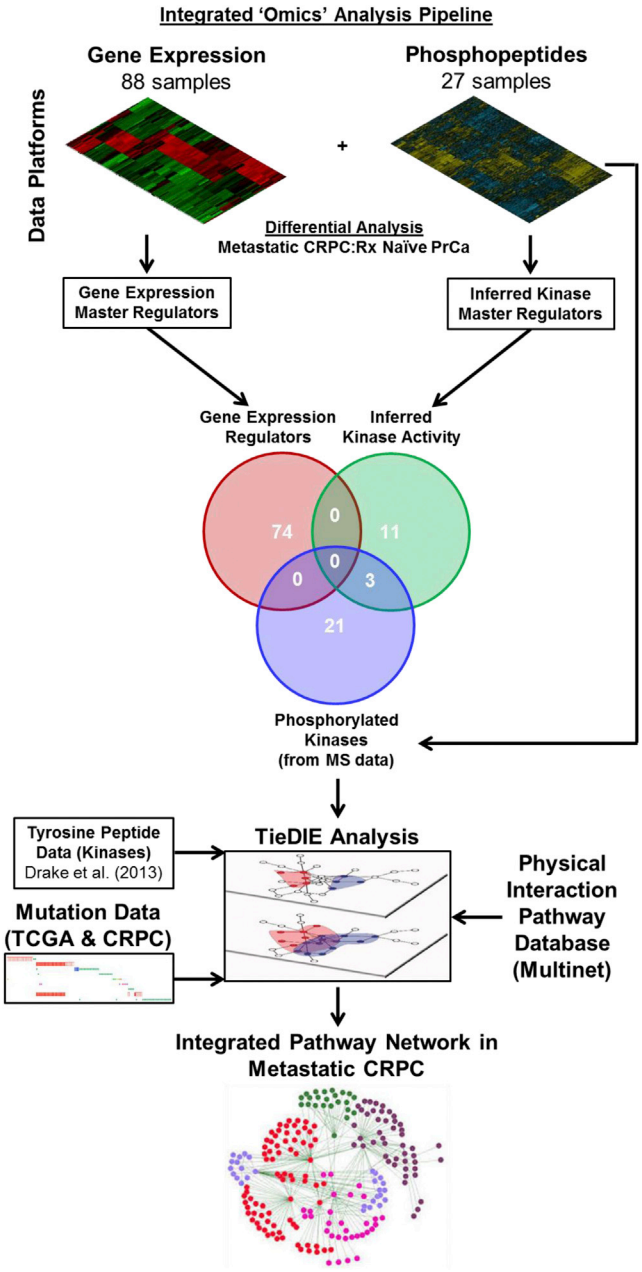

Figure 2. Pipeline for Omic Dataset Integration

Flow diagram depicting the integration pipeline. Twenty-seven gene expression and 16 phosphoproteomic CRPC patient datasets were integrated with mutational data and combined using TieDIE to generate the resulting integrated network. The overlay of input gene expression, kinase master regulators, and phosphorylated kinases are shown as a Venn diagram.

See also Figures S1, S2, and Data S1G–S1J.

have previously been implicated in prostate cancer confirming the validity of our dataset (Gioeli et al., 1999; Li et al., 2014; Lu et al., 1997; Wang et al., 2006). Importantly, the large number of pST identifications enabled an integrated computational approach to identify pathways implicated from this phosphoproteomic dataset.

Integration of Transcriptomic and Phosphoproteomic Datasets Using TieDIE

To prioritize kinases that are likely to regulate the observed gene expression profile of metastatic samples, and be related to genomic aberrations observed in prostate cancer, we developed an original computational pipeline using the TieDIE algorithm, a pathway-based method developed to find protein and gene interactions related to disease (Cancer Genome Atlas Research Network, 2014b; Paull et al., 2013). The approach integrates complementary transcriptomic and genomic datasets collected from different metastatic CRPC tissues or patients, as well as prior knowledge in the form of pathway databases, to find subnetworks of related proteins implicated by multiple forms of biological evidence (Figures 2 and S1A). We first applied the master regulator inference algorithm (MARINa) (Alvarez et al., 2015), a method to infer the activity of a given protein based on the differential expression/phosphorylation of the targets it regulates. This allowed us to identify transcription factors with differential activity (repression/activation) as well as differentially activated kinase regulators (based on the predicted upstream kinases for each phosphopeptide) in metastatic CRPC samples as compared with treatment naive prostate cancers (Data S1G and S1H). In addition, kinases directly identified by the mass spectrometer in our phosphoproteomic dataset (phosphorylated kinases) were merged with the kinase regulators before input to TieDIE.

From this differential analysis, we were able to incorporate 74 transcription factor (TF) regulators, 14 inferred kinases regulators, and 24 differentially phosphorylated kinases (Figure 2). The dataset used for analysis included a matrix of inferred and measured kinases for the same 16 metastatic CRPC samples and a matrix of inferred transcription factors for 27 metastatic samples. Several patients with marked variations in response to therapy (e.g., anti-androgens or chemotherapy; Data S1A) had highly similar transcriptomes as evidenced by the transcription factors identified by MARINa for the 16 metastatic CRPC samples. Thus, the differences in protein level signaling could help explain this observation as well as offer new treatment options that could abrogate the signaling upstream of these TF-driven circuits (Figure S1B). These phosphoproteomic and transcriptomic matrices only overlapped for seven patient samples (from six unique patients) and are used for our patient-specific networks. As a third input to TieDIE, a background of somatic mutations and copy-number aberrations was collected from a large number of prostate cancer samples from multiple datasets. The strength of our approach is that it unites these diverse data, collected on different patient samples, to identify pathways implicated by several viewpoints.

We asked if the kinases inferred by master regulator analysis or identified by phosphorylation status were significantly interrelated to the set of genes involved in somatic mutations or to those genes implicated as transcription factors by master regulator analysis of the expression data. A conservative test that permuted the input gene sets over 1,000 replications demonstrated that the kinases are indeed "nearby" in pathway space to genes with genomic or transcriptomic alterations (Figure S2A). Thus, despite the fact that the inferred TF regulators are not directly targeted for phosphorylation by the kinase regulators

more than we expect by chance, the TFs are "close" in network space suggesting longer paths are needed to encompass the signaling transduced from the phosphoproteome to the transcriptome. The TieDIE solutions were robust to changes in the method's single parameter (alpha) that controls the size of the network solutions (Figure S2B). Using varying settings for alpha, we selected a compact network with a high level of specificity (Figure S2B), which consisted of 338 nodes—40 kinases, 53 transcription factors, 86 amplified/deleted/mutated genes, and 163 linking proteins—connected by 1,889 edges. To simplify this network, interactions that were supported by the phosphoproteomic data were retained. This resulted in a network we refer to as the "scaffold network" for metastatic CPRC that contained 122 nodes and 256 edges (Figure S2C; Data S1I). TieDIE used 61 genes that were not included in the input set, termed "linker" proteins, to produce the scaffold network. Consistent with their predicted embedding in metastatic signaling, these 61 linkers were found to have phospho-residues with significantly higher phosphorylation abundance in metastatic CRPC compared to treatment naive prostate cancer (Figure S2D; $p < 4.5 \times 10^{-6}$).

The diffusion process employed by TieDIE controls for the spurious inclusion of "hub" genes—those genes with many connections in the generic background network potentially as a result of study bias. However, it was possible other factors could influence a linker's inclusion that would undermine the network's relevance to the given input set. Thus, we explicitly tested for inclusion bias in the linker genes by quantifying the frequency with which they were included in random TieDIE solutions constructed using simulated arbitrary input gene sets of the same sizes as the provided inputs. One thousand simulations demonstrated that the linker genes were included at frequencies no higher than other background genes (Figures S2E and S2F). Furthermore, no inclusion bias was observed for linkers with higher connectivity or centrality.

The scaffold network was found to have sub-networks significantly represented by cancer-related MSigDB cancer hallmarks gene sets including AKT/mTOR/MAPK signaling, nuclear receptor signaling (that includes the androgen receptor [AR] pathway), the cell cycle, DNA repair, stemness, and migration (Figures S2G–S2L; Data S1J) as well as established prostate cancer-specific pathways recorded in the KEGG pathway database (8.8-fold enrichment, $p < 4.8e\text{-}15$ or based on DAVID overlap analysis; https://david.ncifcrf.gov). Sub-network views in Figures 3 and S2 show only genes that fall within both the curated hallmark gene sets and the previously generated scaffold network, with gray nodes representing genes that are in the scaffold network but not in the respective hallmark.

To determine the distinct biology revealed by the phosphoproteomic data in metastatic CRPC, we re-ran the same TieDIE analysis to obtain a comparably sized scaffold network without the phosphoproteomics information and compared its cancer hallmark enrichment against the one found when all the data were included (Figures S3A and S3B). We found significant enrichment of AKT/mTOR/MAPK signaling pathways when the phosphoproteomic data were included whereas enrichment was only marginal without inclusion of these data (Figure 3A; 4.6 versus 1.6 -log10 hypergeometric p value). In addition, we found higher relative enrichment of proteins involved in cell cycle, DNA repair, and nuclear receptor pathways when the phosphoproteomic data were included (Figure 3A; cell cycle: 20.5 versus 14.7, -log10 hypergeometric p value; DNA repair: 6.6 versus 5.1; nuclear receptor signaling: 8.1 versus 5.8). Inspecting each sub-network through our phosphoproteomic data revealed several newly discovered enzymatically active phospho-residues enriched in metastatic CRPC. This included MAPK signaling targets (RPS6KA4 S^{343}/S^{347}, S^{682}/T^{687}), cell-cycle targets (MCM2 $S^{40/41}$, S^{27}), and the DNA repair kinase PRKDC T^{2609}, S^{2612} (Figures 3B–3I). Several other kinases within these sub-networks were hyperphosphorylated at residues with unknown function in metastatic CRPC including PRKAA2 S^{337}, MAPK14 S^{2}, STK39 S^{385}, NIPBL S^{318}, and SNW1 S^{14} implicating several more new targets for investigation. Lower relative enrichment in metastatic CRPC was observed for TGF-β or WNT/β-catenin signaling pathways when the phosphoproteomic data were included. This can be partially explained by the lack of overlap between kinases identified directly by the phosphoproteomic data, lowering the relative importance of these gene sets after its inclusion. However, our differential analysis of metastatic CRPC to treatment naive prostate cancer did observe strong enrichment of both TGF-β and WNT/β-catenin signaling pathways after the integration of the phosphoproteomic data in metastatic CRPC (Figure S3B). We also observed that the fraction of proteins overlapping with any of the "hallmark" gene sets to be higher when including the phosphoproteomic data, accounting for any potential study bias. These results provide evidence of actionable phosphorylation events in metastatic CRPC, several of which have previously been implicated in this disease including PRKDC, PRKAA2, and AKT (Goodwin et al., 2015; Yu et al., 2015; Park et al., 2009) while others such as RPS6KA4 and MCM2 represent new drug targets.

Identification of Patient-Specific Integrated Networks

To identify patient-specific signaling routes we used the integrated phosphoproteome-transcriptome network to analyze the six metastatic CRPC patients that had both transcriptomic and phosphoproteomic data available. We ran the VIPER algorithm, a sample-specific version of MARINa that infers the activity of proteins based on measurements of the targets they regulate (Alvarez et al., 2015), to summarize the transcriptomic and phosphoproteomic data vectors of each patient into protein activity inferences of a relatively small number of transcriptional and kinase "master regulators," respectively (Figure 4A). Similar to the full dataset, the transcriptional master regulators were highly similar across this patient cohort but the inferred and phosphorylated kinases were somewhat different between each of the individual patients (Figure 4B). Importantly, we found that phosphoproteomic-driven VIPER inferences of protein activity for patient RA55 were highly correlated and consistent across two metastatic sites (Figures S4A and S4B). Similarly, a second patient, RA43, was found to have higher pairwise correlations (on average) between samples when comparing inferred protein activities from VIPER, than when comparing the relative phosphorylation of peptides (Figures S4C–S4H). We asked if the high differential kinase activities in CRPC compared to primary prostate cancer inferred by VIPER were concordant with the measured phosphorylation levels. We measured the

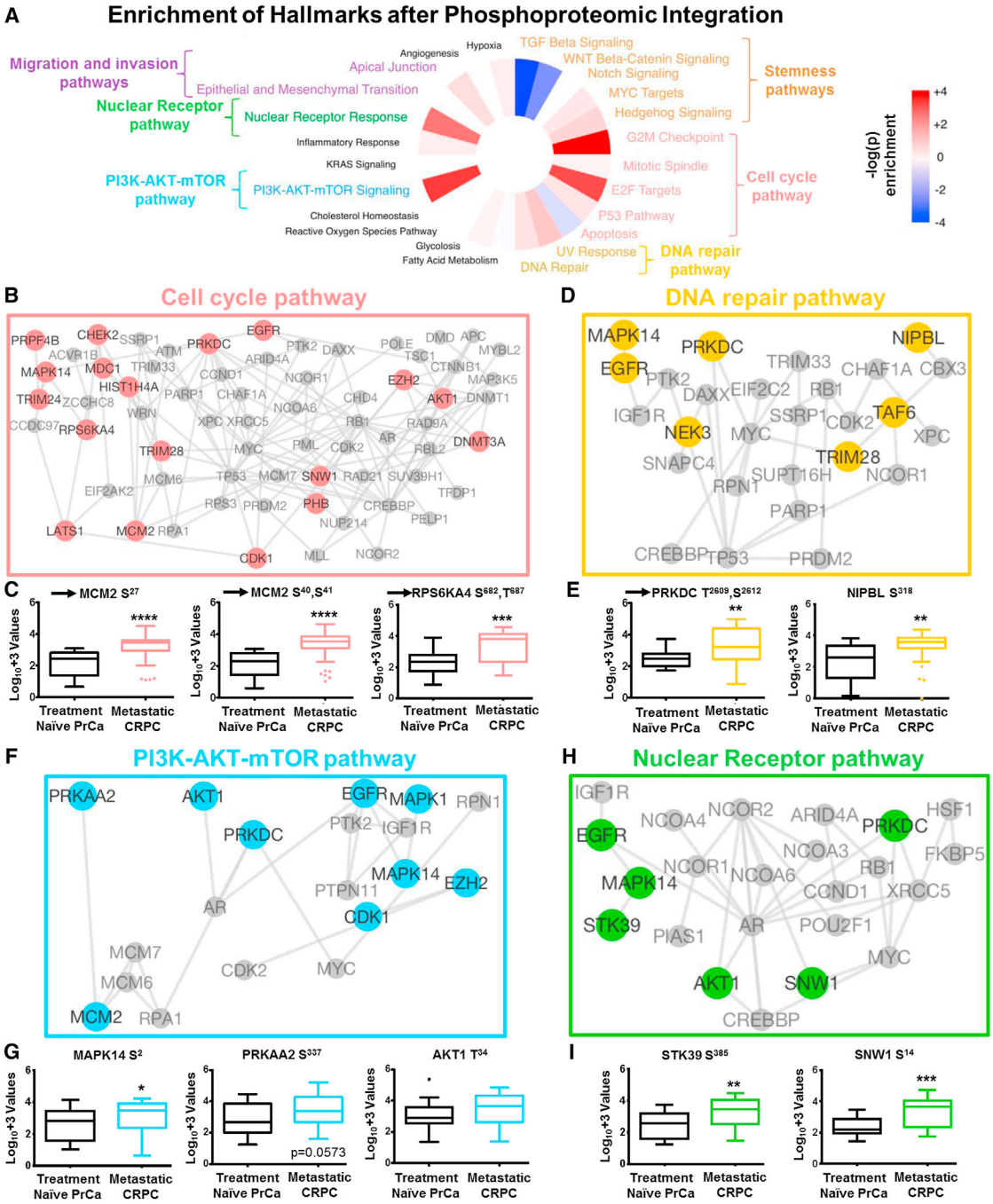

Figure 3. Pathway Analysis of Metastatic CRPC

(A–I) Enriched cancer hallmarks generated by dataset integration using TieDIE after inclusion of the phosphoproteomic and gene expression data relative to gene expression data alone (A). Several cancer hallmarks were enriched after inclusion of the phosphoproteomic data including the cell-cycle pathway (B, red nodes), DNA repair pathway (D, yellow nodes), AKT/mTOR/MAPK pathway (F, blue nodes), and the nuclear receptor pathway (H, green nodes). Detailed analysis of each of these pathways revealed several common and unique players with high connectivity. Assessment of a select number of kinases and phosphoproteins from each network confirmed their elevated phosphorylation state (C, E, G, and I) including some with direct phosphorylation on their enzymatic active residue (C and E). This supports the activation state of the networks observed. Black arrow represents phosphoresidues that result in enzymatic activity of the given protein. These defined subnetworks only contain genes that fall within both the curated hallmark gene sets and the previously generated scaffold network, with colored nodes corresponding to genes that are members of a hallmark and exclusive to the integrated network solution containing the phosphoproteomic data; gray genes are other scaffold members in the surrounding region. A t test was performed to calculate significance. *p < 0.05, **p < 0.01, ***p < 0.001, ****p < 0.0001.

See also Figure S3.

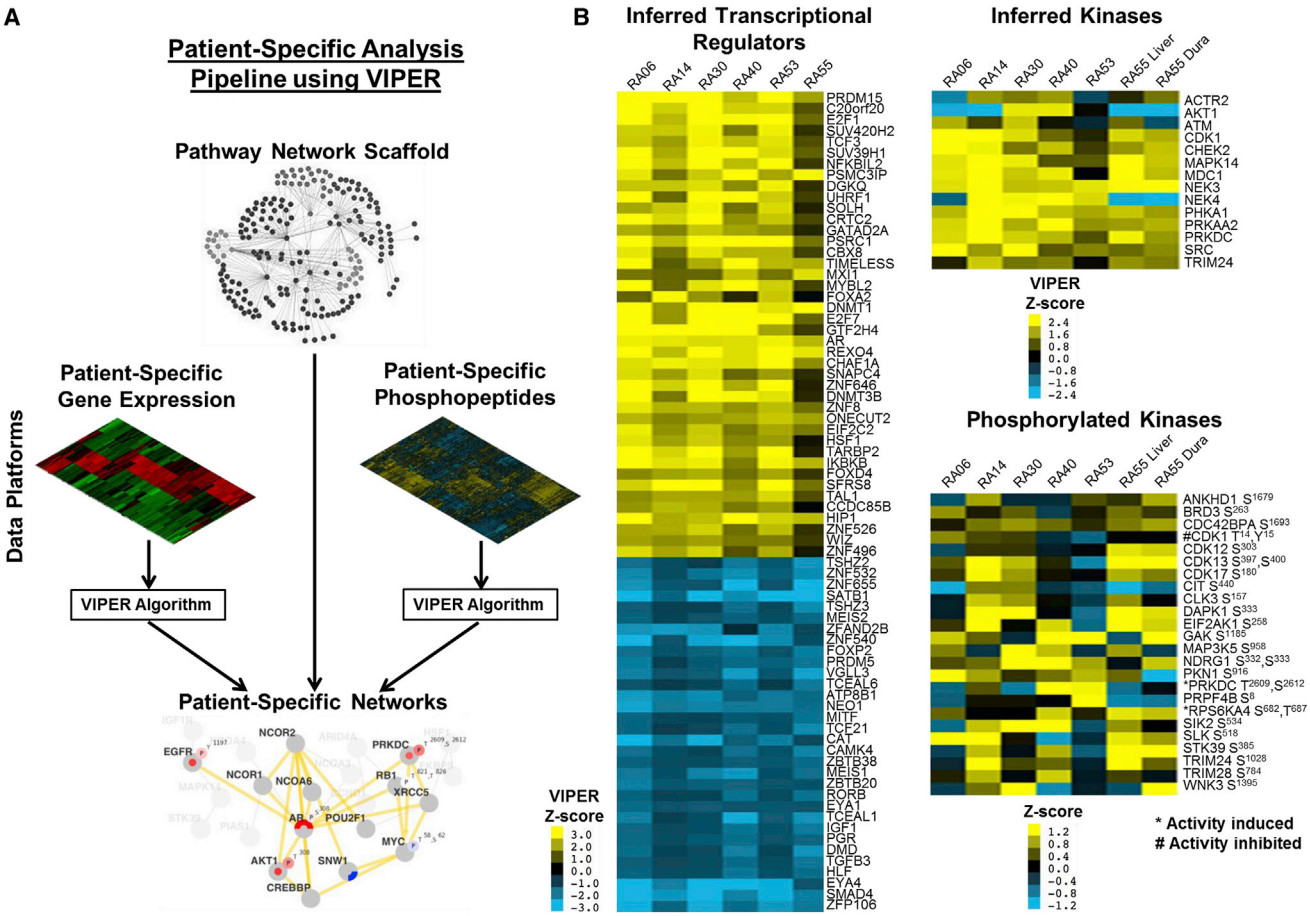

Figure 4. Development of a Patient-Specific Network Using VIPER

(A) Flow diagram depicting the integration of gene expression and phosphoproteomic datasets for VIPER analysis.

(B) Heatmap of the gene expression and kinase master regulators and phosphorylated kinases for all six patients. These data were used as the input for patient-specific network analysis.

See also Figure S4.

correlation between VIPER-inferred and measured activity for 26 phosphoresidues for which functional annotations could be found recorded in the http://phosphosite.org database (Figure S4I). Of these, ten had significant positive correlations with VIPER activity (Benjamini Hochberg [BH] FDR <0.1); none had significant anti-correlations. Of the ten phosphoresidues with positive correlations, eight were annotated on enzymatically active sites, consistent with the higher activity predicted by VIPER for the metastatic samples.

To generate patient-specific network models, we intersected sample-specific VIPER inferences, the phosphorylation abundance of select phosphoresidues, mutations, copy-number gains, and copy-number deletions with the integrated TieDIE "scaffold network" solution. Proteins could then be prioritized by their activities and by their ability to regulate (or be regulated by) other genes implicated in a patient's network. The use of the scaffold allows the cohort-level data to inform the analysis of a single patient's data, which improves the accuracy and robustness of the resulting networks (Figures S4J and S4K). The scaffold network was also found to generalize to unseen patient data based on a leave-one-out test in which the scaffold network was rebuilt after removing the data for each patient in turn as assessed by multiple different sub-sampling tests (Figures S4L–S4N).

Assessment of Actionable Pathways for Personalized Medicine Predictions

We created a visualization scheme we refer to as phosphorylation-based cancer hallmarks using integrated personalized signatures, or pCHIPS (Figures 5A and S5; Data S1K). pCHIPS enables visual inspection and prioritization of the signaling pathways specific to each individual patient and is useful for suggesting personalized treatment options. Dissecting the pCHIPS of patient RA40, we observed four significantly enriched subnetworks including a large active network related to cell-cycle processes (Figures 5B–5F). Interestingly, this was the only patient that we analyzed with a missense mutation and deletion in the tumor-suppressor gene APC. While frequently observed in colorectal cancers, APC mutations can occur in other cancers (Kandoth et al., 2013) where its inactivation leads to increased

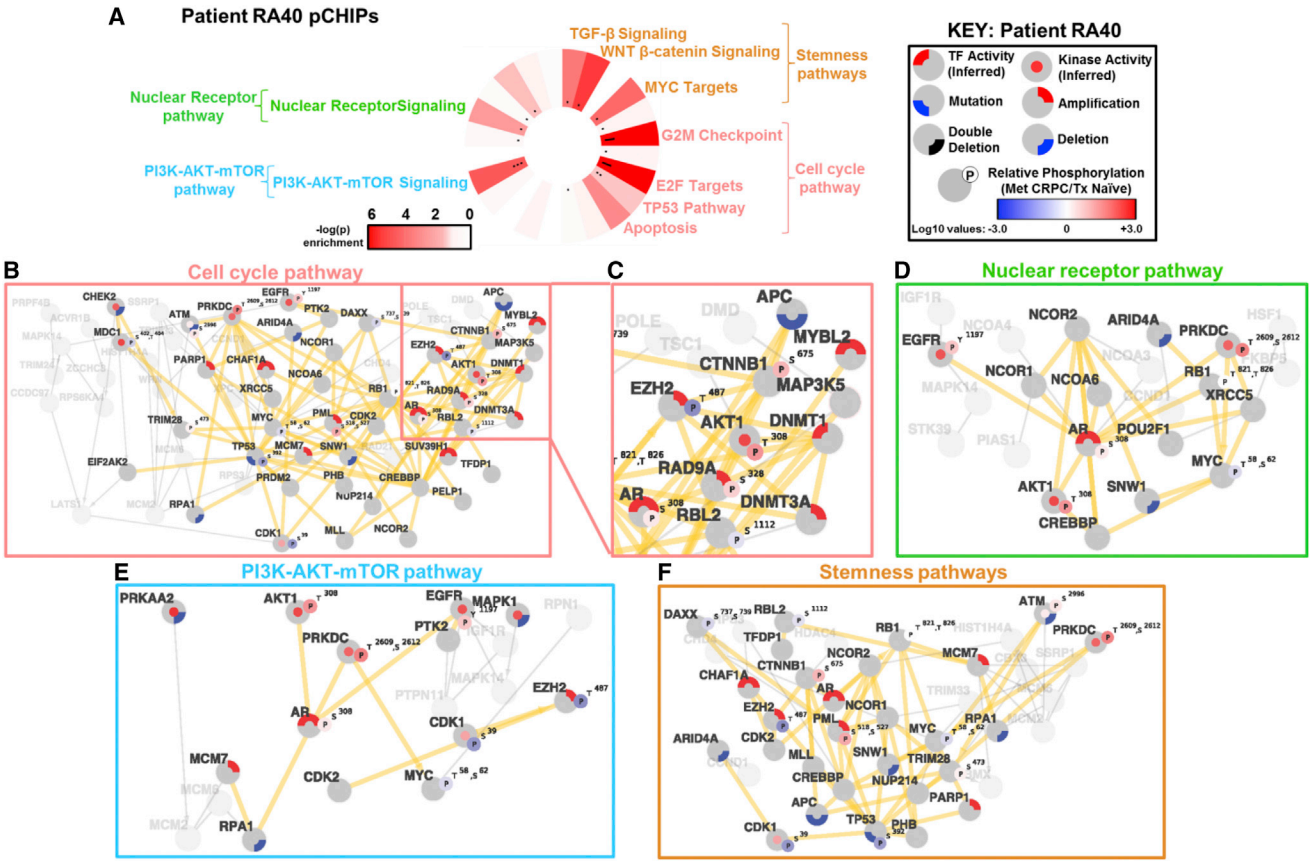

Figure 5. Integrated Pathway Network of Patient RA40

(A–F) Phosphorylation-based cancer hallmarks using integrated personalized signatures (pCHIPS) analysis for patient RA40 revealed strong enrichment of cell cycle and PI3K-AKT-mTOR pathway networks (A). The pCHIPS wheel summarizes enrichment between genes in each patient-specific network and the corresponding pCHIPS category: labels indicate categories with significant enrichment after multi-hypothesis correction (FDR <0.1). Black dots indicate SNV and copy-number genomic events in this patient. Patient-specific network nodes and edges related to cell-cycle pathway (B and C), nuclear receptor pathway (D), PI3K-AKT-mTOR pathway (E), and stemness pathways (F). Edges belonging to both the patient-specific network model and the cell-cycle-related scaffold network are shown as thick yellow edges, while corresponding genes are shaded in dark gray. Yellow arrows indicate that the upstream kinase directly phosphorylates the downstream substrate. "Circleplot" quadrants for each gene summarize genomic, transcriptomic, and phosphoproteomic activity relevant to metastatic CRPC phenotype (upper right, amplification; lower right, deletion; lower left, mutation; upper left, transcriptional regulatory activity; center, kinase regulatory activity). Node "ears" peripherally attached to circleplots represent relative phosphorylation of specific, functionally annotated peptides sites on each protein. Genes and edges that are not represented in the patient-specific network but are in the scaffold network are shown in light gray.
See also Figure S5, Data S1K, and Data S2.

β-catenin activity (Morin et al., 1997). Indeed, we observed strong phosphorylation of the enzymatic active site of β-catenin (S^{675}). The putative activation of EZH2 is also linked to β-catenin activation in several cancers including hepatocellular carcinoma and breast cancer (Chang et al., 2011; Cheng et al., 2011). EZH2 activation in this patient is supported by both low level amplification (Mermel et al., 2011) and hypophosphorylation of residue T^{487} (a marker for ubiquitination of EZH2) as well as amplification of DNA methyltransferase 3 (DNMT3) and predicted transcriptional activity of DNMT1 (Ning et al., 2015) (Figure 5C). Further, the amplification and predicted transcriptional activity of SUV39H1 correlates with EZH2 expression in tumor development (Pandey et al., 2014), consistent with our observations. Mechanistically, EZH2 activity is sufficient for activation of AKT1 (Gonzalez et al., 2011), which we observed through both hyperphosphorylation of the enzymatic active site T^{308} as well as indirectly through the prediction of high AKT activity by VIPER analysis (Data S1H). Together, this information implicates the involvement of β-catenin, AKT1, and EZH2 in contributing to altered cell-cycle regulation and growth and suggests that targeted inhibition within this network could have been useful in this patient. Similar mechanisms related to other signaling pathways for other patients can also be described (Data S2A–S2F) as well as inter-patient pathway differences within the same hallmark (Figure 6).

Given a complex patient-specific network, how do we use it to select an optimal treatment strategy? Under the assumption that we seek to reverse as many altered gene activities found in a patient, we consider here the idea of using a minimum combination of targets that influence the largest area in a patient's network.

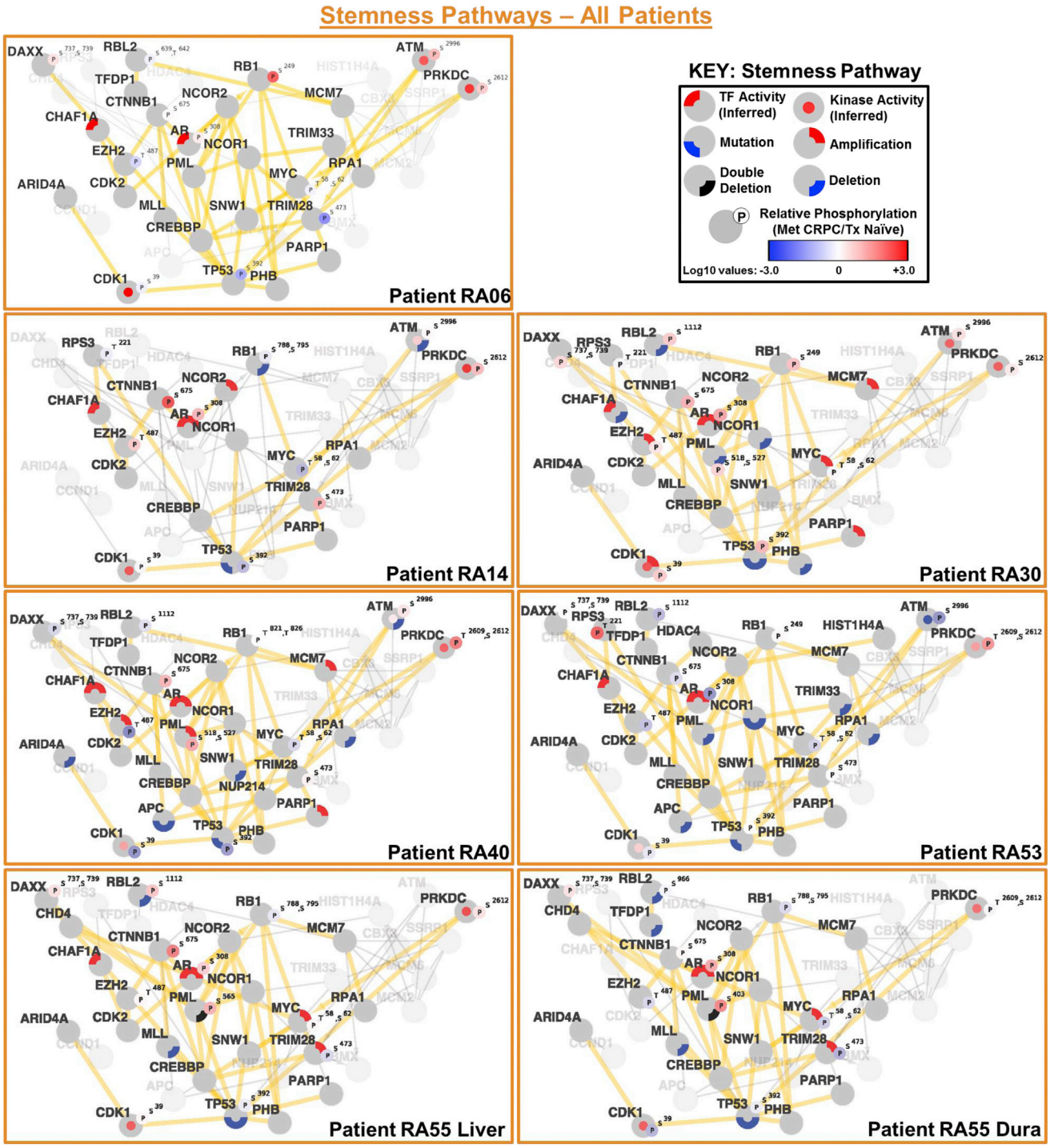

Figure 6. Comparison of the Stemness Pathway Hallmarks across All Seven Patient Samples

Patient-specific networks were developed from the stemness pathway hallmarks and revealed distinct regions of the network were differentially activated across the CRPC patient samples. This suggests that while the stemness pathway hallmarks were enriched in all the patients evaluated, a patient-specific evaluation is needed to determine the precise targets for therapy. Genes and edges that are not represented in the patient-specific network but are in the scaffold network are shown in light gray.

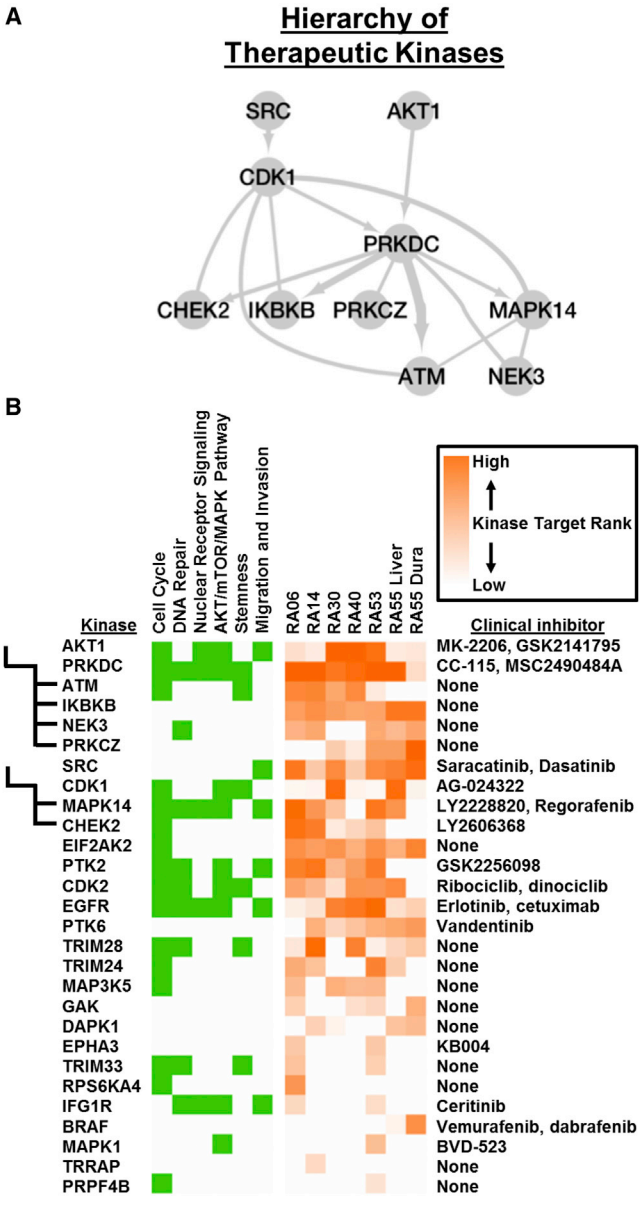

Figure 7. Summary of Kinase Target Potential in Patient-Specific Networks

(A) Network diagram of hierarchy between kinase targets derived from KSEA interactions and potential "coverage" of phosphopeptides activated in CRPC. The thickness of each edge represents the degree of overlap in the set of protein targets that each kinase is predicted to phosphorylate. Directed arrows indicate predicted phosphorylation from a (source) kinase, at a residue on the corresponding target kinase.

(B) Therapeutic potential and summary of kinase targets. Far left: the hierarchy of therapeutic kinase targets shown in (A) is briefly summarized. Left: green boxes indicate kinases (rows) that are members of each of the six major hallmark subnetworks (columns) shown in Figure 3. Right: orange boxes indicate the predicted importance of kinase targets based on the combined evidence from VIPER-inferred kinase activity, phosphorylation status of functionally annotated peptides, and connectivity, for each patient-specific network (columns). Currently available clinical inhibitors for each are listed on the right.

See also Figures S6, S7, and Data S1L–S1M.

Understanding the nesting of gene regulatory signals provides information about how to select genes for this purpose. Therefore, we developed a hierarchy of therapeutic kinase targets based on KSEA-derived relationships between kinases and the sets of peptides each kinase regulates, as well as evaluation of the cancer hallmarks and pathways of each individual patient (Figures 7A, S6A, and S6B). The hierarchy reveals the top kinase targets for every individual patient that we analyzed and the corresponding therapeutic intervention (Figure 7B). Given this structure, targeting of a single kinase such as PRKDC may be sufficient to blunt the activity of other kinases that phosphorylate many of the same targets (NEK3, PRKCZ) and those that are, additionally, predicted to be phosphorylated by PRKDC (ATM, IKBKB).

To assess the validity of our kinase predictions, we developed kinase hierarchies for prostate cancer cell lines, LNCaP, 22Rv1, and DU-145 for which external data were available and for which we had transcriptomic and phosphoproteomic data. Using existing in vitro drug response data from the Genomics of Drug Sensitivity in Cancer (GDSC) (Yang et al., 2013) (http://www.cancerrxgene.org/; Data S1L), we compared the relative sensitivity, measured in $-\ln(IC_{50})$ values, for all of the inhibitors that target the predicted kinases. The relative rank of the personalized network prediction score was significantly correlated to kinase inhibitor sensitivity in an aggressive DU-145 cell line ($p < 0.024$; Kendall-tau rank correlation) but not for a second aggressive cell line 22Rv1 (Figures S7A–S7E). In the case of DU-145 cells, the highest activity corresponded well with the strongest response (MAPK14, EGFR, and PTK2) (Figure S7A). Interestingly, for 22Rv1, PRKDC had the highest inferred activity of all kinases and was found to be essential for 22Rv1 survival in a genome-wide RNA silencing screen performed by the Achilles project (Figure S7F). In addition, the predictions for 22Rv1 were also found to be weakly positively correlated overall with the gene essentiality data ($p < 0.07$; Figure S7F). Indeed, a recent publication evaluated PRKDC function in a panel of prostate cancer cell lines, including 22Rv1, and observed that inhibiting PRKDC activity was effective at delaying metastasis formation after tail vein injection (Goodwin et al., 2015). This result provides evidence that PRKDC activity in the 22Rv1 cell line, as predicted in our models, is essential for development of metastases in vivo and targeting this kinase with a PRKDC selective inhibitor was effective at blocking this process. Taken together, both aggressive cell line predictions could be corroborated with either the external drug sensitivity or gene essentiality data despite the known sources of inherent noise in both profiling studies. Future in vitro and in vivo experiments will be necessary to further confirm the results of these data-induced networks.

DISCUSSION

Targeting the synthesis of androgens or AR directly is the current standard of care in advanced prostate cancer and most tumors are responsive to these therapies. Our network models identified and implicated AR signaling as active in this cohort of patient samples. However, current clinical inhibitors targeting AR alone in late stage prostate cancer patients provide survival benefits of only 3–4 months (de Bono et al., 2011; Scher et al., 2012). Previously, we analyzed the abundance of phosphotyrosine peptides

using unbiased quantitative mass spectrometry to identify tyrosine kinase signaling pathways in metastatic CRPC (Drake et al., 2013). Together with this work, we have provided clues into the signaling pathways that are activated in metastatic prostate cancer patients who had received, and became resistant to, anti-androgen therapy and that individual patients with multiple metastatic lesions displayed similar kinase signaling profiles (Drake et al., 2013). If kinase activity is one mechanism by which prostate tumors bypass anti-androgen therapy, then an interesting concept would be the implementation of kinase inhibitor therapies in combination with AR targeted agents. One exception would be patients who develop a lethal variant of CRPC termed small cell neuroendocrine carcinoma (SCNC) as these tumors, on average, lack AR signaling and have been shown to be driven by oncogenes such as MYCN or aurora kinase A (AURKA) (Beltran et al., 2011; Lee et al., 2016). For patients with intact AR signaling, several clinical trials are underway to address combinatorial therapy in metastatic prostate cancer including inhibition of AKT, MET/VEGFR2, or SRC in combination with AR blockade (ClinicalTrials.gov Identifiers: NCT01485861, NCT01995058, NCT01685125). While the results of these trials are still pending, the need for models to predict combinatorial therapies through joint analysis of high-throughput datasets that interrogate multiple aspects of the cell in clinical tissues are essential to identify the key biomarkers for patient stratification and therapy.

We presented pCHIPS as a method to capture multiple perspectives of cellular biology from phosphoproteomic and transcriptomic data integration and present these data at the individual level. Our analysis implicated several signaling proteins such as PRKDC, PRKAA2, PTK2, RPS6KA4, and CDK family members within these pathways as possible new therapeutic targets and/or biomarkers in prostate cancer. In nearly every case, we note a different implicated therapy suggested by the phosphoproteomic data. Interestingly, the transcriptional regulators were found to be more consistent across the metastatic samples while the kinase activities were found to vary. This suggests that the dominant signaling networks driving the biology of each patient may converge on the downstream transcriptional programs identified by the gene expression data. Several patients with marked differences in response to therapy (e.g., anti-androgens or chemotherapy; Data S1A) have highly similar transcriptomes as evidenced by the transcription factors identified by VIPER for the 16 metastatic CRPC samples. The differences in protein level signaling could help explain the variable responses and offer new treatment options to abrogate the signaling upstream of these TF-driven circuits.

An intriguing question is whether network-based approaches like the one presented here yield similar or complementary information about treatment strategy compared to those based on so-called actionable mutations. First, for the five patient samples for which we had genomics data, we found cases in which different hallmarks were implicated with the patient-specific networks compared to using only the mutational information. Seven hallmarks were concordant across the patients, seven were discordant, and five agreed in a subset of patients (see Figure S6B). Second, we used the models derived from cell lines to investigate whether the presence of mutations or inferred activated kinases were more informative about drug sensitivity. We tabulated the data and found that the inferred phospho-based activities were as indicative of drug response as the presence of somatic mutations in those pathways and, when averaged across pathways and cell lines, these data suggest one type of data is sufficient to implicate pathway targets (Figure S7G; Data S1L and S1M). Importantly, for an individual patient afflicted with a tumor that lacks mutations in known actionable pathways, phosphoproteomic data could be informative to prioritize treatment.

Continued development of these computational strategies will enable better determination of the specific vulnerabilities in individual tumors as our work sheds light on the diversity of the activated signaling pathways in metastatic CRPC tumors. These data and resulting pathway-based inferences establish a window into the regulation of protein signaling of aggressive tumors and a valuable reference for further investigation. Specifically, cell-line-specific networks and kinase targets could be selected to inhibit cell growth or to test whether inhibition of kinases at higher levels can abrogate those at lower levels of the signaling hierarchy. Ultimately, further interrogation of these networks in appropriate pre-clinical models to assess co-targeting or combination therapies are necessary and warrant future investigation into patient stratification prior to clinical intervention. To facilitate such follow-up investigations, we have made available several modalities of the data and results. The mass spectrometry proteomics data have been deposited to the ProteomeXchange Consortium via the PRIDE partner repository with the dataset identifier PXD002286 (Vizcaíno et al., 2014). In addition to these data, the results are available through the UCSC TumorMap portal (http://tumormap.ucsc.edu/), providing public access to the assayed and predicted phosphorylation levels for primary and metastatic prostate cancer datasets from several public sources. Finally, we provide an online tool (https://sysbiowiki.soe.ucsc.edu/pchips) for users to input gene expression data to develop their own phosphoproteome-guided networks without the need for their own phosphoproteome data.

EXPERIMENTAL PROCEDURES

Quantitative Analysis of Phosphoserine and Phosphothreonine Peptides by Quantitative Mass Spectrometry

Phosphopeptide enrichment was performed as previously described (Zimman et al., 2010) with minor modifications. The desalted peptide mixture was fractionated online using EASY-spray columns (25 cm × 75 μm ID, PepMap RSLC C18 2 μm). The gradient was delivered by an easy-nLC 1000 ultra high-pressure liquid chromatography (UHPLC) system (Thermo Scientific). Tandem mass spectrometry (MS/MS) spectra were collected on a Q-Exactive mass spectrometer (Thermo Scientific) (Kelstrup et al., 2012; Michalski et al., 2011). Samples were run in technical duplicates, and raw MS files were analyzed using MaxQuant version 1.4.1.2 (Cox and Mann, 2008). MS/MS fragmentation spectra were searched using ANDROMEDA against the Uniprot human reference proteome database with canonical and isoform sequences (downloaded January 2012 from http://uniprot.org). N-terminal acetylation, oxidized methionine, and phosphorylated serine, threonine, or tyrosine were set as variable modifications, and carbamidomethyl cysteine (*C) was set as a fixed modification. The false discovery rate was set to 1% using a composite target-reversed decoy database search strategy. Group-specific parameters included max missed cleavages of two and label-free quantitation (LFQ) with an LFQ minimum ratio count of one. Global parameters included match between runs with a match time

window and alignment time window of 5 and 20 min, respectively, and match unidentified features selected.

MS Data Analysis

Quantitative, label-free phosphopeptide data from MaxQuant were $\log_{10}$ transformed and missing data were imputed using random values generated from a normal distribution centered on the 1% quantile and the median SD of all phosphopeptides (Deeb et al., 2012). After missing value imputation, phosphopeptides were quantile normalized. For clustering, phosphopeptide data were filtered using an FDR-corrected ANOVA p value of 0.05. Hierarchical clustering was performed using the Cluster 3.0 program with the Pearson correlation and pairwise complete linkage analysis (Eisen et al., 1998). Java TreeView was used to visualize clustering results (Saldanha, 2004). Quantitative data for each phosphopeptide can be found in Data S1B–S1D.

TieDIE Pathway Analysis of Clinical Prostate Cancer Samples

We used the TieDIE algorithm (Paull et al., 2013) to connect 35 kinases and "kinase regulators," 108 putative cancer driver genes with genomic perturbations in CRPC, and 74 transcription factors, using the "Multinet" (Khurana et al., 2013) pathway database consisting of a diverse set of literature-based gene-gene interactions (43,722 protein-protein interactions; 27,900 direct phosphorylation; 27,914 transcriptional/regulatory; 9,714 metabolic; genetic interactions excluded). Each of these three inputs were treated as a separate, equally weighted, input set for the algorithm, while the gene members of each input set were weighted by the total evidence for each protein: kinases by combined SAM d-statistic and MARINa inferred activity level, transcription factors by MARINa inferred activity level, and genomic events by the number of mutations and copy-number alterations observed in the 49 metastatic prostate cancer samples. The kinase, genomic event and TF gene sets were found to be significantly close in pathway space ($p < 0.012$; Figure S2A), according to a conservative background model run with 1,000 permutations of the input data.

The resulting network consisted of 338 nodes and 1,889 edges (597 direct phosphorylation; 1,184 protein-protein interaction; 102 transcriptional/regulatory; 6 metabolic). This network was filtered further by restricting to protein-protein edges with at least one pair of constituent phosphopeptides with at least modest correlation (Spearman rank correlation, Rho $\geq$ 0.3), resulting in a final "scaffold" network of 122 nodes and 256 edges (190 protein-protein interaction; 131 phosphorylation).

Cancer Hallmark Enrichment Analysis

Cancer hallmark definitions were downloaded from the GSEA/MSigDB (http://www.broadinstitute.org/gsea/msigdb) database and reduced to hallmarks highly linked to cancer (Data S1J). Enrichment analysis was performed by calculating the probability of overlap between the test set (defined by the set of genes in a network model) and the hallmark sets, using the hypergeometric distribution. Hallmark "wheels" were colored proportionally to the negative log p value returned by the hypergeometric test.

Patient-Specific Network Generation and Kinase Target Prediction

To generate sample-specific networks, we used the VIPER package (Alvarez et al., 2015) to infer sample-specific activity and applied thresholds derived from the MARINa analysis to each sample's data, generating binary calls for each of the 35 kinase regulators and 74 TFs, respectively. Scores for the 24 peptides with significant differential phosphorylation activity were z-normalized by gene and thresholded at a Z score of 1.0 or above, while VIPER pseudo Z scores were thresholded at the level corresponding to a 0.1 FDR cutoff in each corresponding Network Enrichment Score for MARINa analysis (Supplemental Experimental Procedures). Functional "high-level" copy-number gain and loss was assessed with the GISTIC algorithm (Mermel et al., 2011). For each sample, we searched all paths connecting any active kinase, mutation or high-level copy-number gain or deletion to any active TF over edges contained in the scaffold network, using the NetworkX python package (Hagberg et al., 2008).

For all proteins in each patient-specific network, we performed three independent rankings based on the phosphorylation activity of functionally annotated peptides, VIPER inferred activity scores, and the network connectivity as measured by the shortest-path betweenness centrality for all genes. These three independent rankings were averaged for each protein providing a patient-specific network (PNET) score, from which a final combined ranking of all proteins for each patient was derived (Figure 7).

Statistical Analysis

All statistical data were presented after either t tests or one-way ANOVA as described in the figure legends. Correlation analysis was performed for each pair of proteins with an edge in the TieDIE network, by calculating the pairwise Spearman correlation between all corresponding peptides; only protein-protein edges with at least moderate positive or anti-correlation (Rho $\geq$ 0.3; Rho $\leq$ 0.3) between one pair of respective peptides were retained.

ACCESSION NUMBERS

The accession number for the mass spectrometry proteomics data reported in this paper is ProteomeXchange Consortium: PXD002286.

SUPPLEMENTAL INFORMATION

Supplemental Information includes Supplemental Experimental Procedures, seven figures, and two data files and can be found with this article online at http://dx.doi.org/10.1016/j.cell.2016.07.007.

AUTHOR CONTRIBUTIONS

Conceptualization and Methodology, J.M.D., E.O.P., N.A.G., T.G.G., J.M.S., and O.N.W.; Investigation, J.M.D., E.O.P., N.A.G., J.K.L., B.A.S., T.S., and C.M.F.; Resources, A.A.V., J.A.W., S.S., C.K.W., Y.N., E.O.P., and D.T.F.; Formal Analysis, J.M.D., E.O.P., N.A.G., J.K.L., B.T., and J.H.; Writing – Original Draft, J.M.D., E.O.P., J.M.S., and O.N.W.; Writing – Review and Editing, all authors.

ACKNOWLEDGMENTS

We thank members of the O.N.W. and J.M.S. labs for helpful comments and discussion on the manuscript and the University of Michigan for supplying material from their rapid autopsy program. J.M.D. is supported by the Department of Defense Prostate Cancer Research Program W81XWH-14-1-0148, Prostate Cancer Foundation Young Investigator Award, and a New Jersey Health Foundation Research grant. N.A.G. is supported by UCLA Scholars in Oncologic Molecular Imaging (SOMI) program, NIH grant R25T CA098010. J.K.L. is supported by Specialty Training and Advanced Research (STAR) Program at UCLA, Prostate Cancer Foundation Young Investigator Award, and Tower Cancer Research Foundation Career Development Award. B.A.S. is supported by the UCLA Tumor Immunology Training grant T32 CA009120, American Cancer Society Postdoctoral Fellowship PF-16-082-01-TBE, and Prostate Cancer Foundation Young Investigator Award. T.S. is supported by Prostate Cancer Foundation Young Investigator Award and NIH/National Cancer Institute K99 Pathway to Independence Award 4R00CA184397. C.M.F. is supported by the UCLA Medical Scientist Training Program. J.H. is supported by NIH grants 5R01CA172603-02, 2P30CA016042-39, 1R01CA181242-01A1, 1R01CA195505, the Department of Defense Prostate Cancer Research Program W81XWH-12-1-0206, UCLA SPORE in prostate cancer, Prostate Cancer Foundation Honorable A. David Mazzone Special Challenge Award, and UCLA Jonsson Comprehensive Cancer Center Impact Grant. J.A.W. is supported by NIH GM089778. T.G.G. is supported by the NCI/NIH P01 CA168585, an American Cancer Society Research Scholar Award RSG-12-257-01-TBE, the CalTech-UCLA Joint Center for Translational Medicine, the UCLA Jonsson Cancer Center Foundation, the National Center for Advancing Translational Sciences UCLA CTSI grant UL1TR000124, and a Concern Foundation CONquer CanCER Now Award. J.M.S. is supported by NCI/NIH U24-CA143858, NCI/NIH 1R01CA180778, NHGRI/NIH 5U54HG006097, and NIGMS/NIH 5R01GM109031 grants. O.N.W. is an Investigator of the Howard Hughes Medical Institute and is supported by the Zimmerman Family, the Concern Foundation, and by a Prostate Cancer Foundation Challenge Award.

J.H., T.G.G., J.M.S., and O.N.W. are supported by the West Coast Prostate Cancer Dream Team supported by Stand Up to Cancer/AACR/Prostate Cancer Foundation SU2C-AACR-DT0812 (O.N.W. co-PI). This research grant is made possible by the generous support of the Movember Foundation. Stand Up To Cancer is a program of the Entertainment Industry Foundation administered by the American Association for Cancer Research.

Received: November 30, 2015
Revised: March 15, 2016
Accepted: July 7, 2016
Published: August 4, 2016

REFERENCES

Alvarez, M.J., Giorgi, F., and Califano, A. (2015). Using VIPER, a package for virtual inference of protein-activity by enriched regulon analysis (Bioconductor).

Aytes, A., Mitrofanova, A., Lefebvre, C., Alvarez, M.J., Castillo-Martin, M., Zheng, T., Eastham, J.A., Gopalan, A., Pienta, K.J., Shen, M.M., et al. (2014). Cross-species regulatory network analysis identifies a synergistic interaction between FOXM1 and CENPF that drives prostate cancer malignancy. Cancer Cell *25*, 638–651.

Beltran, H., Rickman, D.S., Park, K., Chae, S.S., Sboner, A., MacDonald, T.Y., Wang, Y., Sheikh, K.L., Terry, S., Tagawa, S.T., et al. (2011). Molecular characterization of neuroendocrine prostate cancer and identification of new drug targets. Cancer Discov. *1*, 487–495.

Cancer Genome Atlas Network (2012a). Comprehensive molecular characterization of human colon and rectal cancer. Nature *487*, 330–337.

Cancer Genome Atlas Network (2012b). Comprehensive molecular portraits of human breast tumours. Nature *490*, 61–70.

Cancer Genome Atlas Research Network (2013). Comprehensive molecular characterization of clear cell renal cell carcinoma. Nature *499*, 43–49.

Cancer Genome Atlas Research Network (2014a). Integrated genomic characterization of papillary thyroid carcinoma. Cell *159*, 676–690.

Cancer Genome Atlas Research Network (2014b). Comprehensive molecular characterization of urothelial bladder carcinoma. Nature *507*, 315–322.

Cancer Genome Atlas Research Network (2015). The molecular taxonomy of primary prostate cancer. Cell *163*, 1011–1025.

Casado, P., Rodriguez-Prados, J.-C., Cosulich, S.C., Guichard, S., Vanhaesebroeck, B., Joel, S., and Cutillas, P.R. (2013). Kinase-substrate enrichment analysis provides insights into the heterogeneity of signaling pathway activation in leukemia cells. Sci. Signal. *6*, rs6.

Chang, C.-J., Yang, J.-Y., Xia, W., Chen, C.-T., Xie, X., Chao, C.-H., Woodward, W.A., Hsu, J.-M., Hortobagyi, G.N., and Hung, M.-C. (2011). EZH2 promotes expansion of breast tumor initiating cells through activation of RAF1-β-catenin signaling. Cancer Cell *19*, 86–100.

Chen, J.C., Alvarez, M.J., Talos, F., Dhruv, H., Rieckhof, G.E., Iyer, A., Diefes, K.L., Aldape, K., Berens, M., Shen, M.M., and Califano, A. (2014). Identification of causal genetic drivers of human disease through systems-level analysis of regulatory networks. Cell *159*, 402–414.

Cheng, A.S.L., Lau, S.S., Chen, Y., Kondo, Y., Li, M.S., Feng, H., Ching, A.K., Cheung, K.F., Wong, H.K., Tong, J.H., et al. (2011). EZH2-mediated concordant repression of Wnt antagonists promotes β-catenin-dependent hepatocarcinogenesis. Cancer Res. *71*, 4028–4039.

Cox, J., and Mann, M. (2008). MaxQuant enables high peptide identification rates, individualized p.p.b.-range mass accuracies and proteome-wide protein quantification. Nat. Biotechnol. *26*, 1367–1372.

de Bono, J.S., Logothetis, C.J., Molina, A., Fizazi, K., North, S., Chu, L., Chi, K.N., Jones, R.J., Goodman, O.B., Jr., Saad, F., et al.; COU-AA-301 Investigators (2011). Abiraterone and increased survival in metastatic prostate cancer. N. Engl. J. Med. *364*, 1995–2005.

Deeb, S.J., D'Souza, R.C.J., Cox, J., Schmidt-Supprian, M., and Mann, M. (2012). Super-SILAC allows classification of diffuse large B-cell lymphoma subtypes by their protein expression profiles. Mol. Cell. Proteomics *11*, 77–89.

Drake, J.M., Graham, N.A., Stoyanova, T., Sedghi, A., Goldstein, A.S., Cai, H., Smith, D.A., Zhang, H., Komisopoulou, E., Huang, J., et al. (2012). Oncogene-specific activation of tyrosine kinase networks during prostate cancer progression. Proc. Natl. Acad. Sci. USA *109*, 1643–1648.

Drake, J.M., Graham, N.A., Lee, J.K., Stoyanova, T., Faltermeier, C.M., Sud, S., Titz, B., Huang, J., Pienta, K.J., Graeber, T.G., and Witte, O.N. (2013). Metastatic castration-resistant prostate cancer reveals intrapatient similarity and interpatient heterogeneity of therapeutic kinase targets. Proc. Natl. Acad. Sci. USA *110*, E4762–E4769.

Eisen, M.B., Spellman, P.T., Brown, P.O., and Botstein, D. (1998). Cluster analysis and display of genome-wide expression patterns. Proc. Natl. Acad. Sci. USA *95*, 14863–14868.

Gioeli, D., Mandell, J.W., Petroni, G.R., Frierson, H.F., Jr., and Weber, M.J. (1999). Activation of mitogen-activated protein kinase associated with prostate cancer progression. Cancer Res. *59*, 279–284.

Gonzalez, M.E., DuPrie, M.L., Krueger, H., Merajver, S.D., Ventura, A.C., Toy, K.A., and Kleer, C.G. (2011). Histone methyltransferase EZH2 induces Akt-dependent genomic instability and BRCA1 inhibition in breast cancer. Cancer Res. *71*, 2360–2370.

Goodwin, J.F., Kothari, V., Drake, J.M., Zhao, S., Dylgjeri, E., Dean, J.L., Schiewer, M.J., McNair, C., Jones, J.K., Aytes, A., et al. (2015). DNA-PKcs-mediated transcriptional regulation drives prostate cancer progression and metastasis. Cancer Cell *28*, 97–113.

Grasso, C.S., Wu, Y.-M., Robinson, D.R., Cao, X., Dhanasekaran, S.M., Khan, A.P., Quist, M.J., Jing, X., Lonigro, R.J., Brenner, J.C., et al. (2012). The mutational landscape of lethal castration-resistant prostate cancer. Nature *487*, 239–243.

Hagberg, A.A., Schult, D.A., and Swart, P.J. (2008). Exploring network structure, dynamics, and function using NetworkX. In Proceedings of the 7th Python in Science Conference, G. Varoquaux, T. Vaught, and J. Millman, eds. (SciPy2008), pp. 11–15.

Huang, S.-S.C., Clarke, D.C., Gosline, S.J.C., Labadorf, A., Chouinard, C.R., Gordon, W., Lauffenburger, D.A., and Fraenkel, E. (2013). Linking proteomic and transcriptional data through the interactome and epigenome reveals a map of oncogene-induced signaling. PLoS Comput. Biol. *9*, e1002887.

Hunter, T. (2009). Tyrosine phosphorylation: thirty years and counting. Curr. Opin. Cell Biol. *21*, 140–146.

Kandoth, C., McLellan, M.D., Vandin, F., Ye, K., Niu, B., Lu, C., Xie, M., Zhang, Q., McMichael, J.F., Wyczalkowski, M.A., et al. (2013). Mutational landscape and significance across 12 major cancer types. Nature *502*, 333–339.

Kelstrup, C.D., Young, C., Lavallee, R., Nielsen, M.L., and Olsen, J.V. (2012). Optimized fast and sensitive acquisition methods for shotgun proteomics on a quadrupole orbitrap mass spectrometer. J. Proteome Res. *11*, 3487–3497.

Khurana, E., Fu, Y., Chen, J., and Gerstein, M. (2013). Interpretation of genomic variants using a unified biological network approach. PLoS Comput. Biol. *9*, e1002886.

Lee, J.K., Phillips, J.W., Smith, B.A., Park, J.W., Stoyanova, T., McCaffrey, E.F., Baertsch, R., Sokolov, A., Meyerowitz, J.G., Mathis, C., et al. (2016). N-Myc drives neuroendocrine prostate cancer initiated from human prostate epithelial cells. Cancer Cell *29*, 536–547.

Li, W., Ai, N., Wang, S., Bhattacharya, N., Vrbanac, V., Collins, M., Signoretti, S., Hu, Y., Boyce, F.M., Gravdal, K., et al. (2014). GRK3 is essential for metastatic cells and promotes prostate tumor progression. Proc. Natl. Acad. Sci. USA *111*, 1521–1526.

Lu, S., Tsai, S.Y., and Tsai, M.J. (1997). Regulation of androgen-dependent prostatic cancer cell growth: androgen regulation of CDK2, CDK4, and CKI p16 genes. Cancer Res. *57*, 4511–4516.

Mermel, C.H., Schumacher, S.E., Hill, B., Meyerson, M.L., Beroukhim, R., and Getz, G. (2011). GISTIC2.0 facilitates sensitive and confident localization of the targets of focal somatic copy-number alteration in human cancers. Genome Biol. *12*, R41.

Michalski, A., Damoc, E., Hauschild, J.-P., Lange, O., Wieghaus, A., Makarov, A., Nagaraj, N., Cox, J., Mann, M., and Horning, S. (2011). Mass spectrometry-based proteomics using Q Exactive, a high-performance benchtop quadrupole Orbitrap mass spectrometer. Mol. Cell. Proteomics *10*, M111.011015.

Morin, P.J., Sparks, A.B., Korinek, V., Barker, N., Clevers, H., Vogelstein, B., and Kinzler, K.W. (1997). Activation of beta-catenin-Tcf signaling in colon cancer by mutations in beta-catenin or APC. Science *275*, 1787–1790.

Newman, R.H., Hu, J., Rho, H.-S., Xie, Z., Woodard, C., Neiswinger, J., Cooper, C., Shirley, M., Clark, H.M., Hu, S., et al. (2013). Construction of human activity-based phosphorylation networks. Mol. Syst. Biol. *9*, 655.

Ning, X., Shi, Z., Liu, X., Zhang, A., Han, L., Jiang, K., Kang, C., and Zhang, Q. (2015). DNMT1 and EZH2 mediated methylation silences the microRNA-200b/a/429 gene and promotes tumor progression. Cancer Lett. *359*, 198–205.

Pandey, M., Sahay, S., Tiwari, P., Upadhyay, D.S., Sultana, S., and Gupta, K.P. (2014). Involvement of EZH2, SUV39H1, G9a and associated molecules in pathogenesis of urethane induced mouse lung tumors: potential targets for cancer control. Toxicol. Appl. Pharmacol. *280*, 296–304.

Park, H.U., Suy, S., Danner, M., Dailey, V., Zhang, Y., Li, H., Hyduke, D.R., Collins, B.T., Gagnon, G., Kallakury, B., et al. (2009). AMP-activated protein kinase promotes human prostate cancer cell growth and survival. Mol. Cancer Ther. *8*, 733–741.

Paull, E.O., Carlin, D.E., Niepel, M., Sorger, P.K., Haussler, D., and Stuart, J.M. (2013). Discovering causal pathways linking genomic events to transcriptional states using Tied Diffusion Through Interacting Events (TieDIE). Bioinformatics *29*, 2757–2764.

Pawson, T. (2004). Specificity in signal transduction: from phosphotyrosine-SH2 domain interactions to complex cellular systems. Cell *116*, 191–203.

Robinson, D., Van Allen, E.M., Wu, Y.-M., Schultz, N., Lonigro, R.J., Mosquera, J.-M., Montgomery, B., Taplin, M.-E., Pritchard, C.C., Attard, G., et al. (2015). Integrative clinical genomics of advanced prostate cancer. Cell *161*, 1215–1228.

Rubin, M.A., Putzi, M., Mucci, N., Smith, D.C., Wojno, K., Korenchuk, S., and Pienta, K.J. (2000). Rapid ("warm") autopsy study for procurement of metastatic prostate cancer. Clin. Cancer Res. *6*, 1038–1045.

Saldanha, A.J. (2004). Java Treeview–extensible visualization of microarray data. Bioinformatics *20*, 3246–3248.

Scher, H.I., Fizazi, K., Saad, F., Taplin, M.-E., Sternberg, C.N., Miller, K., de Wit, R., Mulders, P., Chi, K.N., Shore, N.D., et al.; AFFIRM Investigators (2012). Increased survival with enzalutamide in prostate cancer after chemotherapy. N. Engl. J. Med. *367*, 1187–1197.

Smith, B.A., Sokolov, A., Uzunangelov, V., Baertsch, R., Newton, Y., Graim, K., Mathis, C., Cheng, D., Stuart, J.M., and Witte, O.N. (2015). A basal stem cell signature identifies aggressive prostate cancer phenotypes. Proc. Natl. Acad. Sci. USA *112*, E6544–E6552.

Subramanian, A., Tamayo, P., Mootha, V.K., Mukherjee, S., Ebert, B.L., Gillette, M.A., Paulovich, A., Pomeroy, S.L., Golub, T.R., Lander, E.S., and Mesirov, J.P. (2005). Gene set enrichment analysis: a knowledge-based approach for interpreting genome-wide expression profiles. Proc. Natl. Acad. Sci. USA *102*, 15545–15550.

Taylor, B.S., Schultz, N., Hieronymus, H., Gopalan, A., Xiao, Y., Carver, B.S., Arora, V.K., Kaushik, P., Cerami, E., Reva, B., et al. (2010). Integrative genomic profiling of human prostate cancer. Cancer Cell *18*, 11–22.

Vaske, C.J., Benz, S.C., Sanborn, J.Z., Earl, D., Szeto, C., Zhu, J., Haussler, D., and Stuart, J.M. (2010). Inference of patient-specific pathway activities from multi-dimensional cancer genomics data using PARADIGM. Bioinformatics *26*, i237–i245.

Vizcaíno, J.A., Deutsch, E.W., Wang, R., Csordas, A., Reisinger, F., Ríos, D., Dianes, J.A., Sun, Z., Farrah, T., Bandeira, N., et al. (2014). ProteomeXchange provides globally coordinated proteomics data submission and dissemination. Nat. Biotechnol. *32*, 223–226.

Wang, G., Ahmad, K.A., Unger, G., Slaton, J.W., and Ahmed, K. (2006). CK2 signaling in androgen-dependent and -independent prostate cancer. J. Cell. Biochem. *99*, 382–391.

Yang, W., Soares, J., Greninger, P., Edelman, E.J., Lightfoot, H., Forbes, S., Bindal, N., Beare, D., Smith, J.A., Thompson, I.R., et al. (2013). Genomics of Drug Sensitivity in Cancer (GDSC): a resource for therapeutic biomarker discovery in cancer cells. Nucleic Acids Res. *41*, D955–D961.

Yu, G., Lee, Y.-C., Cheng, C.-J., Wu, C.-F., Song, J.H., Gallick, G.E., Yu-Lee, L.-Y., Kuang, J., and Lin, S.-H. (2015). RSK promotes prostate cancer progression in bone through ING3, CKAP2, and PTK6-mediated cell survival. Mol. Cancer Res. *13*, 348–357.

Zimman, A., Chen, S.S., Komisopoulou, E., Titz, B., Martínez-Pinna, R., Kafi, A., Berliner, J.A., and Graeber, T.G. (2010). Activation of aortic endothelial cells by oxidized phospholipids: a phosphoproteomic analysis. J. Proteome Res. *9*, 2812–2824.

Activation of Notch1 synergizes with multiple pathways in promoting castration-resistant prostate cancer

Tanya Stoyanova[a,b,1], Mireille Riedinger[c], Shu Lin[d], Claire M. Faltermeier[b], Bryan A. Smith[b], Kelvin X. Zhang[e], Catherine C. Going[a], Andrew S. Goldstein[d,f,g], John K. Lee[h], Justin M. Drake[b,i,j], Meghan A. Rice[a], En-Chi Hsu[a], Behdokht Nowroozizadeh[k,l], Brandon Castor[l], Sandra Y. Orellana[b], Steven M. Blum[b,m], Donghui Cheng[f], Kenneth J. Pienta[n], Robert E. Reiter[d], Sharon J. Pitteri[a], Jiaoti Huang[l,o], and Owen N. Witte[b,c,f,p,1]

[a]Department of Radiology, Canary Center at Stanford for Cancer Early Detection, Stanford University School of Medicine, Palo Alto, CA 94304; [b]Department of Microbiology, Immunology, and Molecular Genetics, University of California, Los Angeles, CA 90095; [c]Department of Molecular and Medical Pharmacology, University of California, Los Angeles, CA 90095; [d]Department of Urology, University of California, Los Angeles, CA 90095; [e]Department of Biological Chemistry, University of California, Los Angeles, CA 90095; [f]Eli and Edythe Broad Center of Regenerative Medicine and Stem Cell Research, University of California, Los Angeles, CA 90095; [g]Department of Molecular, Cell and Developmental Biology, University of California, Los Angeles, CA 90095; [h]Division of Hematology and Medical Oncology, University of California, Los Angeles, CA 90095; [i]Rutgers Cancer Institute of New Jersey, New Brunswick, NJ, 08903; [j]Department of Medicine, Rutgers-Robert Wood Johnson Medical School, New Brunswick, NJ, 08901; [k]Department of Pathology, University of California, Irvine, CA 92697; [l]Department of Pathology and Laboratory Medicine, University of California, Los Angeles, CA 90095; [m]Department of Internal Medicine, Brigham and Women's Hospital, Boston, MA 02115; [n]Brady Urological Institute, Johns Hopkins School of Medicine, Baltimore, MD 21287; [o]Department of Pathology, Duke University School of Medicine, Durham, NC 27710; and [p]Howard Hughes Medical Institute, University of California, Los Angeles, CA 90095

Contributed by Owen N. Witte, August 31, 2016 (sent for review May 16, 2016; reviewed by Warren S. Pear and Robert L. Vessella)

Metastatic castration-resistant prostate cancer (CRPC) is the primary cause of prostate cancer-specific mortality. Defining new mechanisms that can predict recurrence and drive lethal CRPC is critical. Here, we demonstrate that localized high-risk prostate cancer and metastatic CRPC, but not benign prostate tissues or low/intermediate-risk prostate cancer, express high levels of nuclear Notch homolog 1, translocation-associated (Notch1) receptor intracellular domain. Chronic activation of Notch1 synergizes with multiple oncogenic pathways altered in early disease to promote the development of prostate adenocarcinoma. These tumors display features of epithelial-to-mesenchymal transition, a cellular state associated with increased tumor aggressiveness. Consistent with its activation in clinical CRPC, tumors driven by Notch1 intracellular domain in combination with multiple pathways altered in prostate cancer are metastatic and resistant to androgen deprivation. Our study provides functional evidence that the Notch1 signaling axis synergizes with alternative pathways in promoting metastatic CRPC and may represent a new therapeutic target for advanced prostate cancer.

prostate | cancer | Notch1

The first line of treatment for men with advanced prostate cancer is androgen deprivation therapy. However, the disease commonly relapses to a lethal metastatic form referred to as "castration-resistant prostate cancer" (CRPC) (1). Current therapies for CRPC include second-generation androgen inhibitors (enzalutamide and abiraterone acetate), chemotherapeutic agents (docetaxel), and immunotherapy (Sipuleucel-T). Unfortunately, these agents improve median overall survival by only 4 months (2, 3). There is an urgent need to define the pathways that drive metastatic CRPC, possibly gaining insights into new therapeutic strategies for targeting the advanced disease.

The Notch family of receptors regulates cell-fate determination throughout development in many organ systems, including the prostate (4–7). In neonatal and adult mouse prostate tissues, disruption of Notch signaling inhibits prostate epithelial cell differentiation (4). Notch homolog 1, translocation-associated (Notch1) was also shown to promote mouse luminal prostate cell survival and proliferation through the activation of the prosurvival NF-κB pathway (5). Elevated expression of the Notch ligand Jagged1 has been associated with metastatic prostate cancer (8, 9), and downregulation of Notch1 and Jagged1 in human prostate cancer cell lines decreases in vitro invasion and cell growth (10). In addition, chemoresistance in human prostate cancer cells has been linked to the activation of Notch2 receptors (11, 12). Despite these studies, direct evaluation of Notch receptors as drivers of aggressive prostate cancer and the relationship of Notch receptors with other commonly altered pathways in prostate tumorigenesis remain unclear.

The canonical Notch pathway is activated through binding of Notch ligands (Jagged1/2 and Delta-like 1/3/4) to Notch receptors (1/2/3/4) (13–19). Ligand binding induces Notch-receptor cleavage through regulated intramembrane proteolysis (13–21), a multistep process carried out by members of the A Disintegrin and Metalloprotease (ADAMs) family within the extracellular region and by the γ-secretase complex within the transmembrane domain of Notch cell-surface receptors. Upon cleavage, the Notch intracellular domain (NICD) is released and translocates to the nucleus, where it is referred to as "activated Notch" (13–21). NICD serves as a transcriptional coactivator that in turn regulates a set of genes involved in proliferation, self-renewal, survival, and differentiation (20, 21).

Significance

A high nuclear Notch homolog 1, translocation-associated (Notch1) intracellular domain level distinguishes high-risk prostate cancer and castration-resistant prostate cancer from benign and low/intermediate-risk prostate cancer. Chronic activation of Notch1 cooperates with multiple oncogenic pathways altered in early prostate cancer, including AKT, Myc, and Ras/Raf/MAPK, to promote progression to androgen ablation-resistant prostate adenocarcinoma.

Author contributions: T.S., S.L., A.S.G., J.K.L., J.M.D., and O.N.W. designed research; T.S., M.R., C.M.F., B.A.S., K.X.Z., C.C.G., M.A.R., E.-C.H., B.N., B.C., S.Y.O., S.M.B., D.C., and S.J.P. performed research; K.J.P. and J.H. contributed new reagents/analytic tools; T.S., M.R., S.L., C.M.F., B.A.S., K.X.Z., C.C.G., A.S.G., J.K.L., J.M.D., M.A.R., E.-C.H., B.N., B.C., S.Y.O., S.M.B., D.C., R.E.R., S.J.P., J.H., and O.N.W. analyzed data; and T.S. and O.N.W. wrote the paper.

Reviewers: W.S.P., University of Pennsylvania; and R.L.V., University of Washington.

The authors declare no conflict of interest.

Freely available online through the PNAS open access option.

Data deposition: The sequences reported in this paper have been deposited in the Gene Expression Omnibus (GEO) database, www.ncbi.nlm.nih.gov/geo (accession no. GSE87448).

[1]To whom correspondence may be addressed. Email: stanya@stanford.edu or owenwitte@mednet.ucla.edu.

This article contains supporting information online at www.pnas.org/lookup/suppl/doi:10.1073/pnas.1614529113/-/DCSupplemental.

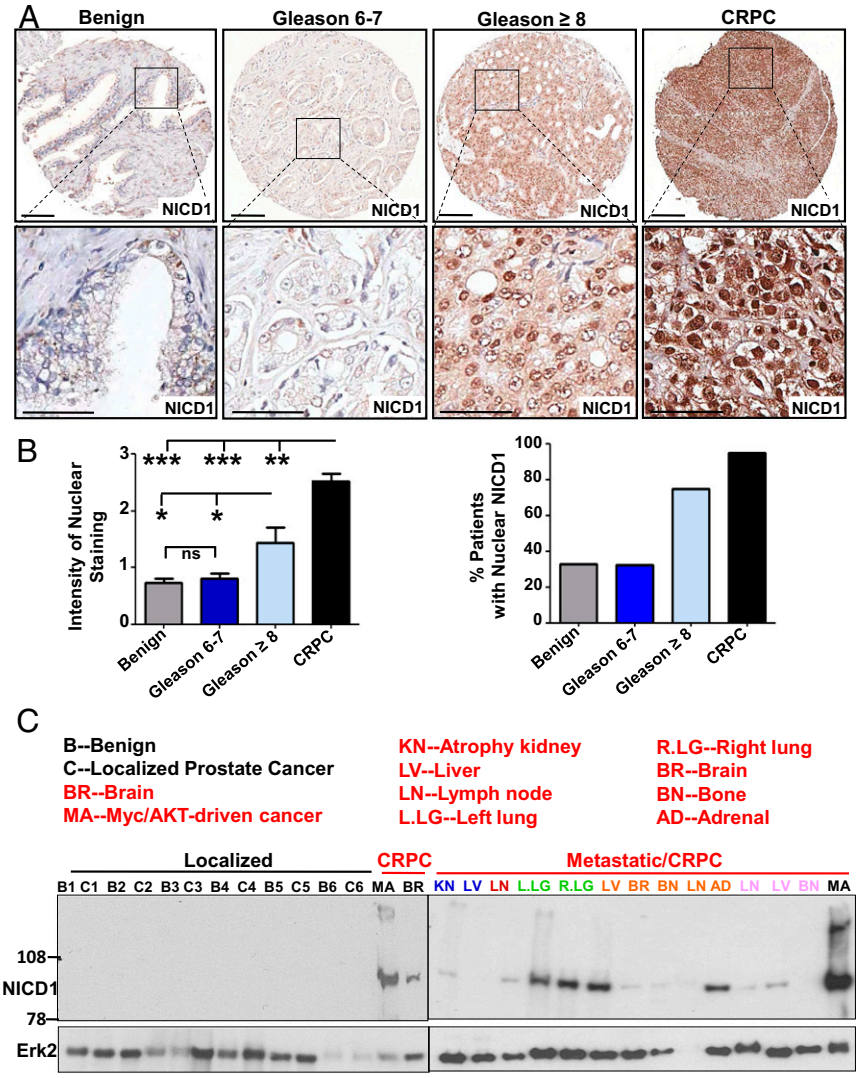

Fig. 1. The Notch1 receptor intracellular domain is highly elevated in advanced human prostate cancer. (*A*) Human prostate TMAs were stained with an antibody against NICD1 (Novus Biologicals). Representative images are shown. (Scale bars: 100 microns in *Upper Row* and 50 microns in *Lower Row*.) (*B*) NICD1 expression was scored from 0–3 in benign tissue (n = 221), localized low- to intermediate-risk prostate cancer (Gleason score 6 or 7) (n = 207), localized high-risk prostate cancer (Gleason score 8–10) (n = 23), and CPRC (n = 19) specimens. (*Left*) The intensity of nuclear staining was plotted. ***$P < 0.0001$. **$P < 0.005$; *$P < 0.05$; ns, nonsignificant; one-way ANOVA. (*Right*) Percentage of patients exhibiting nuclear NICD1. (*C*) Western blot analyses were performed with anti-NICD1 antibody (Epitomics/Abcam) and anti-Erk2 used as loading control using the following specimens. (*i*) Human specimens were separated into regions of benign tissue and low- to intermediate-risk prostate cancer by a urologic pathologist. (*ii*) Metastatic CRPC tissues were obtained from the rapid autopsy program at the University of Michigan. (*iii*) The Myc/myrAKT CRPC model initiated in primary human cells. Metastatic CRPC tissues were obtained from total of eight different patients (including the samples presented in Fig. S1). Twenty-three distinct metastatic sites are shown. Each distinct patient is indicated by a different color.

Components of the Notch signaling pathway are altered in multiple cancers (21–32). Interestingly, Notch signaling previously has been reported to function as both a tumor suppressor and an oncogene (21–32). The dependency of Notch1 function in cancer may be tissue specific and context dependent (21–32). Loss-of-function mutations in Notch receptors support their tumor-suppressive role in multiple malignances, including bladder cancer and squamous cell carcinoma (22–24). Constitutive activation of the Notch receptors through gene rearrangements or mutations leads to Notch receptors' oncogenic function in 55–60% of patients with T-cell acute lymphoblastic leukemia (26, 27). An oncogenic role of Notch1 also has been demonstrated in chronic lymphocytic leukemia and in solid tumors such as lung adenocarcinoma and others (28–31). Mutations within Notch1 receptor are rare (3% frequency) in metastatic prostate cancer (32, 33).

Here we report significantly elevated levels of nuclear NICD1 in hormone-naive high-risk prostate cancer and nearly all metastatic CRPC specimens but not in benign tissues or low- and intermediate-risk localized prostate cancer. Although overexpression of NICD1 alone was not sufficient to drive prostate tumorigenesis, NICD1 in combination with components of pathways commonly altered in early prostate cancer, such as myristoylated AKT, Myc, and Ras/Raf/MAPK, promoted the development of aggressive prostate adenocarcinoma and progression to CRPC. Consistent with their aggressiveness, these tumors displayed an epithelial-to-mesenchymal (EMT) transition phenotype, high self-renewal, and the potential for metastatic colonization. Tumors driven by NICD1 in combination with myristoylated AKT, Myc, and the Ras/Raf/MAPK pathway are also resistant to androgen deprivation. Our results indicate that Notch1 receptor signaling plays a central role in the development and progression of prostate cancer and may serve as a rational therapeutic target in high-risk prostate cancer and metastatic CRPC.

Results

Nuclear NICD1 Is Highly Elevated in High-Risk Prostate Canter and CRPC. To determine if alterations in the Notch signaling axis are associated with prostate tumorigenesis, we first assessed the levels of Notch1 in benign prostate tissue and different stages of human prostate cancer including low- to intermediate-risk (Gleason score 6 and 7) and high-risk (Gleason score 8–10) prostate cancer and CRPC. Immunohistochemical analysis of human prostate tissue microarrays (TMAs) showed a significant (more than two-fold) increase in the average intensity of nuclear NICD1 staining in high-risk prostate cancer in comparison with benign prostate tissue or localized low- to intermediate-risk prostate cancers (Fig. 1 *A* and *B* and Fig. S1). The average intensity of the staining was even higher in CRPC samples and showed a dramatic increase, by more than threefold, compared with benign prostate tissue or localized low- to intermediate-risk prostate cancers (Fig. 1 *A* and *B* and Fig. S1). Analysis of NICD1

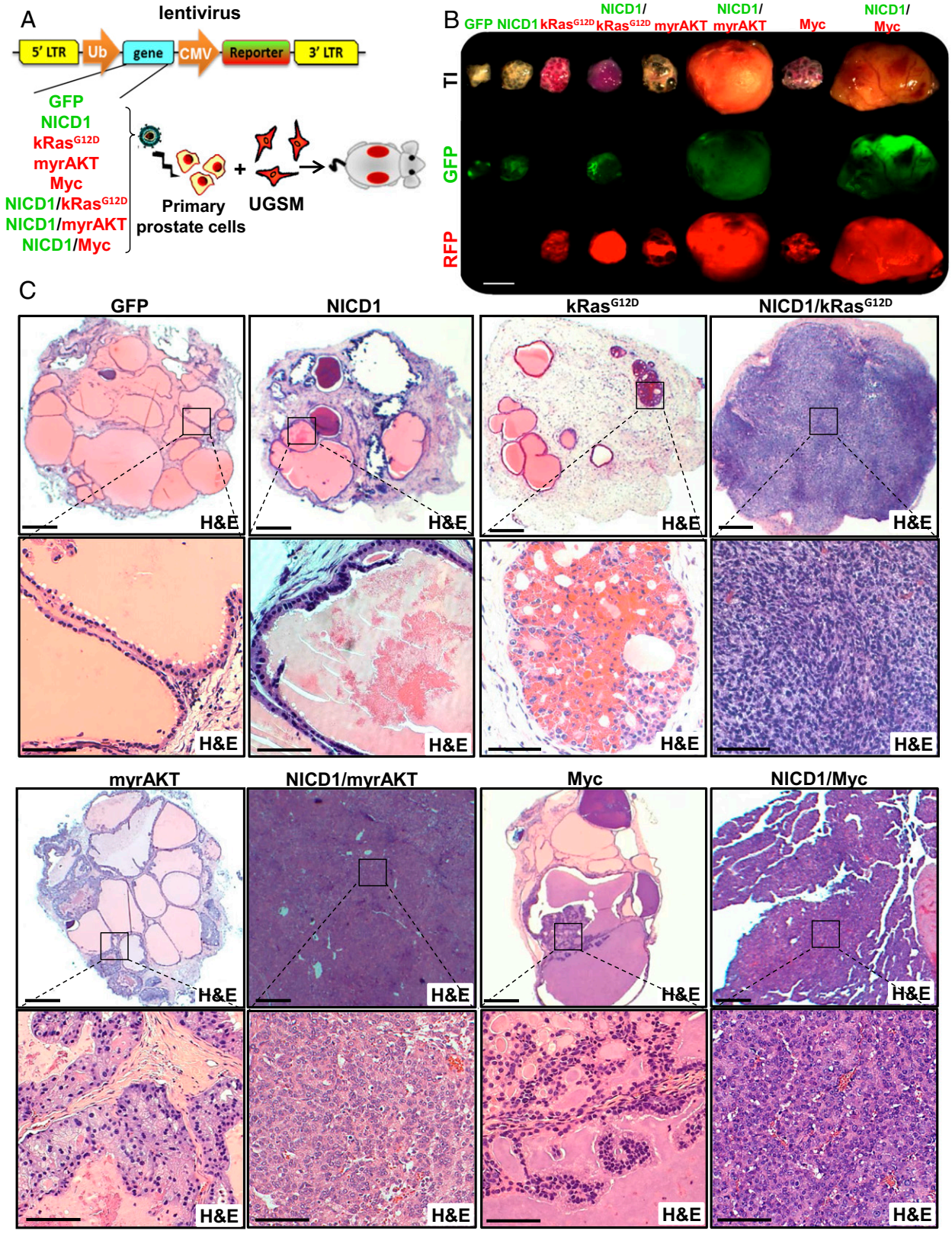

Fig. 2. NICD1 synergizes with multiple oncogenic pathways to drive prostate cancer. (*A*, *Left*) Schematic representation of the in vivo mouse tissue regeneration assay. Lentiviral transduction was used to overexpress GFP alone (GFP), human NICD1 and GFP (NICD1), mutant $kRas^{G12D}$ and RFP ($kRas^{G12D}$), myristoylated/activated AKT and RFP (myrAKT), or Myc and RFP (Myc), alone or in combination with NICD1 (NICD1/$kRas^{G12D}$, NICD1/myrAKT, NICD1/Myc). (*Right*) Transduced epithelial cells were combined with UGSM and implanted under the kidney capsule of SCID mice. Twelve weeks later the grafts were evaluated histologically. (*B*) Representatives of the grafts recovered 12 wk after implantation are shown for each condition. (Scale bar: 5 mm.) One of the five experiments performed is shown. (*C*) The recovered grafts from each condition were stained with H&E and were evaluated histologically. Representatives of the recovered grafts are shown. (Scale bars: 500 microns in upper panels; 100 microns in lower panels.)

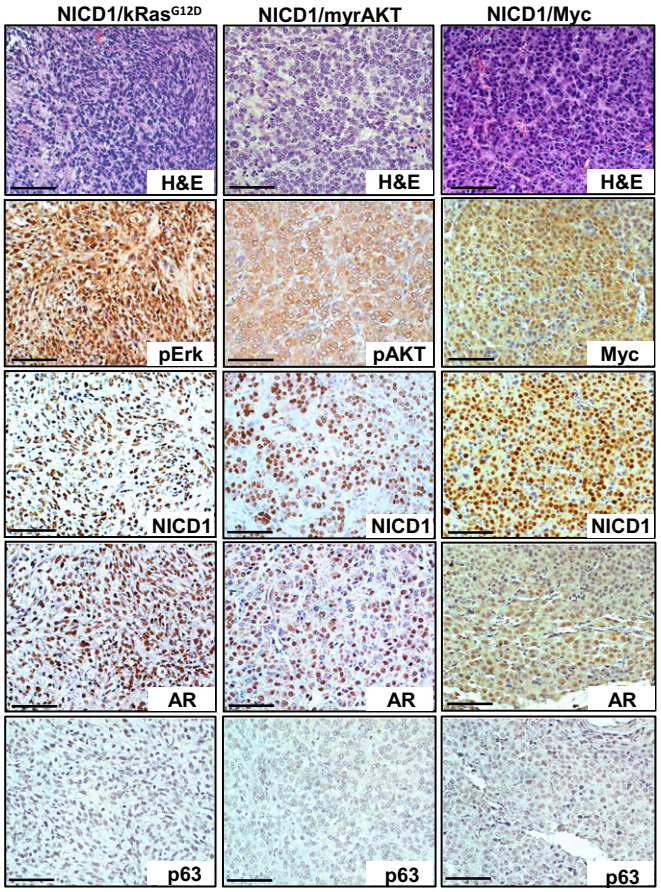

Fig. 3. Characterization of NICD1/myrAKT, NICD1/Myc, and NICD1/kRas^{G12D} tumors. Immunohistochemical analysis was performed on 4-μm sections of paraffin-embedded NICD1/myrAKT, NICD1/Myc, and NICD1/kRas^{G12D} tumors stained with H&E or with antibodies against NICD1, pErk, pAKT, Myc, p63, or AR. (Scale bars: 100 microns.)

subcellular localization indicated the presence of nuclear NICD1 in 75% of samples from high-risk prostate cancers ($n = 23$) and in 95% of CRPC samples ($n = 19$) (Fig. 1 *A* and *B*). In contrast, nuclear NICD1 was found in 32% of benign prostate tissue samples ($n = 221$) and in 33% of localized low- to intermediate-risk prostate cancers ($n = 207$) but at low intensity (Fig. 1 *A* and *B*). Similar results were observed through Western blot analysis of benign tissue, localized low- to intermediate-risk prostate cancers. and CRPC from distinct metastatic sites. Prostate tissues designated as low-risk localized prostate tumor, benign tissue adjacent to the tumor, or CRPC from distinct metastatic sites obtained from rapid autopsies performed in eight different patients (34, 35) were subjected to Western blot analysis (Fig. 1*C* and Fig. S2). As a positive control, we used a human CRPC model initiated in primary human cells and driven by the combination of Myc and myristoylated/activated AKT (myrAKT) oncogenes that express high levels of NICD1 (36). NICD1 (100 kDa) was observed only in the human metastatic CRPC samples and the Myc/myrAKT human CRPC model (36) but not in the benign tissue or in localized low- to intermediate-risk prostate cancers (Fig. 1*C* and Fig. S2). Cleavage of Notch1 at valine1744 in human metastatic CRPC was confirmed by Western blot with antibody against cleaved Notch1 (Fig. S3). These results demonstrate that high levels of nuclear NICD1 distinguish low- to intermediate-risk prostate cancer from high-risk prostate cancer and metastatic CRPC and prompted us to investigate the functional role of NICD1 in prostate tumorigenesis.

NICD1 Synergizes with the myrAKT, Myc, and Ras/Raf/MAPK Pathways to Promote the Development of Aggressive Prostate Adenocarcinoma. High levels of nuclear NICD1 are observed predominantly in high-risk prostate cancer and CRPC, suggesting a role for the pathway in prostate cancer progression. We sought to determine whether NICD1 promotes prostate tumorigenesis through collaboration with early genetic alterations. Deletion of the PTEN tumor suppressor is observed in up to 70% of prostate cancers and results in the activation of AKT (37, 38). Other common alterations in advanced human prostate cancer include elevated expression of the Myc oncogene and activation of the Ras/Raf/MAPK signaling pathway (38, 39). To mimic the loss of PTEN, we used myrAKT. Activation of Ras/Raf/MAPK was achieved through overexpression of mutant kRas^{G12D}. Dissociated mouse prostate cells can regrow prostate-like structures in vivo when combined with urogenital sinus mesenchyme (UGSM) followed by implantation under the kidney capsule of SCID mice (Fig. 2*A*) (40). This prostate regeneration model allows testing the functional role of single genes or combinations of genes in vivo (Fig. 2*A*) (40). Overexpression of a single oncogene such as myrAKT, kRas^{G12D}, or Myc initiates prostate intraepithelial neoplasia (PIN) in our model but is not sufficient to drive prostate adenocarcinoma. Therefore these genes are suitable for addressing the role of NICD1 in promoting tumor progression (Fig. 2).

Overexpression of NICD1 alone or in combination with kRas^{G12D} (NICD1/kRas^{G12D}), myrAKT (NICD1/myrAKT), or Myc (NICD1/Myc) was investigated for its ability to drive prostate tumorigenesis using the in vivo mouse prostate regeneration model (Fig. 2*A*). NICD1 alone was not sufficient to drive prostate cancer initiation, because we observed normal prostate tubular structures similar to the GFP-expressing control cells (Fig. 2). In contrast, NICD1 strongly synergized with kRas^{G12D}, myrAKT, and Myc, giving rise to prostate adenocarcinoma (Fig. 2 *B* and *C*). RFP and GFP signals in the recovered tissues were used as a control for infection efficiency (Fig. 2*B*). Importantly, the level of NICD1 overexpression in our in vivo regeneration assay was comparable to the levels observed in human CRPC specimens (Fig. S4). Oncogene expression or pathway activity was confirmed through immunohistochemical analysis (Fig. 3 and Fig. S5).

NICD1/kRas^{G12D}, NICD1/myrAKT, and NICD1/Myc tumors were highly proliferative as measured by proliferating cell nuclear antigen (PCNA), exhibit loss of basal cell marker p63, and express androgen receptors (ARs) (Fig. 3 and Fig. S5). These results demonstrate the functional role of NICD1 in synergizing with alternative pathways to promote the development of advanced prostate adenocarcinoma.

Gene-Expression Profiling of Tumors Driven by NICD1 in Combination with Alternative Pathways Reveals the EMT Signature. To gain insight into how NICD1 promotes advanced prostate cancer, we performed genome-wide transcriptome profiling of NICD1-driven tumors. Tumors initiated by the combination of NICD1/kRas^{G12D}, NICD1/myrAKT, or NICD/Myc and normal mouse prostate were subjected to high-throughput RNA-sequencing and differential gene-expression analysis (Fig. 4*A* and Fig. S6*A*). We identified 4,238 genes significantly up-regulated or down-regulated in NICD1/kRas^{G12D} tumors, 4,433 genes in NICD1/myrAKT tumors, and 3,502 genes in NICD1/Myc tumors compared with normal mouse prostate. Of the differentially expressed genes, 1,944 were common for all three tumors (Fig. 4*A* and Fig. S6*A*). Ingenuity pathway analysis identified "cell movement" and "migration" as one of the top regulatory networks across all NICD1-driven tumors (Fig. 4*A*). As expected, we observed a significant increase in direct transcriptional targets of Notch1 such as Hey2, Hey1, Heyl, Notch3, and Nrarp in NICD1/kRas^{G12D}, NICD1/myrAKT, and NICD/Myc tumors compared with normal mouse prostate (Fig. S6*B*).

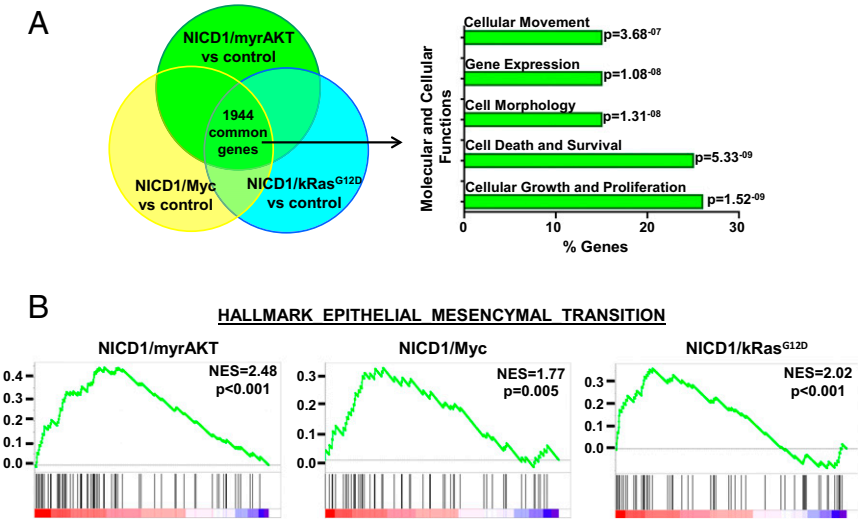

Fig. 4. Expression profiling of NICD1-driven tumors reveals the EMT signature. (*A*) Venn diagram of genes differentially expressed in NICD1/kRas^{G12D}, NICD1/myrAKT, and NICD1/Myc versus normal mouse prostate. A total of 1,944 common differentially expressed genes were analyzed for molecular and cellular functions using Ingenuity engine software. The top statistically significant molecular and cellular functions are presented with the corresponding *P* values. (*B*) The plots show the GSEA of genes differentially expressed in NICD1/myrAKT, NICD1/Myc, or NICD1/kRas^{G12D} versus normal mouse prostate. NES, normalized enrichment score.

Gene set enrichment analysis (GSEA) (41) of differentially expressed genes across all NICD1-driven tumors revealed enrichment of previously published EMT signatures (Fig. 4*B* and Fig. S7). Our results demonstrate that tumors driven by NICD1 in combination with kRas^{G12D}, myrAKT, and Myc exhibit EMT features, a phenotype that may characterize invasive, poorly differentiated carcinoma (42–45).

Tumors Driven by NICD1 in Combination with Pathways Altered in Prostate Cancer Exhibit High Self-Renewal Activity. EMT is a morphological change in which epithelial cells acquire mesenchymal features and is commonly associated with self-renewal activity, an invasive tumor phenotype, and metastasis (46). EMT has been previously demonstrated to stimulate cancer stem cell self-renewal (47). We performed limiting dilution experiments to assess functionally the acquisition of cancer self-renewal activity and stem cell properties and to evaluate the minimum number of cells required to regenerate new tumors upon transplantation. Regenerated NICD1/kRas^{G12D} and NICD1/Myc tumors were dissociated into single cells and subjected to FACS based on expression of RFP and GFP (Fig. 5*A* and Fig. S8*A*). The RFP color marker identified cells expressing kRas^{G12D} or Myc, and GFP allowed the detection of NICD1-expressing cells. GFP/RFP double-positive cells were isolated, and 10, 100, 1,000, or 10,000 RFP/GFP double-positive cells were combined with Matrigel and transplanted s.c. into SCID mouse recipients (Fig. 5*A* and Fig. S8*A*). By 4 wk as few as 10 cancer cells were sufficient to regenerate the original tumor, demonstrating the high frequency of cancer cells with self-renewing activity within the tumors (Fig. 5*B* and Fig. S8 *B* and *C*). Histological analysis identified a phenotype consistent with the original NICD1/kRas^{G12D}- and NICD1/Myc-driven tumors (Fig. 5*B* and Fig. S8*B*).

Tumors Driven by NICD1 in Combination with Pathways Altered in Prostate Cancer Exhibit High Metastatic Colonization Potential. Self-renewal activity of tumor cells is a necessary property during metastasis that allows cancer cells to colonize tumors at new sites. The metastatic potential of tumors driven by NICD1 in combination with alternative pathways was assessed using an in vivo lung-colonization assay. Regenerated NICD1/kRas^{G12D} and NICD1/Myc tumors were dissociated to single cells and infected with a luciferase-expressing lentivirus. As negative control, we used a previously characterized Myc-CAP cancer cell model derived from Myc transgenic mouse prostates (48) expressing luciferase. Immunocompromised mice were subjected to tail-vein injection with 8×10^5 cells. Twenty-eight days after injection we observed large lung tumors in animals injected with NICD1/kRas^{G12D} and NICD1/Myc tumor cells but not in the control animals injected with Myc-CAP cells (Fig. 5 *C* and *D* and Fig. S9). Histological and immunohistochemical analyses showed that these tumors closely resembled the primary tumors and exhibited high levels of nuclear AR (Fig. S9*A*). These results demonstrate that NICD1/kRas^{G12D} and NICD1/Myc tumor cells can survive and regrow tumors at a distant site, revealing the metastatic potential of NICD1 combination tumors.

Tumors Driven by NICD1 in Combination with Pathways Altered in Prostate Cancer Exhibit a Castration-Resistant Phenotype. The frequent activation of NICD1 in clinical CRPC samples coupled with the high frequency of cancer stem cells and metastatic phenotype of NICD1-driven tumors led us to investigate the role of NICD1 in the development of castration resistance. To test if castration can affect tumor growth, we used cells derived from hormone-naive NICD1/kRas^{G12D}, NICD1/myrAKT, and NICD1/Myc tumors (Fig. 6*A* and Fig. S10*A*). Myc-CAP mouse prostate cancer cells, previously demonstrated to be castration sensitive, were used as a control (Fig. 6*C*) (48). Tumor cells (6×10^5) were implanted s.c. into immunocompromised recipients. Upon detection of palpable tumors (average tumor volume, 50 mm^3), recipients were subjected to surgical castration. Myc-CAP cells grew only in intact mice and failed to grow in castrated mice, whereas NICD1/kRas^{G12D}, NICD1/myrAKT, and NICD1/Myc tumors continued to grow rapidly after androgen deprivation (Fig. 6 *A* and *C* and Fig. S10*A*).

To establish the capacity of NICD1/kRas^{G12D}, NICD1/myrAKT, and NICD1/Myc tumors to resist androgen deprivation, cancer cells were implanted into castrated SCID mouse recipients. No significant difference in size and histology was seen in the NICD1/kRas^{G12D}, NICD1/myrAKT, and NICD1/Myc secondary tumors recovered from intact or castrated recipients (Fig. 6*B* and Fig. S10 *B* and *C*). These results establish that NICD1 in combination with the activation of other pathways promotes the development of prostate cancer and the progression to CRPC.

Loss of Notch1 and Pharmacological Inhibition of γ-Secretase Delay Prostate Cancer Cell and Tumor Growth. The γ-secretase complex cleaves Notch cell-surface receptors within the transmembrane domains, leading to the release of the NICD from the membrane to the nucleus, where it is referred to as "activated Notch" (13–21). To evaluate the therapeutic potential of Notch1 inhibition, we first used the γ-secretase inhibitor (GSI) (S)-tert-butyl 2-((S)-2-(2-(3,5-difluorophenyl)acetamido)propanamido)-2-phenylacetate

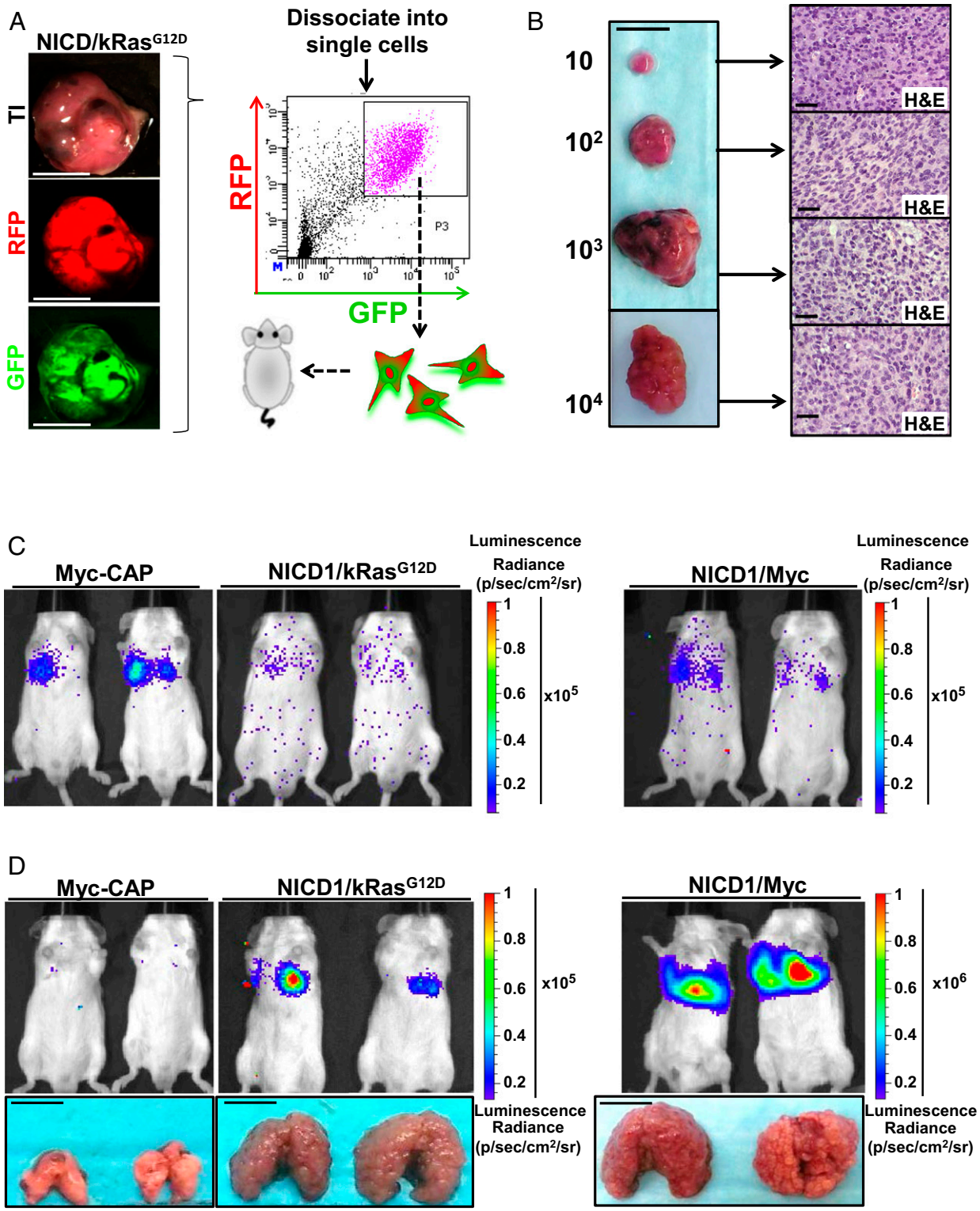

Fig. 5. Tumors driven by NICD1 in combination with pathways altered in prostate cancer exhibit the acquisition of self-renewal activity and metastatic potential. (*A*) Primary NICD/kRas^{G12D} tumor was dissociated into single cells and subjected to FACS. (Scale bars: 1 cm.) GFP/RFP double-positive cells were sorted, and 10, 100, 1,000, or 10,000 cells were implanted into SCID recipient mice. (*B*, *Left*) Representative recovered tumors initiated from 10, 100, 1,000, or 10,000 cells. (Scale bar: 1 cm.) (*Right*) Histology of each tumor is shown. (Scale bar: 50 microns.) One of the three independent experiments is presented. (*C*) Tumors driven by NICD1 in combination with pathways altered in prostate cancer exhibit metastatic potential. Primary tumors driven by NICD1/kRas^{G12D} and NICD1/Myc were dissociated into single cells, infected with lentivirus expressing luciferase and YFP, and cultured. One week after infection cells were sorted by FACS for YFP. As a negative control, we used Myc-CAP cells expressing luciferase with YFP. Cells (8×10^5) were introduced to immunocompromised mice via tail veil injection. Bioluminescent images taken on the day of injection are shown. One of the three independent experiments is shown. (*D*, *Upper*) Bioluminescent images taken day 28 after injection are shown. (*Lower*) Recovered lungs are presented. (Scale bars: 1 cm.) The size of the recovered lungs, histology of the lungs, and immunohistochemistry for NICD1, pErk, myc, and AR are presented in Fig. S9.

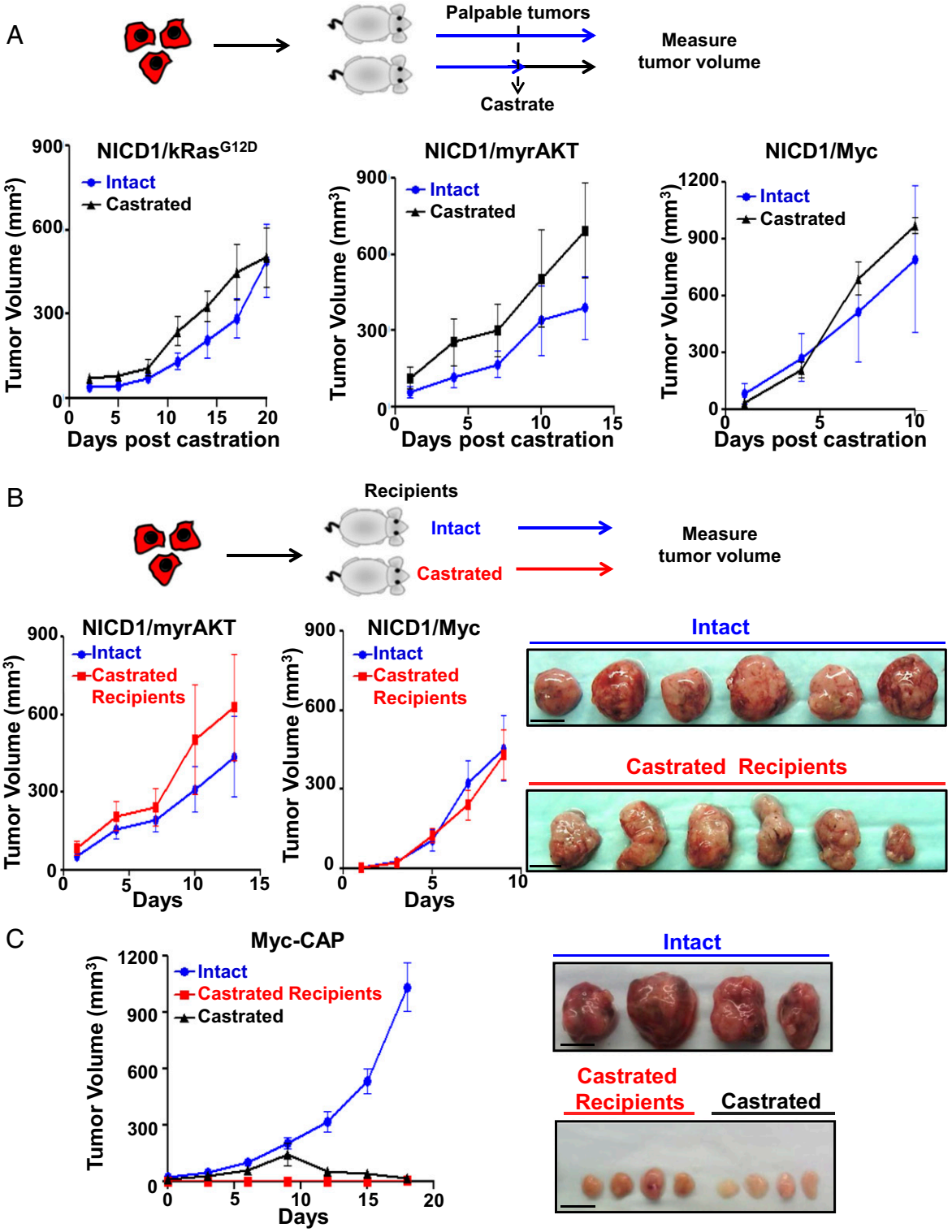

Fig. 6. NICD1 in combination with the Ras/Raf/MAPK, myrAKT, or Myc pathways drives CRPC. (*A*, *Upper*) Schematic representation of the experimental design. Primary tumors driven by NICD1/kRas^{G12D}, NICD1/myrAKT, or NICD1/Myc were dissociated into single cells. NICD1/kRas^{G12D}, NICD1/myrAKT, or NICD1/Myc tumor cells (6×10^5) were mixed with Matrigel and transplanted s.c. into six to eight mice per condition. Upon detection of palpable tumors (50 mm^3), six to eight mice carrying a total of six to eight tumors were castrated (marked as day 1). Tumor length, width, and height were measured every 3 d for a total of 10–20 d. (*Lower*) Tumor volumes were calculated by multiplying length × width × height/2 and were plotted. One of the two independent experiments for each tumor type (NICD1/kRas^{G12D}, NICD1/myrAKT, or NICD1/Myc) is shown. (*B*, *Upper*) The experimental design. NICD1/myrAKT or NICD1/Myc tumor cells (6×10^5) were mixed with Matrigel and transplanted s.c. into six castrated or six intact recipient mice. (*Lower Left*) Upon detection of palpable tumors (50 mm^3), marked as day 1, tumor volumes were measured every 3 d. (*Lower Right*) Recovered NICD1/Myc secondary tumors from intact or castrated recipients are shown. (Scale bars: 1 cm.) One of the two independent experiments for each tumor type (NICD1/myrAKT or NICD1/Myc) is presented. (*C*, *Left*) Myc-CAP cells (6×10^5) were mixed with Matrigel and implanted s.c. into eight intact or four castrated immunodeficient recipient mice. Upon detection of palpable tumors, one group of intact mice ($n = 4$) was subjected to surgical castration. (*Right*) Images of the recovered tumors. (Scale bars: 1 cm.)

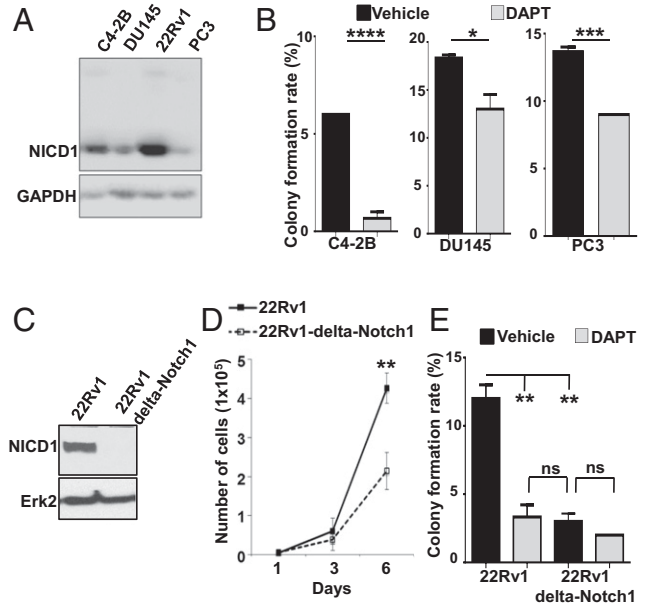

Fig. 7. Notch1 down-regulation and γ-secretase inhibition delay prostate cancer cell growth. (*A*) C4-2B, DU145, 22Rv1, and PC3 cells were lysed and subjected to Western blot analysis with antibodies against NICD1 and GAPDH. (*B*) C4-2B, DU145, and PC3 cells were subjected to a colony-formation assay. Plated cells were treated with DMSO (vehicle) or 25 μM GSI-IX (DAPT) every 48 h for 9 d. The mean colony-formation rate is plotted. Statistical analysis was performed by Student *t* test. ****$P < 0.0001$; *** $P < 0.005$; *$P < 0.05$; ns, nonsignificant. One of the two independent experiments is shown. (*C*) 22Rv1 and 22Rv1 ΔNotch1 cells were lysed and subjected to Western blot analysis with antibodies against NICD1 and Erk-2. (*D*) 22Rv1 or 22Rv1Δ Notch1 cells (1×10^4) were plated. Cell number was counted 1, 3, and 6 d after plating. Student *t* test was used for statistical analysis. **$P < 0.01$. (*E*) 22Rv1 and 22Rv1 ΔNotch1 cells were subjected a colony-formation assay. Cells were treated with DMSO (vehicle) or 25 μM GSI-IX (DAPT) every 48 h for 9 d. The mean colony-formation rate is shown. Student *t* test was used for statistical analysis. **$P < 0.01$; ns, nonsignificant.

(DAPT) (GSI-IX). We tested multiple prostate cancer cell lines for expression of NICD1 (Fig. 7*A*). The androgen-independent prostate cancer cell lines C4-2B, DU145, 22Rv1, and PC3 express different levels of NICD1 (Fig. 7*A*). All four prostate cancer cell lines were subjected to a colony-formation assay in the presence of DAPT or vehicle (Fig. 7*B*). Treatment of C4-2B, DU145, 22Rv1, and PC3 cells with DAPT significantly inhibited cell growth as measured by colony formation in vitro (Fig. 7 *B* and *E*). Additionally, we generated a 22Rv1 Notch1-knockout cell line via CRISPR/Cas9 to demonstrate the effect of Notch1 loss on cell growth and colony formation (Fig. 7*C*). Deletion of Notch1 in 22Rv1 cells (22Rv1 ΔNotch1) significantly delayed cell growth (Fig. 7*D*). Comparable to the effect of DAPT on colony formation, the deletion of Notch1 in 22Rv1 cells led to a significant decrease in colony-formation potential. DAPT had no significant effect on cell growth in ΔNotch1 22Rv1 cells, demonstrating the specificity of the Notch1 effect on prostate cancer cell growth (Fig. 7*E*).

To evaluate the therapeutic potential of Notch1 inhibition in vivo, mice harboring androgen ablation-resistant 22Rv1 xenograft tumors were treated with either vehicle ($n = 4$) or DAPT (GSI-IX) ($n = 4$) at 50 mg/1 kg (Fig. S11*A*). Treatment was initiated upon the detection of palpable tumors, and tumor volume was assessed every 4 d after treatment induction. Treatment with DAPT delayed tumor growth of 22Rv1 xenografts. To confirm the on-target effect of DAPT in vivo, the 22Rv1 tumors were harvested and analyzed for NICD1 and cleaved Notch1 levels (Fig. S11*B*). These results demonstrate that loss or inhibition of Notch1 may represent a promising therapeutic strategy for CRPC.

Discussion

Defining the mechanisms that drive CRPC is critical for the development of new therapies for the lethal form of the disease. Here we demonstrate that NICD1 is localized to the nucleus in 70% of the high-risk prostate cancer and in 95% of CRPC samples analyzed. These findings suggest that nuclear NICD1 may distinguish between low- to intermediate-risk and high-risk prostate cancer and may predict prostate cancer that will recur as CRPC. Although activating mutations of Notch receptors are found in several cancers, there is no evidence of Notch1-activating mutations in advanced prostate cancer. Nuclear NICD1 in prostate cancer may arise as a consequence of Notch1 cleavage caused by elevated levels of Notch ligands, such as Jagged1, which has been reported to be overexpressed in metastasis (7). Mechanisms underlying the activation of Notch1 in advanced prostate cancer are yet to be elucidated.

Because the nuclear localization of Notch receptors reflects their activation state, we devised a strategy to mimic the high expression of Notch1 observed in clinical metastatic CRPC by engineering the overexpression of the NICD in primary mouse prostate epithelium. NICD1 strongly synergized with a broad range of pathways commonly altered in prostate cancer, such as myrAKT, Myc, and Ras/Raf/MAPK. These combinations resulted in advanced prostate adenocarcinoma (Fig. 8). Our observation that NICD1 alone is not sufficient to drive prostate cancer initiation but instead synergizes with other pathways that can initiate only low-grade PIN lesions to drive prostate adenocarcinoma suggests that the Notch 1 receptor has a critical role in the progression of prostate cancer. These results are consistent with previous findings in osteogenic sarcoma and lung adenocarcinoma in which NICD1 strongly synergizes with p53 loss or Myc overexpression to accelerate tumor progression (49, 50).

Transcriptome profiling of tumors driven by NICD1 in combination with myrAKT, Myc, and Ras/Raf/MAPK revealed features of EMT. During development, Notch1 is known to drive EMT (51), a process by which epithelial cells lose their polarity and acquire mesenchymal features. These changes are accompanied by down-regulation of epithelial and adhesion genes such as E-cadherin and cytokeratins and elevated expression of mesenchymal markers such as vimentin and N-cadherin. Acquisition of an EMT phenotype is characteristic of invasive carcinoma, metastasis, and increased tumor cell self-renewal (47). In prostate cancer, down-regulation of E-cadherin is associated with poor prognosis and survival (40), whereas increased expression of the mesenchymal marker N-cadherin correlates with a high Gleason

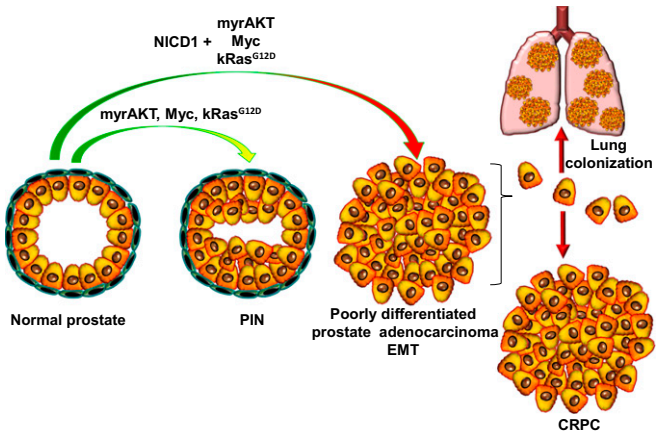

Fig. 8. NICD1 in combination with the myrAKT, Myc, or Ras/Raf/MAPK pathways promotes metastatic CRPC. The schematic representation summarizes our results.

score and drives CRPC (42, 44). Consistent with the acquisition of EMT features, we found NICD1/myrAKT, NICD1/Myc, and NICD1/Ras^{G12D} tumors to be highly metastatic and capable of self-renewal activity. Notch signaling may serve a more general role in cancer stem cell maintenance in multiple tumor types (47).

Promising strategies targeting individual Notch receptors, ligand-receptor interactions, and Notch transcriptional activity have been developed and have demonstrated anticancer activity in animal models (52–54). Humanized monoclonal antibodies that block the ligand–receptor interaction between Notch and its ligand DLL4 demonstrate potent anticancer activity in patient-derived xenograft models (52). Another class of antibodies that targets individual Notch receptors, locking them in an inactive conformation, has also demonstrated promising therapeutic potential (53). Another strategy to inhibit Notch receptors is the use of GSIs that block regulated intramembrane proteolysis and subsequent Notch receptor activation (55). Our finding that Notch1 cooperates with a range of common genetic alterations in prostate cancer suggests that Notch1 inhibition may represent an effective therapy for advanced prostate cancer. Indeed, here we demonstrate that GSI and loss of Notch1 decrease prostate cancer cell growth. Additionally, GSI treatment delays the tumor growth of prostate cancer xenografts. Consistent with our findings, previous study has shown that the GSI PF-03084014 results in a significant decrease in tumor growth in two xenograft models of prostate cancer (PC3 and DU145) (12). PF-03084014 demonstrated an even greater antitumor effect in prostate cancer growth when combined with the chemotherapeutic agent docetaxel, which is currently in clinical use (12).

We provide functional evidence that NICD1 synergizes with multiple pathways in driving poorly differentiated prostate adenocarcinoma and metastatic CRPC in vivo (Fig. 8). Our results suggest that activation of Notch1 may serve as a biomarker to predict the potential benefit of Notch1 inhibition and as a therapeutic target for patients suffering from metastatic CRPC.

Materials and Methods

TMAs. Seventy-five prostatectomy specimens from patients never treated with hormonal therapy were reviewed, and areas of normal prostate (indicated as benign tissue) and low- to intermediate-risk prostate cancer (Gleason patterns 6–7) were marked for sampling. Two cores per sample, each measuring 0.6 mm in diameter, were taken from selected regions in each paraffin block and transferred to a recipient paraffin block containing a total of 150 benign or cancer cores. Unstained sections of 4-μm thickness were used for immunohistochemical staining. Two additional TMAs were constructed containing (*i*) benign tissues and adjacent low- to intermediate-risk prostate cancer from 40 patients (three cores per sample) and (*ii*) benign tissues and adjacent cancer samples (low- to intermediate-risk and high-risk) from 115 patients. Additional CRPC TMAs were constructed from blocks containing transurethral resection tissues from 20 patients who failed androgen-ablation therapy (i.e., patients with CRPC) and who developed urinary obstruction. Two cores from each patient block were transferred to a new TMA block (CRPC TMA). A section from the TMA blocks was obtained and used for immunohistochemical staining.

Mouse Strains. C57BL/6, CB17$^{Scid/Scid}$, and NSG (NOD-SCID-IL2Rγ–null) mice were purchased from the Jackson Laboratory. Animals were housed at the University of California, Los Angeles animal facilities according to the regulations of the Division of Laboratory Animal Medicine.

Prostate Tissue Regeneration Assays. Housing, breeding, and all surgical procedures were performed in agreement with the guidelines of the Division of Laboratory Animal Medicine of the University of California, Los Angeles. All experimental procedures were approved by the Division of Laboratory Animal Medicine of the University of California, Los Angeles. The details of the regeneration process have been explained previously (56).

Lung Colonization Assay. NICD1/Myc and NICD1/Ras^{G12D} secondary tumors were excised, minced, and incubated in DMEM containing 10% FBS, 1 mg/mL collagenase, and 1 mg/mL Dispase for 1 h at 37 °C. To achieve single-cell dissociation, tumor chucks were spun down, further treated with 0.05% Trypsin-EDTA for 5 min at 37 °C, passed through a 20-gauge syringe, and filtered through a 70-μm filter mesh. Cells were cultured for 2 wk followed by infection with lentivirus-expressing luciferase and YFP. Mice were injected with 8×10^5 NICD1/Myc, NICD1/Ras^{G12D}, and Myc-CAP cells expressing luciferase and YFP via tail vein injection. Thirty minutes after injection, animals were injected i.p. with 150 μL of 15 mg/mL luciferin followed by bioluminescence imaging with the IVIS Lumina II imaging system.

RNA Sequencing. RNA was extracted from mouse tumor tissue using the RNeasy Mini Kit from Qiagen. Libraries for RNA-sequencing were prepared with NuGen Ovation RNA-Seq System V2. The workflow consists of double-stranded cDNA generation using a mixture of random and poly (T) priming, fragmentation of double-stranded cDNA, end repair to generate blunt ends, A-tailing, adaptor ligation, and PCR amplification. Different adaptors were used for multiplexing samples in one lane. Sequencing was performed on an Illumina HiSeq 2500 for a pair-read 100-nt run. Data quality control was done on an Illumina Sequencing Analysis Viewer. Demultiplexing was performed with Illumina CASAVA 1.8.2. The reads were first mapped to the latest University of California, Santa Cruz transcript set using Bowtie2 version 2.1.0, and the gene-expression level was estimated using RSEM v1.2.15. TPM (transcript per million) was used as the normalized gene expression. Differentially expressed genes were identified using the DESeq package. Genes showing altered expression with a false-discovery rate $P < 0.05$ and more than twofold changes were considered differentially expressed.

Vector Production and Viral Packaging. The third-generation lentiviral vectors FUCGW and FUCRW, derived from FUGW, were used for the construction of the human NICD1, kRas^{G12D}, myrAKT, and Myc constructs.

Antibodies. The following antibodies were used: anti-Notch1 [Novus Biologicals 3E12; Abcam ab52627; Cell Signaling Technology C37C7; Cell Signaling Technology (Val1744) (D3B8)]; anti-PCNA (Cell Signaling), anti–AR-N-20 (Santa Cruz), anti-p63 (Santa Cruz), and anti-AKT (Cell Signaling).

Immunohistochemistry. Indicated tissues were fixed in 10% buffer and were embedded in formalin and paraffin. Four-micron sections were deparaffinized in xylene and rehydrated in 100, 95, and 70% ethanol. Antigen retrieval was performed with citrate buffer (pH 6.0) at 95 °C for 20 min. Sections were blocked using mouse-on-mouse blocking reagents (BMK-2202; Vector Labs). The sections were incubated with the indicated antibodies overnight. Slides were washed with 1× PBS and incubated with anti-mouse HRP or anti-rabbit HRP antibodies (DAKO) for 1 h, developed with HRP substrate (DAKO), and counterstained with hematoxylin.

Colony-Formation Assay. Five hundred C4-2B, DU145, 22Rv1, and PC3 cells per well were plated in triplicate in a six-well plate. Cells were treated with DMSO (vehicle) or 25 μM DAPT (GSI-IX; Selleck Chemicals LLC) every 48 h. Nine days after plating colonies were fixed with ice-cold methanol for 30 min at −20 °C and were stained with 0.1% crystal violet in 1× PBS for 30 min at room temperature. Plates were washed for 1 h with water. Colonies were counted, and the colony formation rate (%) was calculated as the number of colonies per 500 cells × 100.

Generation of ΔNotch1 22Rv1 Cell Lines. The 5′ UTR and first exons of Notch1 were used to design guide RNAs. Sequences were loaded on crispr.mit.edu. A sequence spanning the ATG was identified (guide #1 Notch1 CRISPR forward CACCGGGGAGGCATGCCGCCGCTCC; guide #1 Notch CRISPR reverse AAACGGAGCGGCGGCATGCCTCCCC). Overhangs appropriate for cloning onto BbsI sites were added. Oligos were annealed and cloned into the PX458 vector. pSpCas9(BB)-2A-GFP (PX458) (Addgene plasmid no. 48138) was a gift from Feng Zhang, Broad Institute of MIT and Harvard, Cambridge, MA; McGovern Institute for Brain Research, Cambridge, MA; and Departments of Brain and Cognitive Sciences and Biological Engineering, MIT, Cambridge, MA (57). 22RV1 cells (5×10^5 cells per well in 2 mL 10% DMEM in a six-well plate) were transfected with 5 μg DNA using Lipofectamine 2000. GFP$^+$ cells were sorted by FACS 24 h after transfection and were plated in a 96-well plate at four cells per well. Cells were grown until wells with single clones were 50% confluent (4 wk). Loss of Notch1 was confirmed by Western blot.

In Vivo Studies with GSI. NSG mice (8–10 wk old) were injected s.c. in the flank with 1×10^6 22Rv1 cells in Matrigel. When tumors reached palpable size (50 mm^3), animals were randomly assigned to treatment with vehicle (control) or with DAPT (50 mg/kg GSI-IX). Vehicle and DAPT were dissolved in 10% ethanol and 90% corn oil and were administered by oral gavage on the following schedule: 3 d on, 1 d off, 6 d on, and 1 d off. The schedule was

repeated two times. The length (L), width (W), and height (H) of tumors were measured every 4 d. Tumor volume was calculated by (L × W × H)/2.

ACKNOWLEDGMENTS. We thank the University of California, Los Angeles (UCLA) Tissue Procurement Core Laboratories for tissue preparation. T.S. is supported by a Prostate Cancer Foundation Young Investigator Award and NIH/National Cancer Institute (NCI) K99/R00 Pathway to Independence Award 4R00CA184397. C.M.F. is supported by a UCLA Tumor Cell Biology Training Grant. S.L. is supported in part by the American Urological Association/Urology Care Foundation Research Scholar Award Program. B.A.S. is supported by UCLA Tumor Immunology Training Grant T32-CA009120. J.K.L. is supported by the Specialty Training and Advanced Research (STAR) Program at UCLA, a Prostate Cancer Foundation Young Investigator Award, and a UCLA Clinical and Translational Science Institute-KL2 Award KL2TR001882 (principal investigator: Mitchell Wong) from the NIH/National Center for Advancing Translational Sciences. J.M.D. is supported by Department of Defense Prostate Cancer Research Program Grant W81XWH-15-1-0236 and a Prostate Cancer Foundation Young Investigator Award. J.H. is supported by NIH/NCI Grant P50CA092131 [to the UCLA Specialized Program of Research Excellence (SPORE) in prostate cancer; principal investigator: R.E.R.], a Creativity Award from the Prostate Cancer Foundation (PCF) (principal investigator: M. Rettig), and NIH Grant 1R01CA158627 (principal investigator: L. Marks). A.S.G. is supported by the Department of Defense and a Prostate Cancer Foundation Young Investigator Award. O.N.W. is an Investigator of the Howard Hughes Medical Institute and is partly supported by the Eli and Edythe Broad Center of Regenerative Medicine and Stem Cell Research. K.J.P. is supported by a PCF Challenge Award and by the NIH. R.E.R. is supported by NIH/NCI Grant P50CA092131 (to the UCLA SPORE in prostate cancer). A.S.G and O.N.W. are supported by a PCF Creativity Award (principal investigator: O.N.W.). A.S.G, J.H., and O.N.W. are supported by a PCF Challenge Award (principal investigator: O.N.W.) and the UCLA SPORE in prostate cancer (principal investigator: R.E.R.).

1. Feldman BJ, Feldman D (2001) The development of androgen-independent prostate cancer. *Nat Rev Cancer* 1(1):34–45.
2. Kantoff PW, et al.; IMPACT Study Investigators (2010) Sipuleucel-T immunotherapy for castration-resistant prostate cancer. *N Engl J Med* 363(5):411–422.
3. Tannock IF, et al.; TAX 327 Investigators (2004) Docetaxel plus prednisone or mitoxantrone plus prednisone for advanced prostate cancer. *N Engl J Med* 351(15): 1502–1512.
4. Wang XD, et al. (2006) Notch signaling is required for normal prostatic epithelial cell proliferation and differentiation. *Dev Biol* 290(1):66–80.
5. Kwon OJ, et al. (2014) Increased Notch signalling inhibits anoikis and stimulates proliferation of prostate luminal epithelial cells. *Nat Commun* 5:4416.
6. Valdez JM, et al. (2012) Notch and TGFβ form a reciprocal positive regulatory loop that suppresses murine prostate basal stem/progenitor cell activity. *Cell Stem Cell* 11(5):676–688.
7. Gerhardt DM, et al. (2014) The Notch1 transcriptional activation domain is required for development and reveals a novel role for Notch1 signaling in fetal hematopoietic stem cells. *Genes Dev* 28(6):576–593.
8. Santagata S, et al. (2004) JAGGED1 expression is associated with prostate cancer metastasis and recurrence. *Cancer Res* 64(19):6854–6857.
9. Zhu H, Zhou X, Redfield S, Lewin J, Miele L (2013) Elevated Jagged-1 and Notch-1 expression in high grade and metastatic prostate cancers. *Am J Transl Res* 5(3):368–378.
10. Wang Z, et al. (2010) Down-regulation of Notch-1 and Jagged-1 inhibits prostate cancer cell growth, migration and invasion, and induces apoptosis via inactivation of Akt, mTOR, and NF-kappaB signaling pathways. *J Cell Biochem* 109(4):726–736.
11. Domingo-Domenech J, et al. (2012) Suppression of acquired docetaxel resistance in prostate cancer through depletion of notch- and hedgehog-dependent tumor-initiating cells. *Cancer Cell* 22(3):373–388.
12. Cui D, et al. (2015) Notch pathway inhibition using PF-03084014, a γ-Secretase inhibitor (GSI), enhances the antitumor effect of docetaxel in prostate cancer. *Clin Cancer Res* 21(20):4619–4629.
13. Kopan R, Ilagan MX (2009) The canonical Notch signaling pathway: Unfolding the activation mechanism. *Cell* 137(2):216–233.
14. Schroeter EH, Kisslinger JA, Kopan R (1998) Notch-1 signalling requires ligand-induced proteolytic release of intracellular domain. *Nature* 393(6683):382–386.
15. Kidd S, Lieber T, Young MW (1998) Ligand-induced cleavage and regulation of nuclear entry of Notch in Drosophila melanogaster embryos. *Genes Dev* 12(23): 3728–3740.
16. Struhl G, Adachi A (1998) Nuclear access and action of notch in vivo. *Cell* 93(4): 649–660.
17. De Strooper B, et al. (1999) A presenilin-1-dependent gamma-secretase-like protease mediates release of Notch intracellular domain. *Nature* 398(6727):518–522.
18. Maillard I, Adler SH, Pear WS (2003) Notch and the immune system. *Immunity* 19(6): 781–791.
19. Allman D, Punt JA, Izon DJ, Aster JC, Pear WS (2002) An invitation to T and more: Notch signaling in lymphopoiesis. *Cell* 109(Suppl):S1–S11.
20. Jarriault S, et al. (1995) Signalling downstream of activated mammalian Notch. *Nature* 377(6547):355–358.
21. Ntziachristos P, Lim JS, Sage J, Aifantis I (2014) From fly wings to targeted cancer therapies: A centennial for notch signaling. *Cancer Cell* 25(3):318–334.
22. Rampias T, et al. (2014) A new tumor suppressor role for the Notch pathway in bladder cancer. *Nat Med* 20(10):1199–1205.
23. Agrawal N, et al. (2011) Exome sequencing of head and neck squamous cell carcinoma reveals inactivating mutations in NOTCH1. *Science* 333(6046):1154–1157.
24. Wang NJ, et al. (2011) Loss-of-function mutations in Notch receptors in cutaneous and lung squamous cell carcinoma. *Proc Natl Acad Sci USA* 108(43):17761–17766.
25. Klinakis A, et al. (2011) A novel tumour-suppressor function for the Notch pathway in myeloid leukaemia. *Nature* 473(7346):230–233.
26. Ellisen LW, et al. (1991) TAN-1, the human homolog of the Drosophila notch gene, is broken by chromosomal translocations in T lymphoblastic neoplasms. *Cell* 66(4):649–661.
27. Weng AP, et al. (2004) Activating mutations of NOTCH1 in human T cell acute lymphoblastic leukemia. *Science* 306(5694):269–271.
28. Girard L, et al. (1996) Frequent provirus insertional mutagenesis of Notch1 in thymomas of MMTVD/myc transgenic mice suggests a collaboration of c-myc and Notch1 for oncogenesis. *Genes Dev* 10(15):1930–1944.
29. Puente XS, et al. (2011) Whole-genome sequencing identifies recurrent mutations in chronic lymphocytic leukaemia. *Nature* 475(7354):101–105.
30. Westhoff B, et al. (2009) Alterations of the Notch pathway in lung cancer. *Proc Natl Acad Sci USA* 106(52):22293–22298.
31. Lobry C, Oh P, Aifantis I (2011) Oncogenic and tumor suppressor functions of Notch in cancer: It's NOTCH what you think. *J Exp Med* 208(10):1931–1935.
32. Grasso CS, et al. (2012) The mutational landscape of lethal castration-resistant prostate cancer. *Nature* 487(7406):239–243.
33. Robinson D, et al. (2015) Integrative clinical genomics of advanced prostate cancer. *Cell* 161(5):1215–1228.
34. Rubin MA, et al. (2000) Rapid ("warm") autopsy study for procurement of metastatic prostate cancer. *Clin Cancer Res* 6(3):1038–1045.
35. Mehra R, et al. (2011) Characterization of bone metastases from rapid autopsies of prostate cancer patients. *Clin Cancer Res* 17(12):3924–3932.
36. Stoyanova T, et al. (2013) Prostate cancer originating in basal cells progresses to adenocarcinoma propagated by luminal-like cells. *Proc Natl Acad Sci USA* 110(50): 20111–20116.
37. Gray IC, et al. (1998) Mutation and expression analysis of the putative prostate tumour-suppressor gene PTEN. *Br J Cancer* 78(10):1296–1300.
38. Taylor BS, et al. (2010) Integrative genomic profiling of human prostate cancer. *Cancer Cell* 18(1):11–22.
39. Gurel B, et al. (2008) Nuclear MYC protein overexpression is an early alteration in human prostate carcinogenesis. *Mod Pathol* 21(9):1156–1167.
40. Xin L, Ide H, Kim Y, Dubey P, Witte ON (2003) In vivo regeneration of murine prostate from dissociated cell populations of postnatal epithelia and urogenital sinus mesenchyme. *Proc Natl Acad Sci USA* 100(1, Suppl 1):11896–11903.
41. Subramanian A, et al. (2005) Gene set enrichment analysis: A knowledge-based approach for interpreting genome-wide expression profiles. *Proc Natl Acad Sci USA* 102(43):15545–15550.
42. Jaggi M, et al. (2006) N-cadherin switching occurs in high Gleason grade prostate cancer. *Prostate* 66(2):193–199.
43. Tanaka H, et al. (2010) Monoclonal antibody targeting of N-cadherin inhibits prostate cancer growth, metastasis and castration resistance. *Nat Med* 16(12):1414–1420.
44. Gravdal K, Halvorsen OJ, Haukaas SA, Akslen LA (2007) A switch from E-cadherin to N-cadherin expression indicates epithelial to mesenchymal transition and is of strong and independent importance for the progress of prostate cancer. *Clin Cancer Res* 13(23):7003–7011.
45. Lang SH, et al. (2002) Enhanced expression of vimentin in motile prostate cell lines and in poorly differentiated and metastatic prostate carcinoma. *Prostate* 52(4):253–263.
46. Kalluri R, Weinberg RA (2009) The basics of epithelial-mesenchymal transition. *J Clin Invest* 119(6):1420–1428.
47. Mani SA, et al. (2008) The epithelial-mesenchymal transition generates cells with properties of stem cells. *Cell* 133(4):704–715.
48. Watson PA, et al. (2005) Context-dependent hormone-refractory progression revealed through characterization of a novel murine prostate cancer cell line. *Cancer Res* 65(24):11565–11571.
49. Tao J, et al. (2014) Notch activation as a driver of osteogenic sarcoma. *Cancer Cell* 26(3):390–401.
50. Allen TD, Rodriguez EM, Jones KD, Bishop JM (2011) Activated Notch1 induces lung adenomas in mice and cooperates with Myc in the generation of lung adenocarcinoma. *Cancer Res* 71(18):6010–6018.
51. Timmerman LA, et al. (2004) Notch promotes epithelial-mesenchymal transition during cardiac development and oncogenic transformation. *Genes Dev* 18(1):99–115.
52. Moellering RE, et al. (2009) Direct inhibition of the NOTCH transcription factor complex. *Nature* 462(7270):182–188.
53. Takebe N, Nguyen D, Yang SX (2014) Targeting notch signaling pathway in cancer: Clinical development advances and challenges. *Pharmacol Ther* 141(2):140–149.
54. Ridgway J, et al. (2006) Inhibition of Dll4 signalling inhibits tumour growth by deregulating angiogenesis. *Nature* 444(7122):1083–1087.
55. Wu Y, et al. (2010) Therapeutic antibody targeting of individual Notch receptors. *Nature* 464(7291):1052–1057.
56. Lukacs RU, Goldstein AS, Lawson DA, Cheng D, Witte ON (2010) Isolation, cultivation and characterization of adult murine prostate stem cells. *Nat Protoc* 5(4):702–713.
57. Ran FA, et al. (2013) Genome engineering using the CRISPR-Cas9 system. *Nat Protoc* 8(11):2281–2308.

Supporting Information

Stoyanova et al. 10.1073/pnas.1614529113

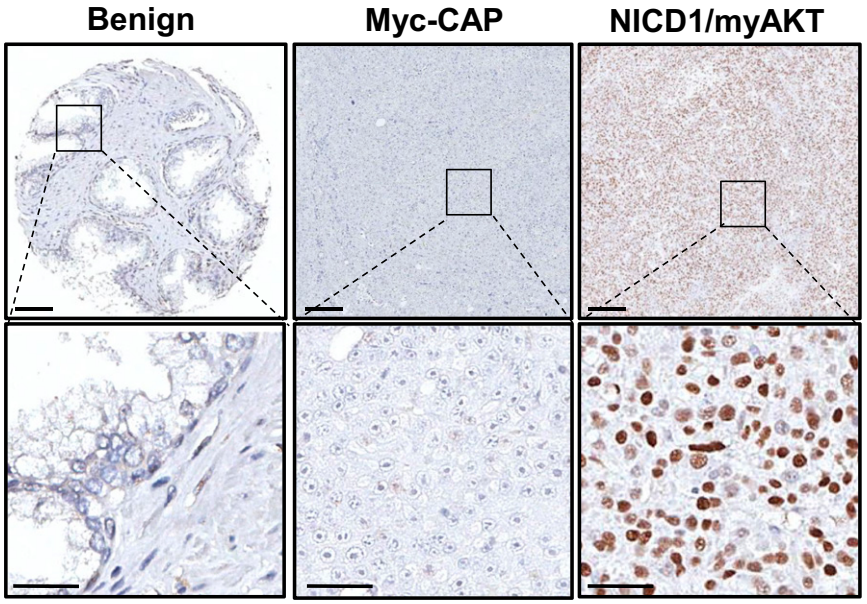

Fig. S1. Nuclear NICD1 is elevated in advanced human prostate cancer. The figure shows negative and positive controls for the human prostate TMA stained with an antibody against the intracellular domain of Notch1 presented in Fig. 1*A*. (*Left*) Benign human tissue; epithelial cells are negative for NICD1. (*Center*) Previously described mouse Myc-CAP xenografts (41). Myc-CAP xenografts are negative for nuclear NICD1. (*Right*) As a positive control we used tumors driven by the combination of NICD1 overexpression and active AKT overexpression (myrAKT). (Scale bars: 100 microns in the upper row; 50 microns in the lower row.)

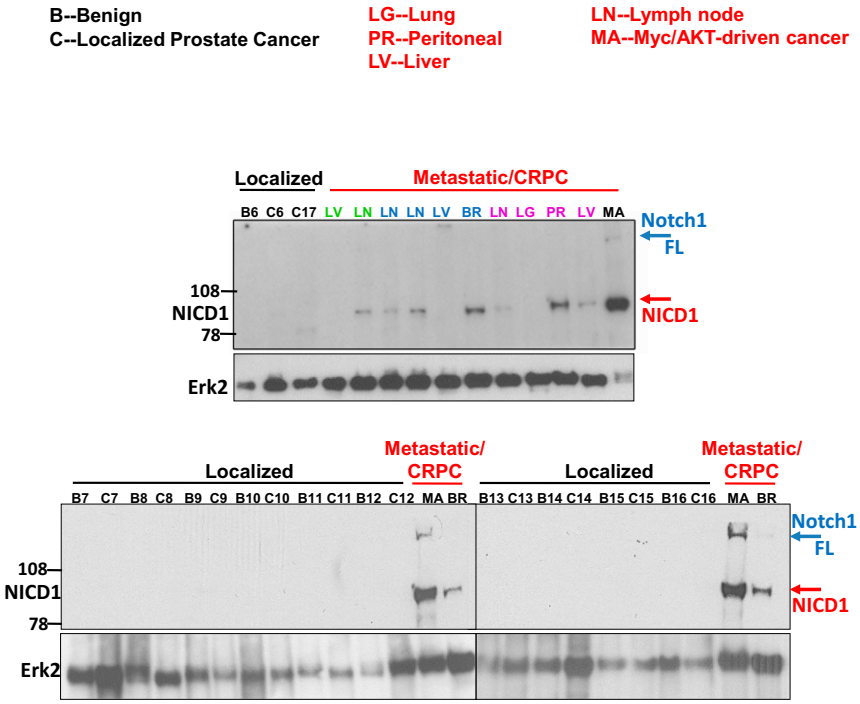

Fig. S2. NICD1 is highly expressed in metastatic prostate cancer but not in benign prostate tissues and low- or intermediate-risk prostate cancer. Western blot analyses were performed using anti-NICD1 antibody (Epitomics; currently Abcam), and anti-Erk2 was used as a loading control. For the Western blot analyses we used (*i*) human prostate tissues separated into benign (B) and low- to intermediate-risk prostate cancer (T) regions; (*ii*) metastatic CRPC tissues obtained from the rapid autopsy program at the University of Michigan; and (*iii*) the Myc/myrAKT CRPC model initiated in primary human cells that express high levels of full-length Notch1 (Notch1 FL, ~300 kDa) and NICD1 (~100 kDa). Distinct patients with metastatic disease are shown in different colors.

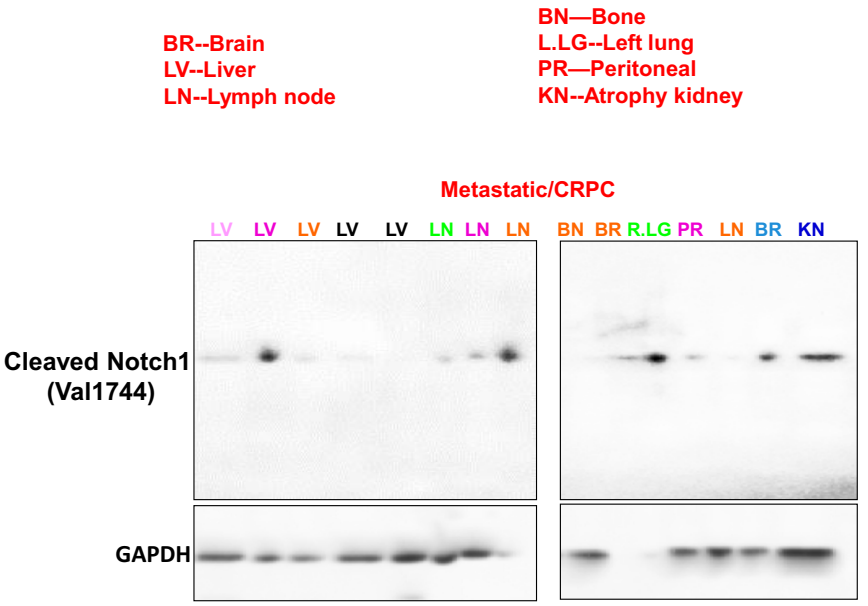

Fig. S3. NICD1 is highly expressed in metastatic prostate cancer. Western blot analyses were performed on metastatic CRPC tissues obtained from the rapid autopsy program at the University of Michigan using anti-cleaved Notch1 V1744 antibody (Cell Signaling Technology). GAPDH was used as a loading control. Distinct patients with metastatic disease are shown in different colors. Different colors and metastatic sites match the patients' samples analyzed in Fig. 1C and Fig. S2.

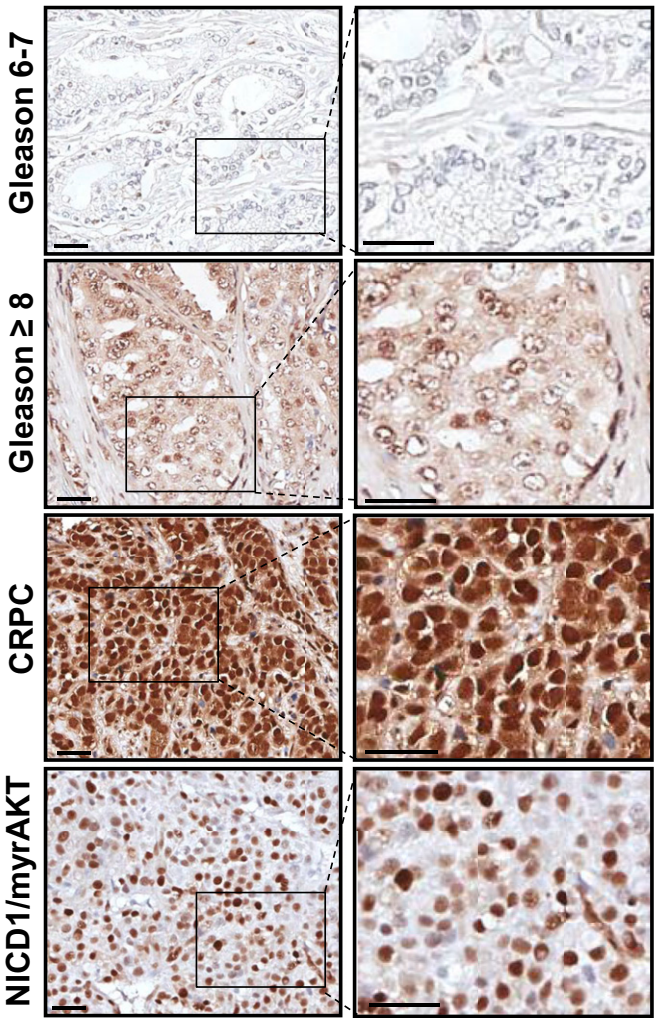

Fig. S4. Expression levels of NICD1 in tumors driven by NICD1 in combination with $kRas^{G12D}$, myrAKT, or Myc resemble levels of nuclear NICD1 in human CRPC specimens. Levels of nuclear NICD1 overexpression mimic the levels of nuclear NICD1 in human CRPC. Immunohistochemical analyses of 4- μm sections of paraffin-embedded human low- to intermediate-risk prostate cancer (Gleason score 6 or 7), localized high-risk prostate cancer (Gleason score 8–10), CRPC specimens, and NICD1/myrAKT tumors with antibodies against NICD1 (Novus Biologicals) are shown. (Scale bars: 100 microns in left panels; 50 microns in right panels.)

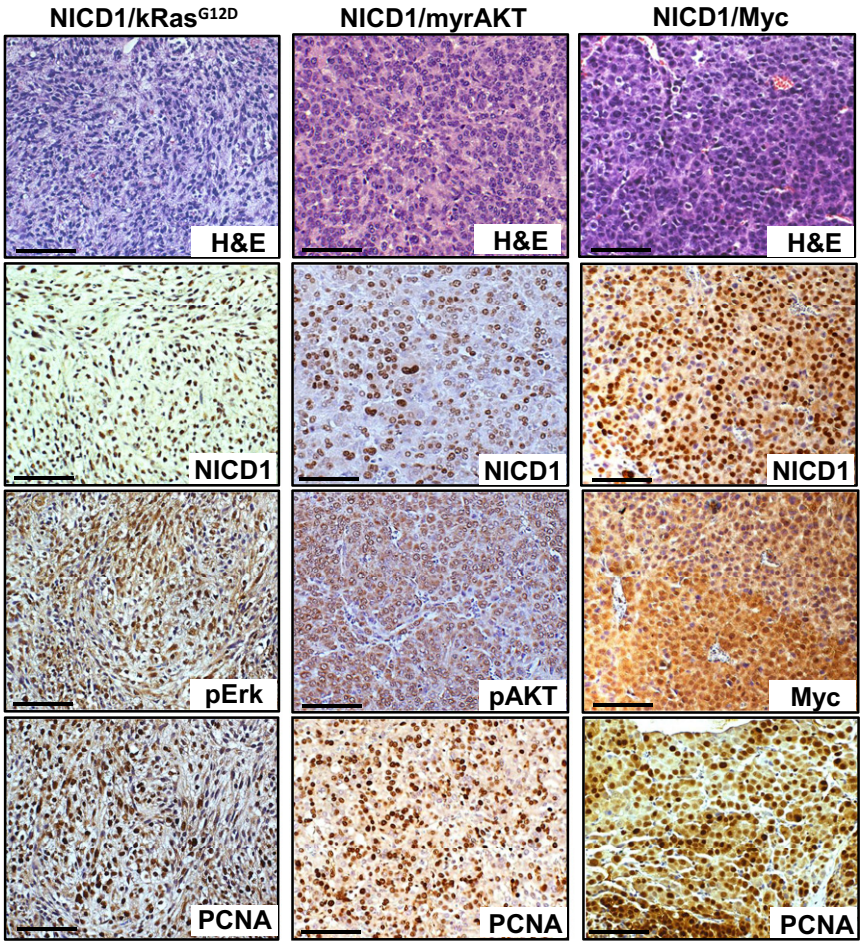

Fig. S5. NICD1/myrAKT, NICD1/Myc, and NICD1/kRas^{G12D} tumors are highly proliferative. Immunohistochemical analysis of 4-μm sections of paraffin-embedded NICD1/myrAKT, NICD1/Myc, and NICD1/kRas^{G12D} tumors stained with H&E or with antibodies against NICD1, pErk, pAKT, Myc, or PCNA. (Scale bars: 100 microns.)

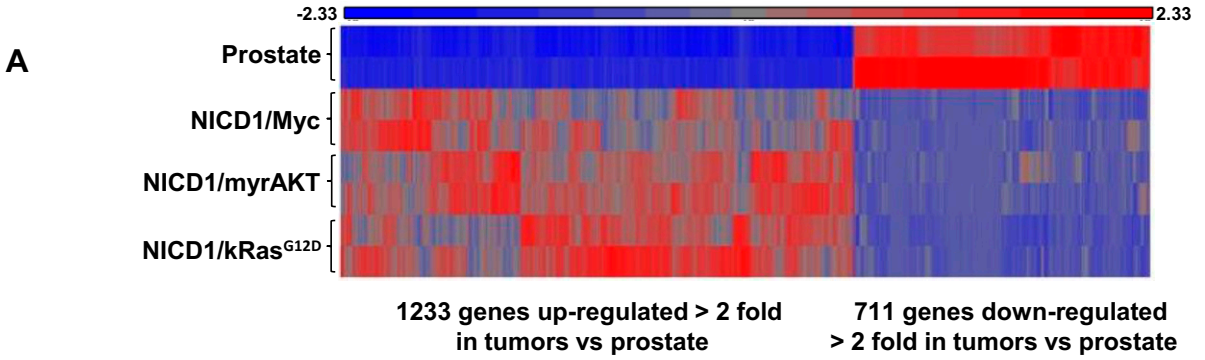

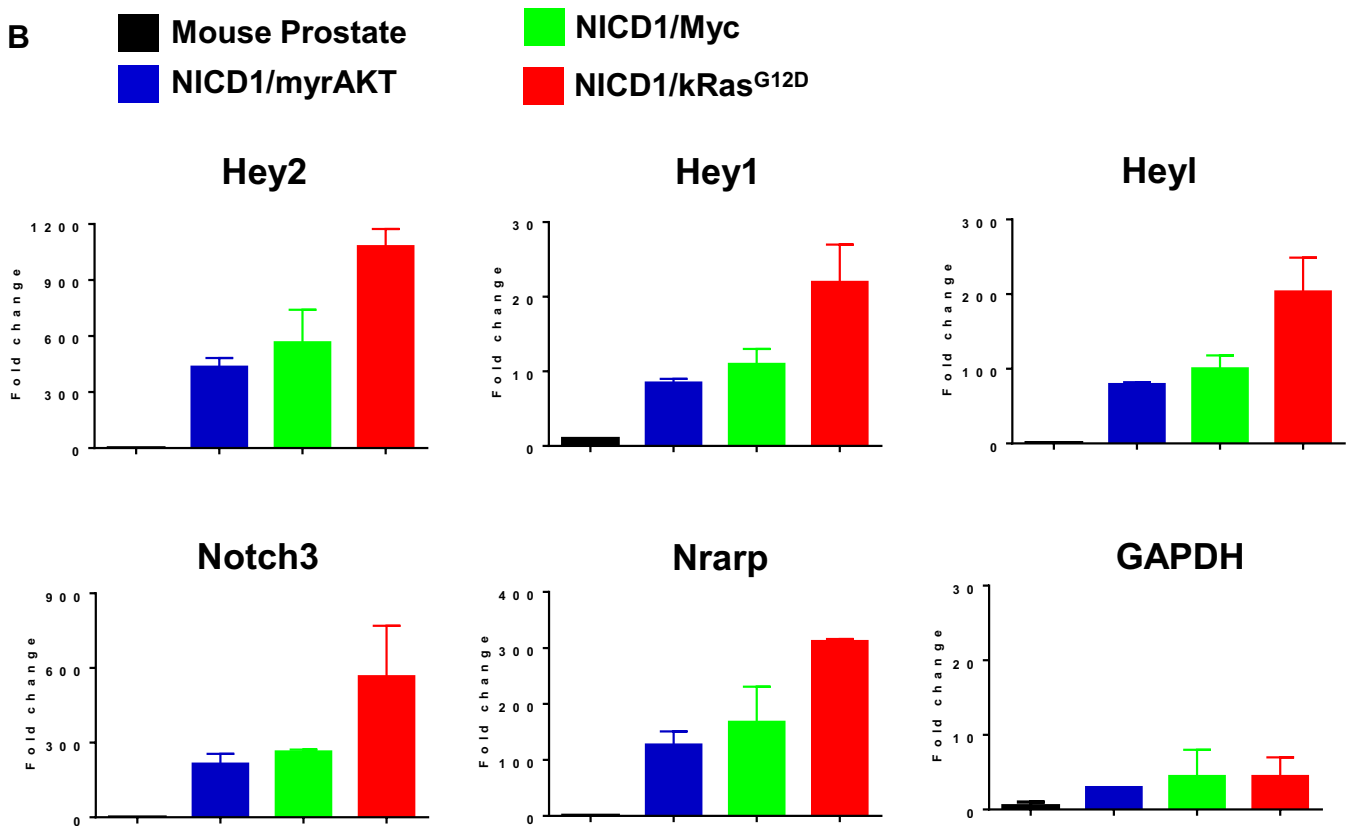

Fig. S6. Tumors driven by NICD1 in combination with pathways altered in prostate cancer express high levels of Notch1 target genes. (*A*) Heat map of common genes differentially expressed in NICD1/Myc, NICD1/myrAKT, and NICD1/kRasG12D tissue versus normal mouse prostate. Red represents genes overexpressed, and blue represents genes down-regulated across all NICD1/Myc, NICD1/myrAKT, and NICD1/kRas^{G12D} tissues versus normal mouse prostate. (*B*) The fold change in reads per kilobase per million mapped reads (RPKM) of transcript of Notch1 target genes (*Hey2*, *Hey1*, *Heyl*, *Notch3*, and *Nrarp*) and GAPDH from our RNA-sequencing analysis is shown. The average of RPKM of each gene in the mouse prostate is considered as 1.

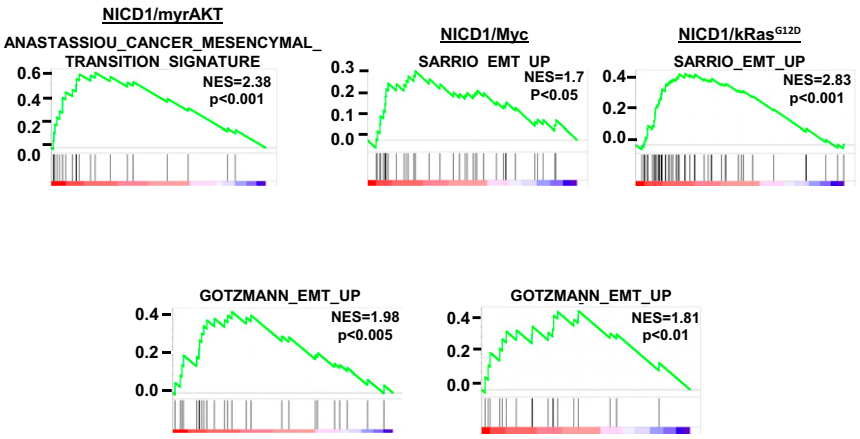

Fig. S7. Tumors driven by NICD1 in combination with pathways altered in prostate cancer exhibit EMT characteristics. Plots representing GSEA of genes differentially expressed in NICD1/myrAKT, NICD1/Myc, and NICD1/kRas^{G12D} versus normal mouse prostate are shown. NES, normalized enrichment score.

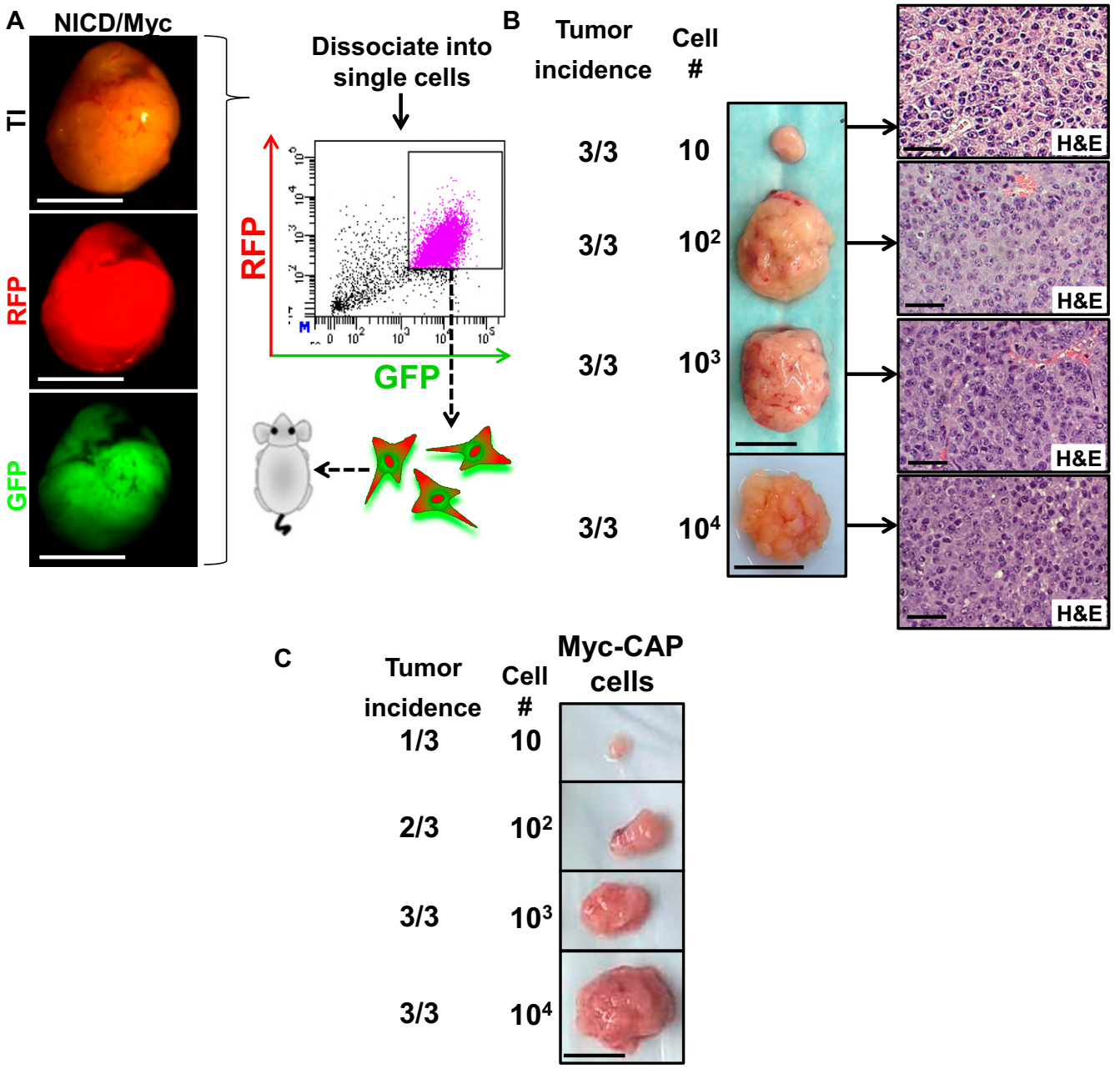

Fig. S8. NICD1 in combination with alternative pathways exhibits high self-renewal activity and metastatic potential in vivo. (*A*) Dissociated single cells from a primary NICD1/Myc tumor were subjected to FACS. GFP/RFP double-positive cells were sorted. GFP/RFP cells were implanted into SCID recipient mice at limiting dilutions of 10, 100, 1,000, or 10,000. (Scale bars: 0.5 cm.) (*B*, *Left*) Representative tumors initiated from 10, 100, or 1,000 cells recovered 4 wk after implantation or from 10,000 cells recovered 3 wk after implantation. (Scale bars: 1 cm.) (*Right*) H&E staining of each tumor is shown. (Scale bars: 50 microns.) One of the two independent experiments is shown. (*C*) The Myc-CAP cell line (44) has lower self-renewal activity and was used as a control. Representative tumors initiated from 10, 100, or 1,000 Myc-CAP cells recovered 8 wk after implantation. (Scale bar: 1 cm.)

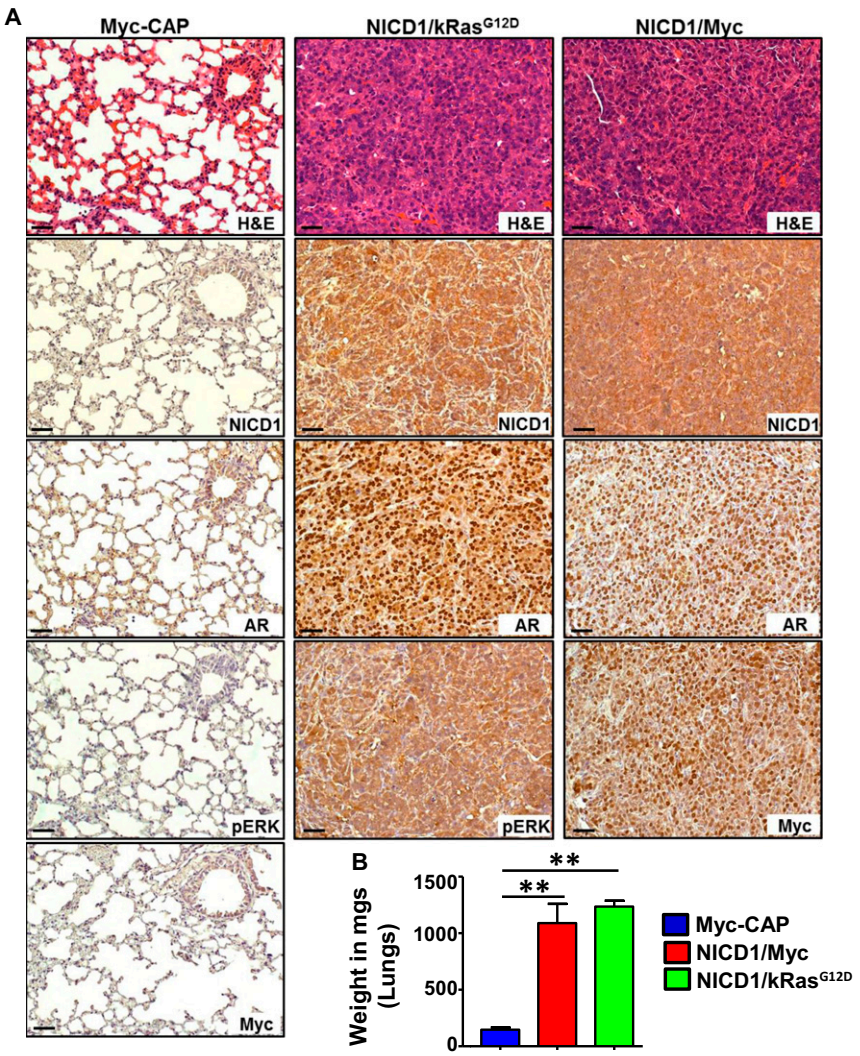

Fig. S9. Tumors driven by NICD1 in combination with other pathways altered in prostate cancer exhibit metastatic potential. (*A*) Immunohistochemistry analysis of paraffin-embedded lungs from the mice injected with NICD1/kRas^{G12D} and NICD1/Myc cells shown in Fig. 5*A* stained with H&E or antibodies against NICD1, pErk, Myc, and AR. (Scale bars: 100 microns in left panels; 50 microns in center and right panels.) (*B*) Weight of the lungs recovered at day 28 after injection from the animals shown in Fig. 5*C* injected with Myc-CAP-Luciferase, NICD1/kRas^{G12D}-Luciferase, or NICD1/Myc-Luciferase was measured in milligrams and plotted. $^{**}P < 0.005$, one-way ANOVA.

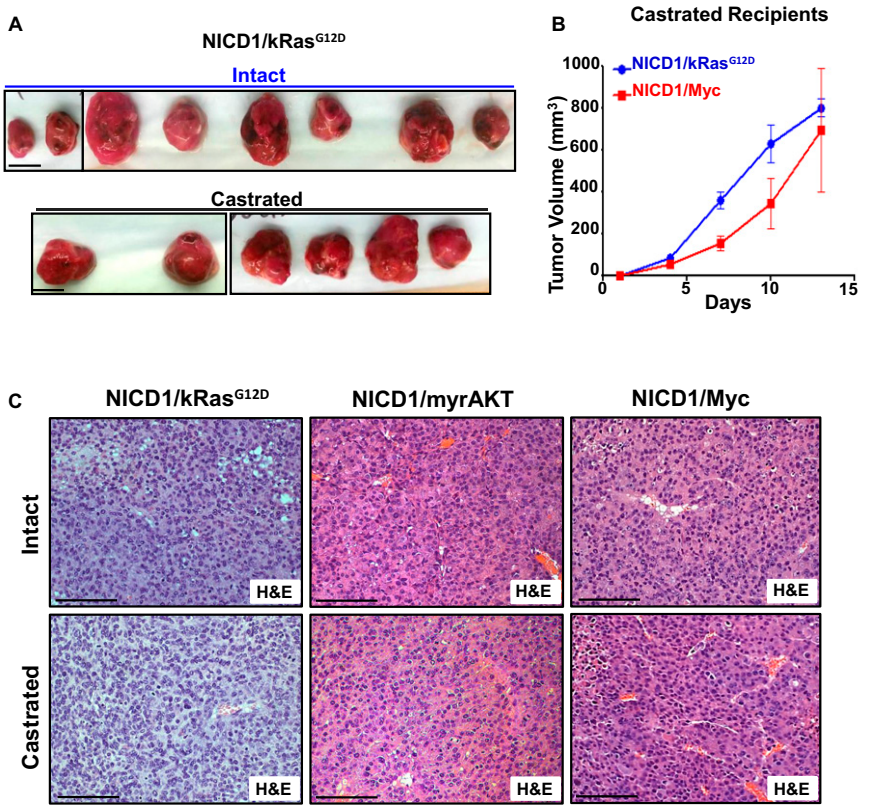

Fig. S10. Tumors driven by NICD1 in combination with other pathways altered in prostate cancer are castration resistant. (*A*) Images of the transplanted tumors driven by NICD1/kRas^{G12D} plotted in Fig. 6*A*. (Scale bars: 1 cm.) (*B*) NICD1/kRas^{G12D} or NICD1/Myc tumor cells (6×10^5) were mixed with Matrigel and were transplanted s.c. into six castrated or six intact recipient mice. Upon detection of palpable tumors (50 mm^3), tumors volumes were measured and plotted. (*C*) Histology of NICD1/kRas^{G12D}, NICD/myrAKT, and NICD1/Myc tumors recovered from intact or castrated recipients. (Scale bars: 100 microns.)

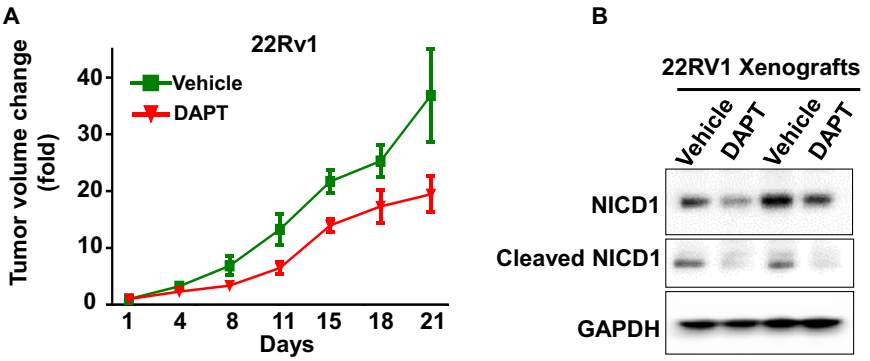

Fig. S11. γ-Secretase inhibition delays prostate cancer tumor growth. (*A*) 22Rv1 cells (1×10^6) were injected s.c. in NSG mice. Upon detection of palpable tumors, animals were treated with either vehicle ($n = 4$) or DAPT (GSI-IX) ($n = 4$) administered for 20 d according to the following schedule: 50 mg/kg DAPT for 3 d followed by 1 d off DAPT, then 50 mg/kg DAPT for 6 d and 1 d off DAPT. Day 1 is the day of treatment initiation. (*B*) Inhibition of Notch1 by DAPT in vivo was confirmed by Western blot for NICD1 and the cleaved Notch1 expression level.

A targeted mass spectrometry approach to identify activated kinases in prostate cancer

Justin M. Drake[a], Sangeeta Bafna[a], Haiyan Zheng[a], Nicholas A. Graham[b], Thomas G. Graeber[c], Peter Lobel[a], Owen N. Witte[c]

[a]Rutgers Cancer Institute of New Jersey, [b]University of Southern California, [c]University of California, Los Angeles

BACKGROUND/OBJECTIVES: Prostate cancer is the second-leading cause of cancer death for men in the United States. Although relatively indolent compared to other epithelial malignancies, prostate cancer is lethal when untamed metastatic castration-resistant dissemination occurs. Mounting evidence suggests that non-mutated, activated kinases are key players in metastatic CRPC. We have previously identified a strong correlation between increased global tyrosine phosphorylation and prostate cancer progression both in a mouse model of prostate cancer and in human clinical samples. We identified several activated kinases using unbiased quantitative phosphopeptide proteomic analysis by tandem mass spectrometry of human metastatic CRPC tissues. Several of these identified kinases are direct targets of current FDA-approved kinase inhibitors opening the door to investigate these kinases as viable therapeutic options. Due to the overwhelming evidence for kinase activation in metastatic CRPC tissues, our **objective** is to utilize a targeted mass spectrometry (MS) approach for the evaluation of current druggable kinases in human CRPC biopsies that will ultimately guide personalized therapy decisions.

METHODOLOGIES: A large panel of approximately 100 phosphopeptides was synthesized and then analyzed on a high resolution Q-Exactive MS to measure the sensitivity of detection and elution time. Information for each phosphopeptide was used to serve as internal standards and surrogates for kinase activity in pre-clinical and clinical tissues.

RESULTS: To date, we have analyzed 100+ phosphopeptide standards via targeted MS. Serial dilutions were evaluated to determine the linearity of the assay over several orders of magnitude as well as sensitivity. We were able to establish high sensitivity into the attomole (10^{-18} moles) range for a majority of the phosphopeptides in a non-mammalian matrix of consisting of plant lysate.

CONCLUSIONS: We have established a list of phosphopeptides that will serve as a predictive biomarker panel to carry forward for pre-clinical proof of concept and clinical testing. Future work will first establish the detection of driver kinases in cell lines with known activating mutations of kinases such as BRAF V600E in melanoma or colorectal cancer cell lines or EGFR mutations in non-small cell lung cancer cell lines. Once established, we will proceed to evaluate several prostate cancer cell lines that have no known driver kinase mutations and measure kinase activity for predicted kinase inhibitor therapies followed by subsequent validation studies.

IMPACT: Advanced predictive tools and effective therapies are necessary to improve the clinical care of patients with metastatic CRPC. The development of a targeted mass spectrometry approach to measure a large panel of druggable, activated kinases in clinical tissues will represent a new clinical paradigm supporting phospho-kinase profiling to determine optimal treatment combinations in patients with metastatic CRPC.